Title:
Nonlinear Time-domain Analysis of Floating Space Frame Structures

Theme:
Floating Offshore Structures

Project Type:
M.Sc. Thesis

Project Period:
02-09-2014 to 16-06-2015

Supervisor:
Lars Damkilde, lic. techn.
Professor,
Aalborg University Esbjerg

Morten E. Nielsen, M.Sc.
Scientific Assistant,
Aalborg University Esbjerg

University:
Aalborg University Esbjerg
Institut for Byggeri og Anlæg
Niels Bohrs Vej 8
6700 Esbjerg

Authors:

Alaa Taha

Arber Kadriu

Number of Pages:
Report: 86
Appendix: A-B

Abstract:
This report concerns the prediction of the loads and global dynamic response of a floating structure consisting of offshore anchoring ropes, a buoy and a slender space frame structure subjected to buoyancy and wave loading. Nonlinear analysis is required as the floating structure undergoes large deformations, and thus a two-dimensional corotational beam formulation is implemented. All structural components are modelled by cylindrical beam elements in both a produced Nonlinear Wave Code in Matlab and in the commercial finite element program Ansys Workbench which is used as validation source for the Nonlinear Wave Code. Via the Nonlinear Wave Code it is possible to evaluate the response of the floating structure in different sea states, including linear waves, nonlinear waves and irregular waves.

The hydrostatics and hydrodynamic forces are modelled by various methods, in which the wave and buoyancy forces are found as a function of the amount of submerged cross-sectional area of the structure. Simple validation examples consisting of vertical and horizontal cylinders are performed continually through the report for the purpose of validating the implemented methods before the dynamic response of the floating space frame structure is predicted.

The floating space frame structure is modelled with a fine mesh to obtain a sufficient representation of the ocean loads and the dynamic response of the structure. A time-domain analysis is performed, in which the structure is subjected to a linear wave. The predicted hydrostatics and hydrodynamic forces and the dynamic response in the Nonlinear Wave Code and Ansys Workbench are consistent. The Nonlinear Wave Code is thus able to predict the dynamic response of a floating slender space frame structure.

Preface

This Master Thesis is formulated by a group of two M.Sc. Engineer students at Aalborg University Esbjerg, on the 9^{th} and 10^{th} semester in the period from the 2^{nd} of September to 16^{th} of June 2015. The theme of the project is Nonlinear Analysis of Floating Offshore Structures. The project consists of a main report and an Appendix. The structural analyses cover modelling of wave loads, buoyancy forces and nonlinear dynamic finite element analysis. It is assumed that the reader has basic literacy concerning technical subjects such as statics, structural dynamics, fluid dynamics, continuum mechanics and the finite element method.

The project is aimed primarily to the projects supervisors, examiners and other interested persons with an understanding of the theory from the considered topics. In the report, equation numbers are given to refer to the requested equations. The notation of the equation numbers is (1.1), (1.2) etc. A reference list is introduced in the end of the report, in which the books are indicated with author, title, publisher, edition while homepages are indicated with link and title.

A copy of the report in PDF format is on the enclosed DVD, and in order to read and use all of the enclosed material, the following programs are required.

- MATLAB
- Ansys Workbench
- Adobe Reader

The report is formulated under supervision of Lars Damkilde, professor at Aalborg University Esbjerg and Morten E. Nielsen, Research Assistant at Aalborg University Esbjerg. The authors of this report express gratitude for the supervisors' guidance.

Table of Content

1 Introduction

One of the major engineering challenges in the near future is to meet the increasing global energy demand, which is expected to double within the next 20 years. [1] The increase in demand for renewable energy in the recent years has entailed a greater attention to offshore renewable energy structures such as wind turbines and the relative new and lesser widespread wave energy converters. The wave energy converters are still at an initial face in the industrial developing, however it may be the new promising renewable energy structure in the near future. The increase of the application of these structures gives rise to a larger utilisation of the ocean. Considering the offshore wind turbines, different types are applied on the ocean as shown in Figure 1.

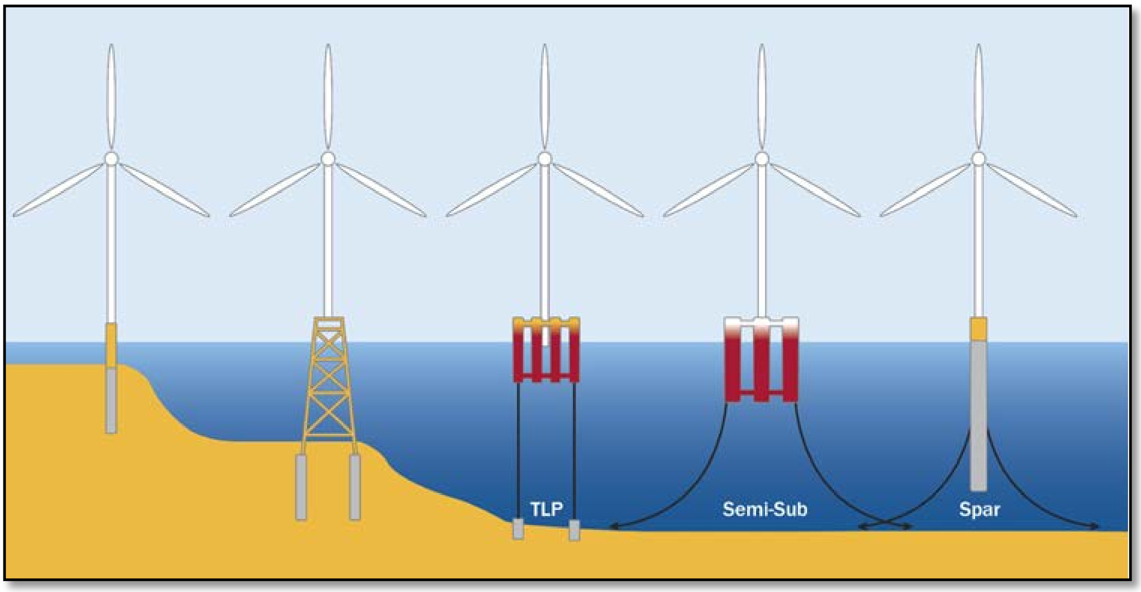

Figure 1: Different types of offshore wind turbines depending on the water depth. **[2]**

The water depth decides the type of foundation of the offshore wind turbines, where the most advanced foundations are those for the floating wind turbines such as the Tension Leg Platform (TLP), semi-submersible structures (Semi-Sub) and spar floating structures (Spar).

The semi-submersible structures have been used for many years in the offshore oil and gas industry operating on deep water. The structure consists of hulls fabricated from large horizontal pontoons onto which vertical steel columns are welded and is held to the seabed by anchors. The TLP has basis on another concept, as it is vertically moored by means of tethers or tendons. The high axial stiffness of the tethers does not allow any vertical motion but allows horizontal motion with wave disturbance, which gives a great stability of the structure. The spar floating structure is a large round hull anchored to the seabed by conventional chains and winches. The structure operates in deep water.

Floating structures allow operation on deep water and thereby the opportunity to apply structures as offshore wind turbines and floating wave energy converter to a greater extend on the ocean.

Furthermore the ocean is a large, relatively untapped renewable energy resource as wave energy is assessed to be a reliable long-term energy source which has the potential to provide 10-15 % of the global electricity need. Mentioning for instance the Weptos, it is a promising wave energy concept, particular due to the drop-shaped rotors which give basis for a high and efficient utilisation of the waves. [1]

Figure 2: Weptos, Wave Energy Converter at sea. **[1]**

The Weptos has the ability to adapt to both small and large waves and wave directional waves. The structure can regulate the amount of incoming wave energy and thus reduce the loads affecting the structure in case of extreme wave conditions. Additionally, the Weptos is anchored to a buoy and is therefore flexible with regard to the waves.

There is a clear interest in utilising the capacity of the ocean which the aforementioned increase in application of both offshore wind turbines and wave energy converters indicates. One of the major challenges when considering floating structures, is however to predict the loads and the dynamic response of the structure. Depending on the design of the structure and the design of the anchor, the structure behaves differently on the ocean and therefor an overall prediction of the loads of a floating structure is complex to accomplish.

1.1 Approach for Analysis of Slender and Large Volume Structures

Marine structures are generally categorised as either large or small volume structures. Large volume offshore structures such as ships and semi-submersible floating platforms are inertia-dominated which implies that radiation/diffraction analyses need to be performed. The global loads are thus due to wave diffraction significantly larger than the drag-dominated global loads. Analysing large volume structures, the hydrodynamic loads are found by potential flow theory by means of a velocity potential of the irrotational motion of an incompressible and inviscid fluid.

The potential flow and the real flow are illustrated in Figure 3.

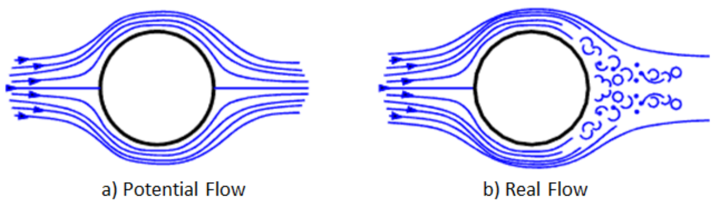

Figure 3: a) Potential flow. b) Real flow **[1]**

Considering small volume structures such as floating slender space frame structures which is the case in this project, the wave loads on the members are predicted by the semi-empirical Morison's formula. Slender structures are drag-dominated and the Morison's formula includes both a drag term and an inertia term. The wave diffraction effect is ignored when applying the Morison's formula, while the viscous drag effect is neglected when using the potential theory. For this reason usually a slender model is used in combination with a large volume structure model in order to include the effect of viscosity through drag forces on the Morison related elements. Figure 4 illustrates an example of a large volume structure in terms of an oil rig while a small slender structure is illustrated in terms of a restrained jacket structure.

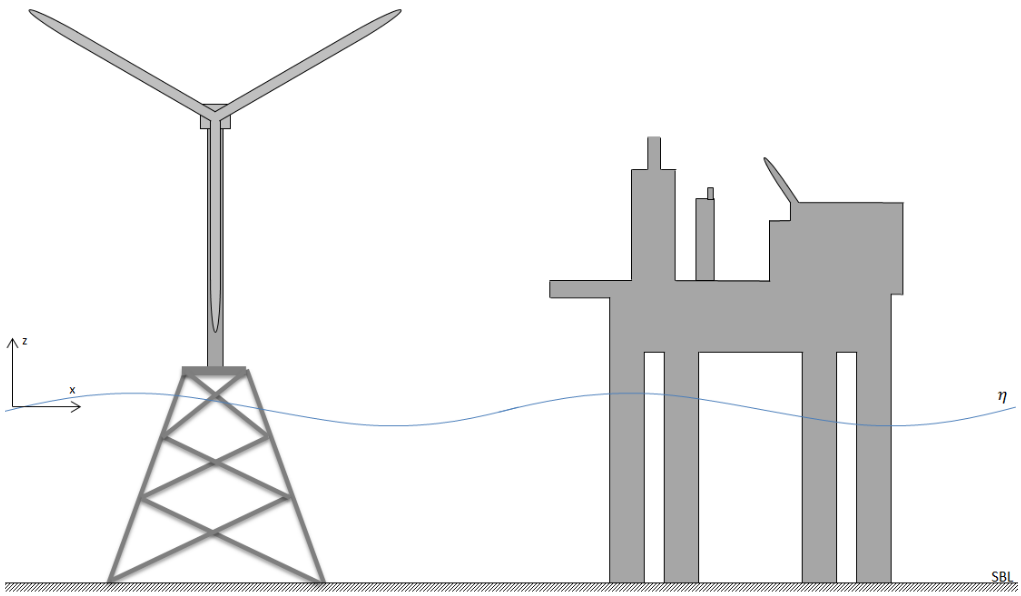

Figure 4: Slender structure in terms of a jacket structure and a large volume structure in terms of an oil rig.

Floating structures are exposed to the same ocean phenomenon as a restrained jacket structure, i.e. wave loading, buoyancy and current. However, a floating slender structure is positioned at the ocean water surface and is in constant motion, which implies that the Morison's formula is expressed in terms of the relative fluid-structure velocities and accelerations. To analyse a floating slender space framed structure it is thus needed to introduce geometric nonlinear analysis as the structure undergoes large displacements and rotations. A more detailed description of the aim and scope of the project are given in the following subsection.

1.2 Aim of Project

The aim of this report is to predict the nonlinear time-domain dynamic response of the floating space frame structure subjected to ocean wave loads and buoyancy illustrated in Figure 5. A dynamic analysis is either performed in the time-domain or in the frequency-domain. The dynamic response of the floating space frame structure is predicted in the time-domain as it is not sufficient to represent the dynamic response of the structure in the frequency-domain. The advantage of the time-domain analysis is that it can deal with higher-order load effects, which is not possible to be captured in the frequency-domain. Main focus is in this project given on the environmental loads subjected to the floating structure consisting of the hydrostatics and hydrodynamic forces while a corotational beam formulation is implemented. The prediction of the loads and the dynamic response is generally valid for any element based structure.

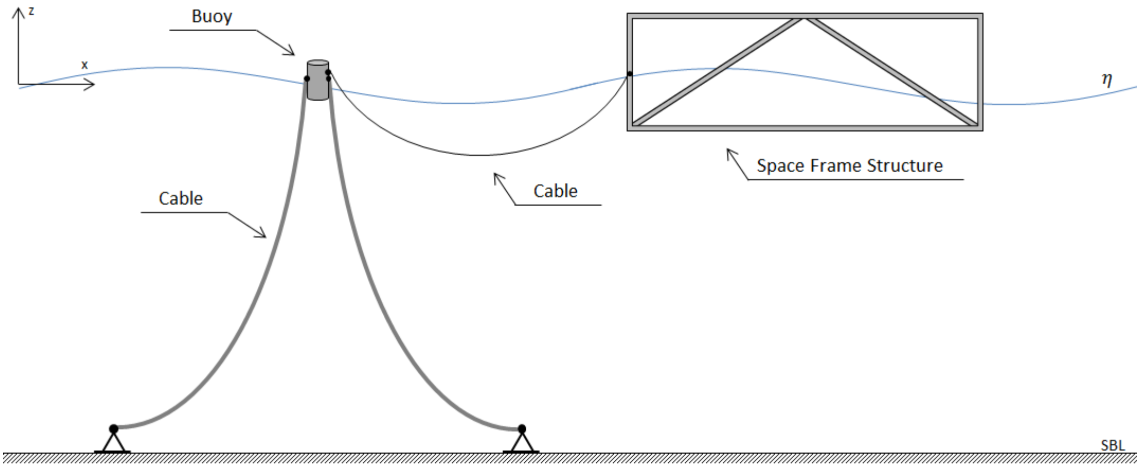

Figure 5: Floating space frame structure consisting of offshore cables, a buoy and a space frame.

The floating space frame structure illustrated in Figure 5 is an integrated dynamic system consisting of a space frame floater, a buoy and moorings. To achieve the aim of predicting the loads and dynamic response of the floating structure the following issues are considered and implemented in the project

- The loads and dynamic response of the structure is predicted in the time-domain.
- All structural components are modelled by cylindrical beam elements.
- The hydrostatics and the hydrodynamic forces are calculated as function of the amount of submerged cross-sectional area of the structure.
- The hydrodynamic forces are found by the semi-empirical Morison's formula expressed in terms of the relative fluid-structure velocities and accelerations.

The simplifications and delimitations made in the project are introduced and described in the following subsections.

Modelling of Nonlinear Wave Code in Matlab

The prediction of the loads and the dynamic response of a floating structure are achieved in the programming language Matlab, as the commercial finite element programme Ansys Workbench is not fully developed with regard to wave modelling on floating structures. The wave modelling in Ansys Workbench is dominated by some important limitations which are discussed continually in the report.

All calculations in the project are thus performed numerically in the programming language Matlab, in which a geometric nonlinear two-dimensional beam element programme is written, denoted the Nonlinear Wave Code. The Nonlinear Wave Code is capable of evaluating buoyancy forces and wave loading on restrained and floating offshore structures in different sea states. The only needed input in the Nonlinear Wave Code to predict the loads and the dynamic response of an arbitrarily designed floating slender structure is the geometry of the structure and the ocean wave specifications. The commercial finite element program Ansys Workbench is used as reference and as validation source for the methods implemented in the Nonlinear Wave Code.

Structural Modelling

All structural components in the project are modelled by cylindrical beam elements including the anchoring cables. By using beam elements it is possible to extract the section forces from the considered model which is decisive for the future structural design of a floating structure.

1.3 Scope of Project

Wave energy converters consist of large structural elements such as rotors or buoys which give a high and efficient utilisation of the wave energy. The energy loss due to these structural elements is an important issue when considering a wave energy converter; however this issue is ignored in the project. Furthermore, the design of these structural elements gives rise to wave disturbance. These phenomenons have thus an important influence on the behaviour of a floating structure as no waves enter through the structure. In this project a simplification is made as focus is only given on the space framed part of a floating structure, by which the diffraction phenomena is neglected and thus only through-going waves are considered as shown in Figure 6.

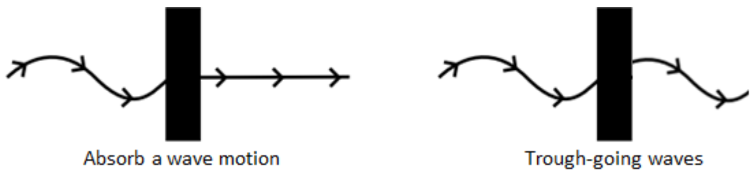

Figure 6: Illustration of wave motion absorption and through-going waves.

The important environmental ocean loads subjected to an offshore structure are waves, current, buoyancy and ice loads. Focus in this project is given on the waves and buoyancy forces, while the current and ice loads are omitted.

No structural design analysis is performed and as aforementioned the fundamental elements for a future structural analysis of a floating structure are considered.

2 Method Consideration

In the present subsection a description of the methods utilised in the project is introduced. Numerical methods which have satisfactorily balanced accuracy and computing resources are defined and used to predict the loads and the response of the floating space frame structure in different sea states.

The corotational beam formulation implemented in the Nonlinear Wave Code follows a paper presentation given by *Louie L. Yaw* [3] and allows the structure to have arbitrarily large displacements and rotations at the global level. The formulation is introduced and described in Chapter 3. An illustration of the floating space frame structure undergoing large displacements and rotations is given in Figure 7.

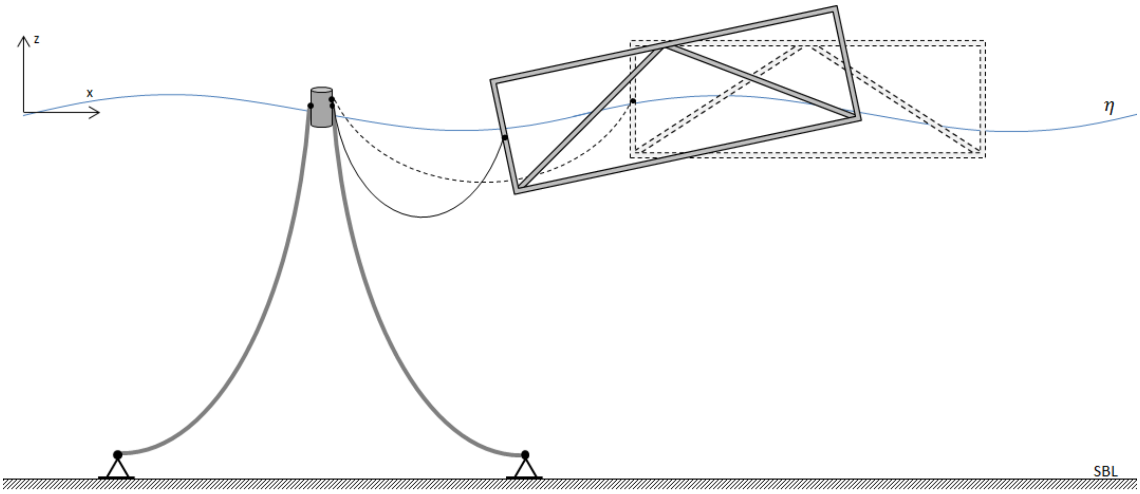

Figure 7: Illustration of the floating space frame structure undergoing large displacements and rotations.

The wave loads acting on the structure are determined in the produced Nonlinear Wave Code in Matlab in which the wave kinematic quantities, that is the wave velocities and accelerations, are numerically calculated. The wave kinematic quantities are calculated based on different sea states, and subsequently used as input in Morison's formula by which the differential hydrodynamic forces are determined. The hydrodynamic forces are transformed into beam loads by means of two methods as stated below.

- In the first method the hydrodynamic forces are transformed into beam loads by means of polynomial regression, i.e. the differential hydrodynamic forces are represented by a higher order polynomial. The forces are subsequently transformed into consistent beam loads by the interpolation functions.
- In the second method the hydrodynamic forces are converted into nodal forces by introducing numerical integration, based on the trapezoidal rule, and by means of interpolation functions.

These methods are validated in their associated subsections by a restrained solid cylinder subjected to the formulated hydrodynamic forces. The most accurate method of representing the hydrodynamic forces is then used in the prediction of the loads subjected to the floating space frame structure.

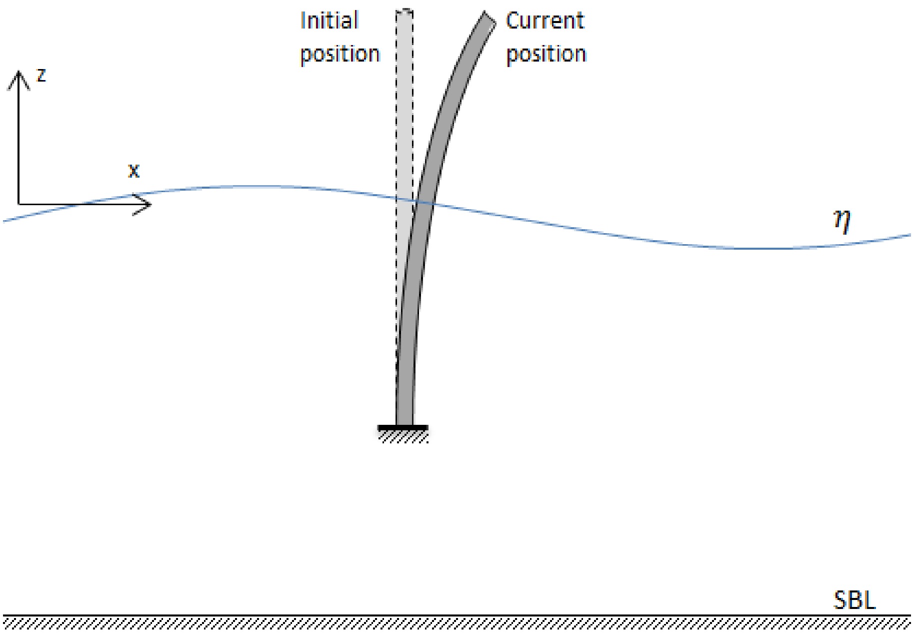

Figure 8: An illustration of a slender restrained cylinder subjected to hydrodynamic forces.

An overall description of the wave theories used for the determination of the wave kinematic quantities and a description of the abovementioned methods applied for calculation and conversion of the differential hydrodynamic forces into nodal forces is given in Chapter 5. The validation of the implemented methods is based on the commercial finite element program Ansys Workbench. For the purpose of this project, no specific location of the structure is given while the wave specifications as well are not given for a specific sea location. Only the linear wave theory is used for the sake of validation in the project. The validity of the used ocean wave specifications is based on the *Le Mehaute* diagram introduced in subsection 4.2.

Furthermore, the hydrostatics is calculated in two manners in which the first method is based on a paper presented by *M. Yazdchi*. [4]

- In the first method, the buoyancy forces are divided into two effects, namely a distributed pressure and a buoyancy term that only exists if the ends are capped. The buoyancy forces are calculated as a function of the submerged element length.
- In the second method, the buoyancy forces are determined as a function of the amount of submerged area, and subsequently transformed into global nodal forces by interpolation functions and numerical integration.

For the purpose of validation of the formulated hydrostatics, two simple buoyancy test example are conducted in the Nonlinear Wave Code. A vertical and a horizontal hollow cylinder are dropped in still water as illustrated in Figure 7, by which the dynamic responses are compared and validated with the buoyancy formulation given in Ansys Workbench.

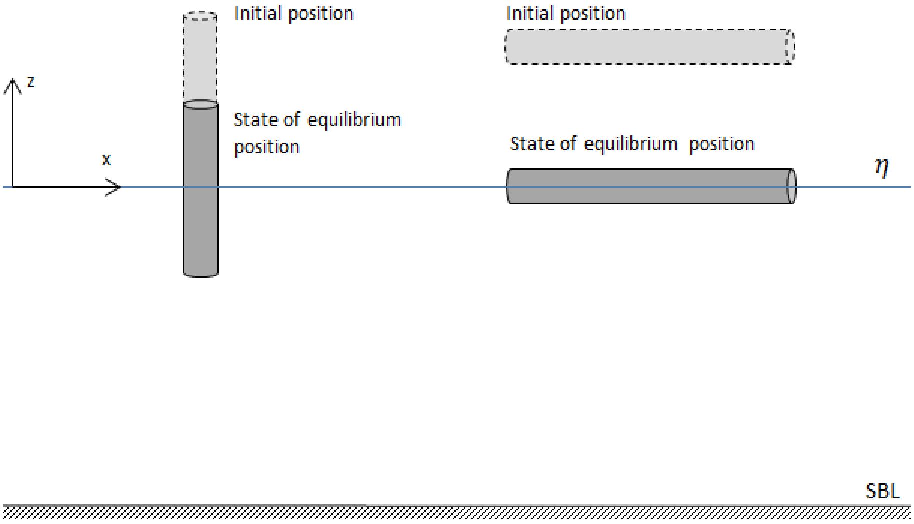

Figure 9: Illustration of a horizontal and vertical hollow cylinder dropped into still water.

The most accurate method of representing the hydrostatics is used in the prediction of the loads and the dynamic response of the floating space frame structure. The modelling and prediction of the response of the floating space frame structure is performed in Chapter 8, in which firstly the anchoring cables and the boundary conditions of the system are modelled.

The Nonlinear Wave Code is completely automated so that the only necessary user input for the wave and buoyancy force analysis is the design of the floating structure and the desired wave specifications. The Nonlinear Wace Code is programmed so that it is possible to evaluate the response of the floating structures in different sea states, including linear waves, non-linear waves and irregular waves. Important scripts of the programmed Nonlinear Wave Code are presented in Appendix B while the full version of the programme is enclosed in the Appendix DVD.

3 Corotational Beam Formulation

In the following chapter a simple two-dimensional corotational beam formulation is introduced and described based on a paper produced by *Louie L. Yaw*. [3] Many of the engineering problems are solved by the assumption of linear elastic, small deflection behavior which means that simple direct solutions are obtained with no need for load incrementation and iterative schemes. However, the displacements and rotations of a floating structure can be so large that it cannot be neglected while loads may change their orientations according to displacements and supports may change during loading. If these occurrences are included then the set of equilibrium equations becomes nonlinear.

Structural nonlinearities can be identified as geometric nonlinearities, material nonlinearities and boundary nonlinearities. Based on this project the material nonlinearities are not presently included. However, considering floating structures the geometric nonlinearities are significant and therefore included in the project. The boundary nonlinearities consisting of the structure supports and insistence of degrees of freedom are likewise included as the modelled forces are set as function of the updated node coordinates and thus as function of the displacements.

3.1 Corotational Concept

The approach used for the geometric nonlinearities is as aforementioned a simple two-dimensional corotational beam formulation, which is valid as long as local beam element strains are small and all beam elements are assumed to remain linear elastic. The most important requirements for a geometric nonlinear formulation is firstly the angle of rotation of a corotating structure, the relations between global and local variables and the determination of a variationally consistent tangent stiffness matrix.

The corotational concept is basically a formulation, where the rigid body motions and the strain producing deformations are kept separate at the local element level. The rigid body rotations and translations are zero with respect to the local corotating coordinate system and thus only the strain causing deformations remains. The local strain causing deformations are related to the internal forces of the beam elements and by some relations between the local and the global variables the global internal forces are obtained.

To separate the rigid body motions from strain producing deformations at the local element level, a corotational local coordinate system for each element is introduced, where the x-axis is directed along the element and the z-axis is perpendicular to the x-axis as illustrated in Figure 10.

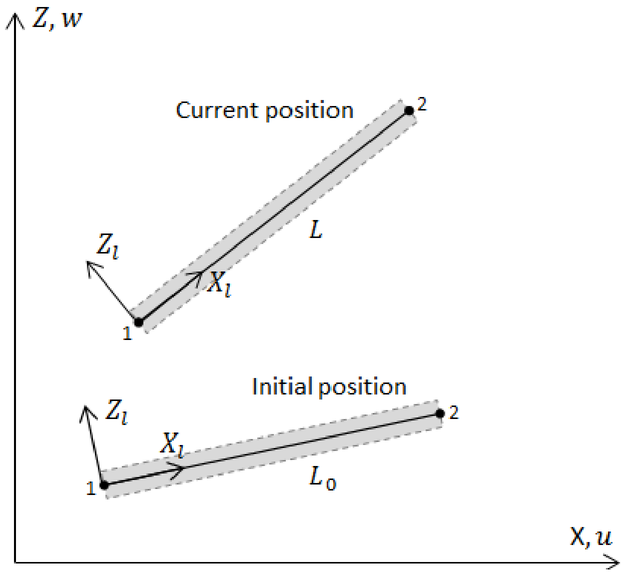

Figure 10: Initial and current configuration of a corotating beam element.

A typical beam element in its initial and current configurations is illustrated in Figure 10, in which the flexural deformations are neglected. In its initial configuration the initial length of the beam element L_0 is defined by the global nodal coordinates of the beam for node 1 and 2 given by (X_1, Z_1) and (X_2, Z_2). Considering the beam element in its current configuration the global nodal displacements of the beam element are considered, and the current length L of the beam element is thus given as

$$L = \sqrt{\left((X_2 + u_2) - (X_1 + u_1)\right)^2 + \left((Z_2 + w_2) - (Z_1 + w_1)\right)^2} \tag{3.1}$$

in which u and w are the global nodal displacements in the X and Z direction, respectively. The initial and current angle of rotation β_0 and β which as well are defined by the global variables are used to calculate the local nodal rotations θ_{1l} and θ_{2l}. These local nodal rotations, which allows the rotation of the two-dimensional beam element to have arbitrarily large rotations, are used to calculate the local end moments M_1 and M_2 of the beam element.

The variationally consistent tangent stiffness matrix is thus generally obtained by evaluating the relation between the global and local variables and by the global internal forces. The global variationally consistent tangent stiffness matrix K is assembled by adding two stiffness contributions: the transformed material stiffness at the global level k_{t1} and the geometric stiffness $k_{t\sigma}$ given as

$$K = k_{t1} + k_{t\sigma} \tag{3.2}$$

The transformed global material stiffness matrix k_{t1} for a two-dimensional beam element is found by

$$k_{t1} = B^T C_l B \tag{3.3}$$

in which B is the transformation matrix given as

$$B = \begin{bmatrix} -c & -s & 0 & c & s & 0 \\ -s/L & c/L & 1 & s/L & -c/L & 0 \\ -s/L & c/L & 0 & s/L & -s/L & 1 \end{bmatrix} \tag{3.4}$$

where c and s are the vectors of cosines and sinus for each beam element angle while L is the beam element length. C_l is a matrix obtained by considering the axial force and the local end moments of the beam which leads to

$$C_l = \frac{EA}{L_0} \begin{bmatrix} 1 & 0 & 0 \\ 0 & 4r^2 & 2r^2 \\ 0 & 2r^2 & 4r^2 \end{bmatrix} \tag{3.5}$$

where r is the radius of gyration calculated by the moment of inertia and the area of the beam element $r = \sqrt{I/A}$ and L_0 is the original length of the beam element. The geometric stiffness contribution $k_{t\sigma}$ is determined by evaluating the local axial forces and the local nodal rotations in the beam and by combining with the material stiffness the variationally consistent tangent matrix is obtained.

For a more detailed description of the theory behind the corotational beam formulation reference is made to the paper presented by *Louie L. Yaw*. [3]

3.2 Load Control Algorithm for Corotational Beam Analysis

A program implementing the corotational beam algorithm has been written in the Nonlinear Wave Code. The algorithm is performed implicit and uses Newton-Raphson iterations at the global level to achieve equilibrium during each incremental load step. The Newton-Raphson method is based on the simple idea of linear approximations and is a very effective mathematically tool for solving equations numerically. The method provides continuously better approximations to the roots of a real-valued function and only needs one initial guess to start the iteration. Given a real-valued function f with the reals x and the equation

$$f(x) = 0 \tag{3.6}$$

An approximation of x is provided by making an initial guess x_0 and obtaining a better approximation x_1 by means of the initial guess x_0, the function $f(x_0)$ and the derivative $f'(x_0)$ as stated in

$$x_1 = x_0 - \frac{f(x_0)}{f'(x_0)} \tag{3.7}$$

The process is repeated until a sufficiently accurate value is obtained

$$x_{n+1} = x_n - \frac{f(x_n)}{f'(x_n)} \tag{3.8}$$

Geometrically, the process is illustrated in Figure 11, where the function f appears in a coordinate system with an approximation x_n of x and a better approximation x_{n+1}.

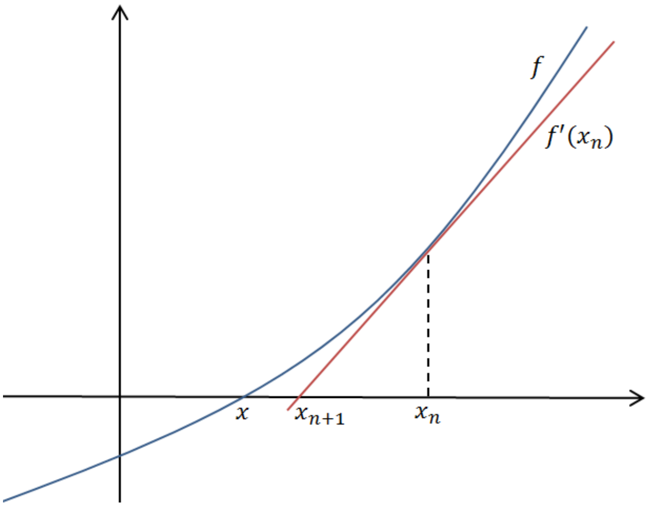

Figure 11: An iteration by the Newton-Raphson method.

As seen in Figure 11 the point $(x_{n+1}, 0)$ is the intersection of the x-axis with the tangent to the function f at point $(x_n, f(x_n))$.

One of the major advantages of the Newton-Raphson iteration is that the method fulfils square convergence, which means that the method provides a doubling of the number of significant figures of x. However, there are some disadvantages by use of the Newton-Raphson iteration method. Each step in the iterative solution requires solution of a linearized set of equations which requires a high computational effort. Furthermore the method is sometimes not reliable, as the method for some examples never converges.

The corotational beam algorithm solution consists of three important steps which are not described in the report. For a more detailed description of the algorithm, reference is made to the Nonlinear Wave Code script *MainNonlinear.m* represented in Appendix B.

3.1 Validation of Corotational Beam Algorithm

Two geometric nonlinear analysis examples are evaluated to validate the corotational nonlinear algorithm implemented in the Nonlinear Wave Code. In the first example it is assumed that large displacement, small rotation and small strains occur.

The first example concerns the geometric nonlinear behaviour of a single bar truss subjected to lateral loading. The geometric nonlinear behaviour of the truss is determined by both an analytical solution, the Nonlinear Wave Code and by a large deflection analysis in Ansys Workbench.

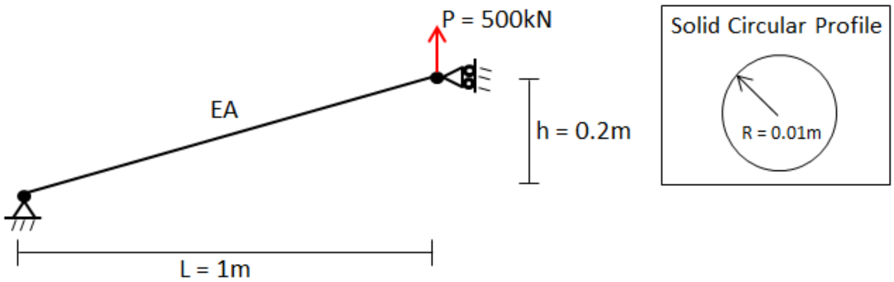

Figure 12: Single bar truss subjected to a lateral loading with the cross-section shown to the right of the figure.

The load displacement illustrated in Figure 14 is linear for small loads but as the load increases the curve becomes nonlinear. As the load increases further the bar truss becomes stiffer due to the geometric stiffness of the bar. The initial configuration and deformed state of the bar truss is shown in Figure 13.

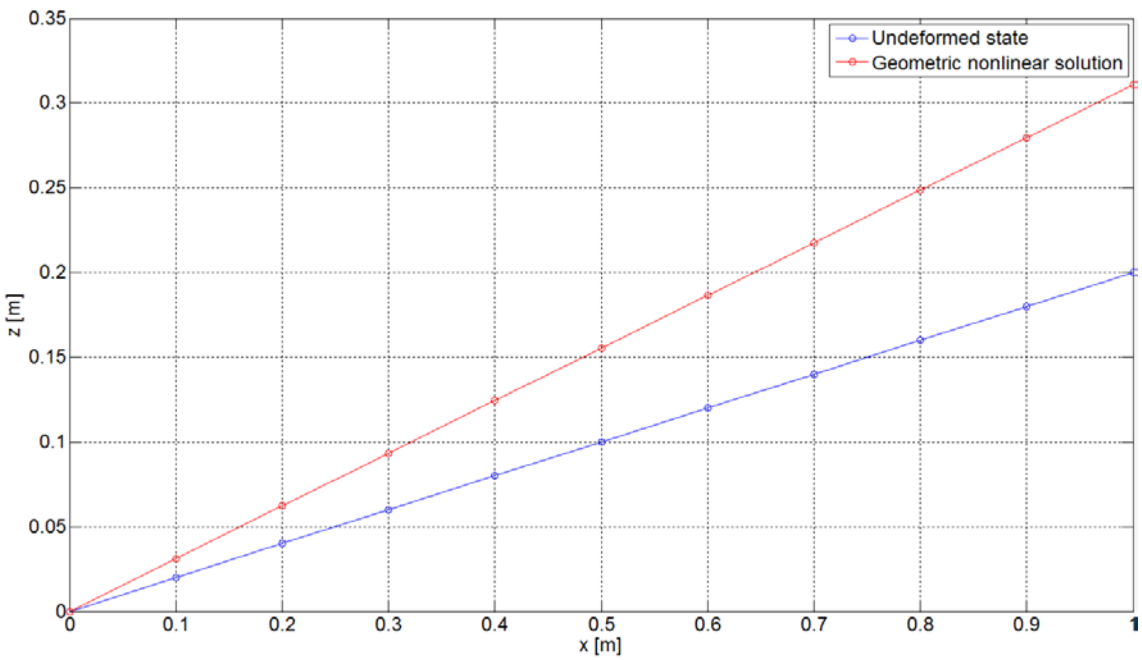

Figure 13: The initial configuration (blue line) and deformed state (red line) of the bar truss.

As remarked from Figure 13 the height h increases from $0.2m$ to $0.311m$. The load displacement results from the analysis are plotted and compared in Figure 14.

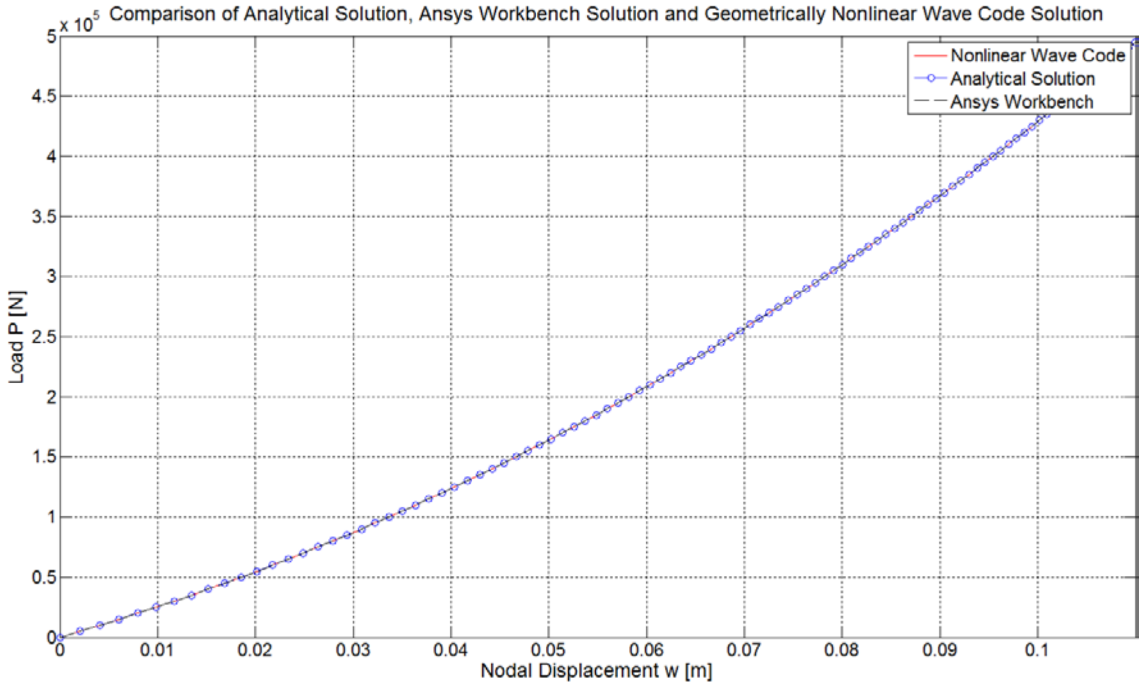

Figure 14: Comparison of the load versus displacement plot between the analytical, Ansys and Matlab solution.

It is remarked from Figure 15 that the results are consistent. By this validation example it is demonstrated that the Nonlinear Wave Code is capable of representing beam elements that are allowed to have arbitrarily large displacements.

The second verification example concerns a beam loaded by a moment at its free end as shown in Figure 16. The purpose of this example is to validate that the Nonlinear Wave Code is able to represent the behaviour of beam elements with large rotations.

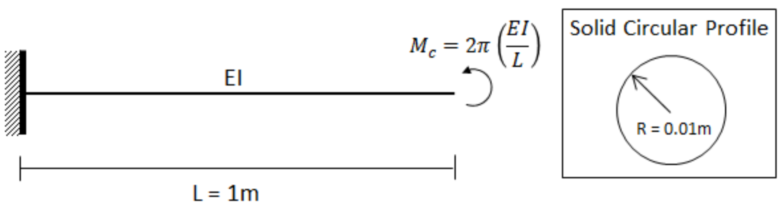

Figure 16: Cantilever beam subjected to an end moment.

The initial and deformed state of the beam is shown in Figure 17.

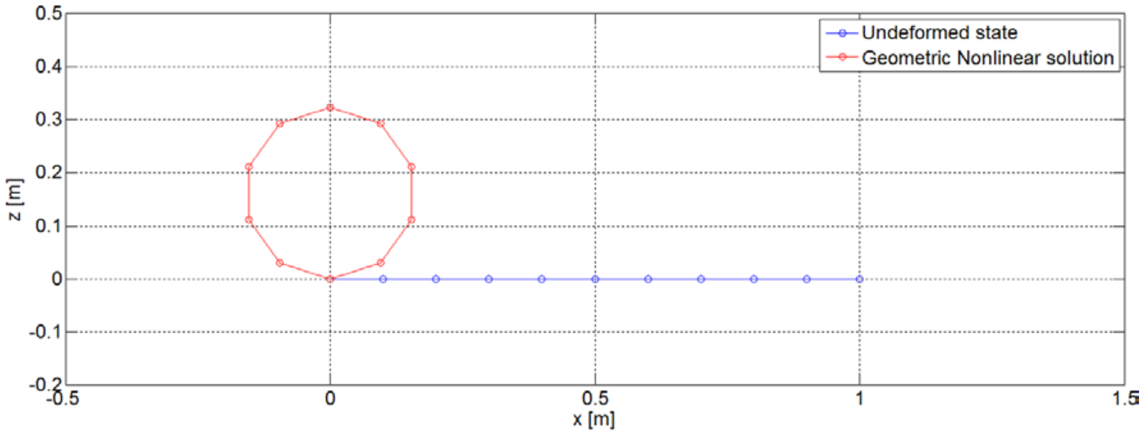

Figure 17: Cantilever beam loaded with end moment.

It is observed from Figure 17 that the cantilever beam is rolled up into a circle, which is due to that the moment has reached a value of $Mc = 2\pi(EI/L)$. The moment versus vertical displacement plot is given in Figure 18.

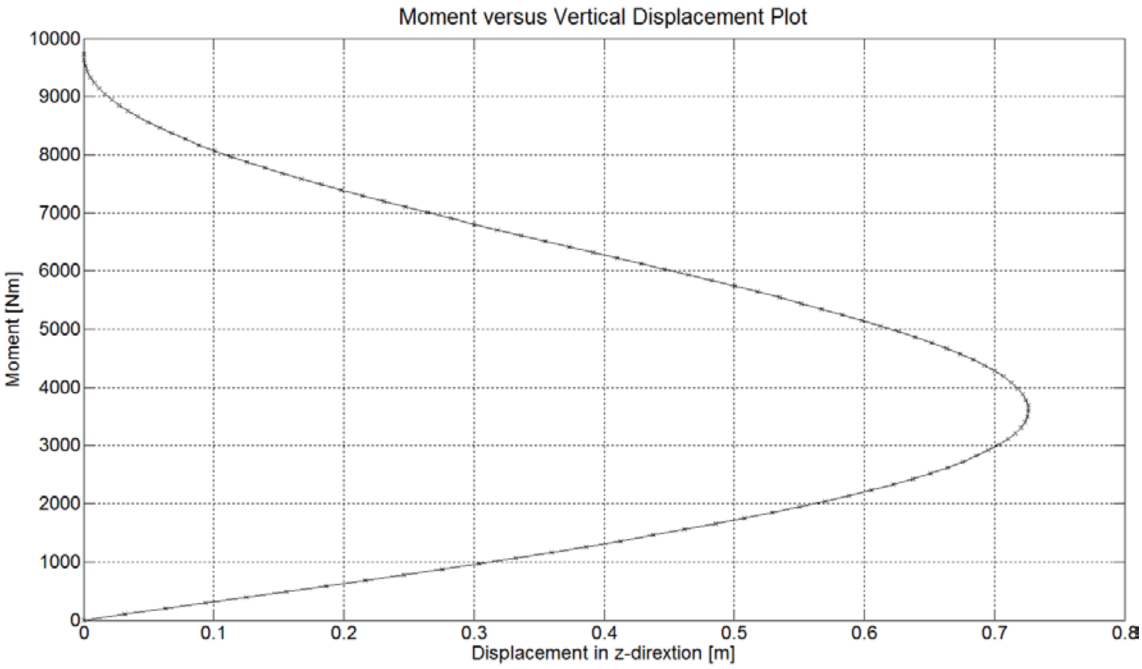

Figure 18: Moment versus displacement plot.

It is again remarked that the load displacement is linear for small loads, but as the load increases the curve becomes nonlinear. The displacement in the z-direction remains positive in consequence of the positive bending moment, which rotates the beam counterclockwise. The displacement reaches maxima at a given point and decreases as the cantilever beam is rolled up into a circle.

In preparation for the nonlinear dynamic analyses in the further project, it is necessary to extend the Newmark algorithm to consider nonlinear dynamic problems. The nonlinear Newmark algorithm is introduced in the following subsection 3.2.

3.2 Nonlinear Newmark Algorithm

Linear structural dynamic problems are extensively solved by the linear Newmark algorithm which is a direct integration method. To consider nonlinear dynamic problems it is necessary to extend the Newmark algorithm so that iteration is performed at each time step in order to satisfy equilibrium.

The Newmark solution method is thus rearranged so that the prediction relates to the velocity $\dot{u}$ and the acceleration $\ddot{u}$, respectively, whereas the displacement u is solved in the iterative solution of the equation of motion. As the equation of motion is satisfied at time increments $\dots, t_n, t_{n+1}$ the solution at t_{n+1} is given from the equation of motion by

$$M\ddot{u}_{n+1} + g(u_{n+1}, \dot{u}_{n+1}) = f_{n+1} \tag{3.9}$$

in which the solution is given by Newton iterations on the residual r obtained from

$$r = f_{n+1} - M\ddot{u}_{n+1} - g(u_{n+1}, \dot{u}_{n+1}) \tag{3.10}$$

The residual r depends thus on u, $\dot{u}$ and $\ddot{u}$. The first step of the nonlinear Newmark algorithm is to initialize the vectors u, $\dot{u}$ and $\ddot{u}$ in which the displacement and velocity vectors are assumed to be known and are thus defined as zero vectors. The steps in the nonlinear Newmark algorithm is introduced below, where the acceleration vector is defined as following in the first step of the solution method

(1) Initial conditions $u_0, \dot{u_0}$

$$\ddot{u}_0 = M^{-1}(f_0 - C\dot{u_0} - Ku_0) \tag{3.11}$$

(2) A loop over time is performed and predicted values of u and $\dot{u}$ are defined

$$\begin{aligned}\ddot{u}_{n+1} &= \ddot{u}_n \\ \dot{u}_{n+1} &= \dot{u}_n + dt \cdot \ddot{u}_n \\ u_{n+1} &= u_n + dt \cdot \dot{u}_n + \frac{1}{2} dt^2 \ddot{u}_n\end{aligned} \tag{3.12}$$

where dt is defined as the time increment.

(3) The aforementioned residual r is calculated as

$$r = F_{n+1} - M\ddot{u}_{n+1} - C\dot{u}_{n+1} - F_{int} \tag{3.13}$$

where F_{int} is the global internal force vector and F_{n+1} is a vector containing the global nodal forces.

(4) Modification of the global tangent stiffness matrix and increment correction

$$K^* = K + M\frac{1}{dt\beta^2} + C\frac{\gamma dt}{\beta dt^2}$$
$$\delta u = \frac{K^*}{r} \tag{3.14}$$

The corrected values of $u_{n+1}, \dot{u}_{n+1}$ and $\ddot{u}_{n+1}$ are then defined as

$$u_{n+1} = u_n + \delta u$$
$$\dot{u}_{n+1} = \dot{u}_n + \frac{\gamma dt}{\beta dt^2}\delta u \tag{3.15}$$
$$\ddot{u}_{n+1} = \ddot{u}_{n+1} + \frac{1}{dt\beta^2}\delta u$$

If the norm of the residual $R > tolerance$ a new iteration starts, i.e. it returns to step 3.

(5) The algorithm returns now to step 2 for a new time step or stop.

The nonlinear Newmark algorithm is implemented in the Nonlinear Wave Code in *MainNonlinear.m*. In the following subsection 3.3 the programmed nonlinear Newmark algorithm is validated by means of Ansys Workbench.

3.3 Validation of Nonlinear Newmark Algorithm

The programmed nonlinear Newmark algorithm is validated by the following example, in which a cantilever beam is exposed to a harmonic excitation force at the free end as illustrated in Figure 19.

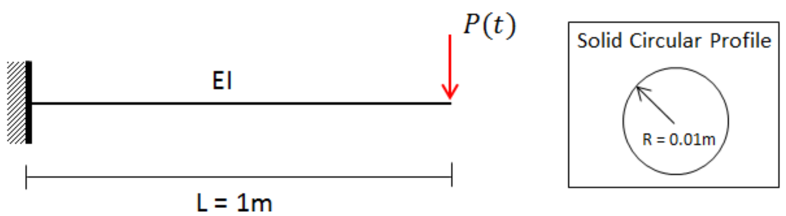

Figure 19: Cantilever beam exposed to a harmonic force at the free end.

The harmonic excitation force is given as $P(t) = P_0 \sin(\omega t)$ in which $P_0 = 1500N$ and $\omega = 2$. The initial configuration and deformed state of the beam is illustrated in Figure 20.

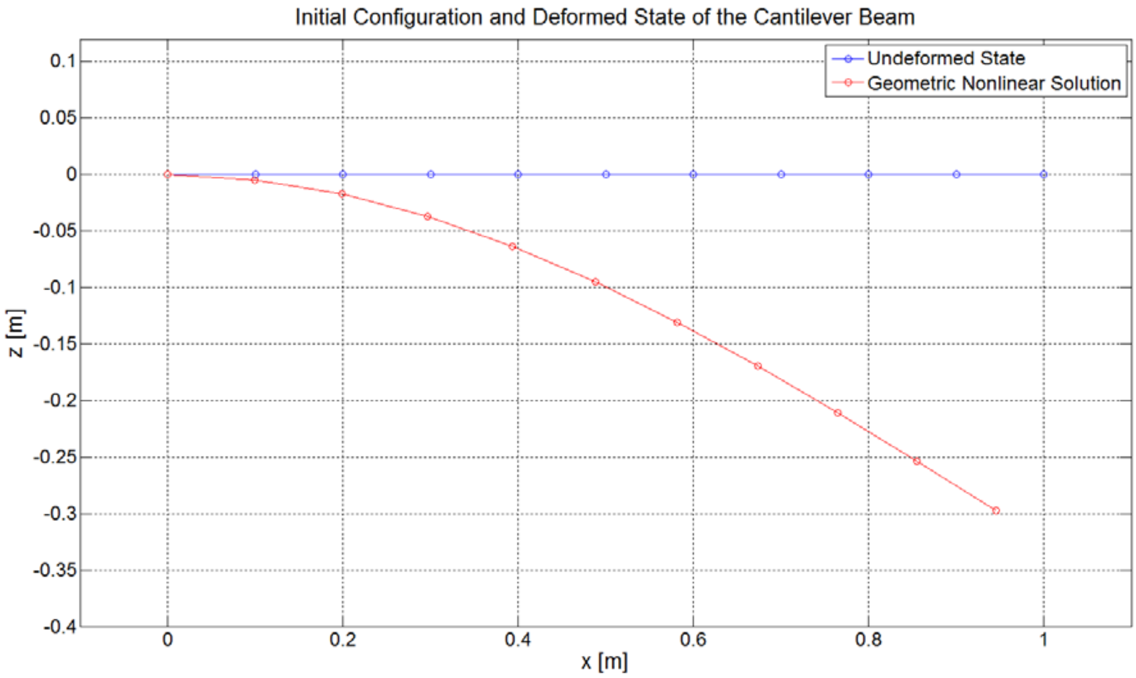

Figure 20: The initial configuration and the maximum deformed state of the cantilever beam.

The dynamic problem is solved by the nonlinear Newmark algorithm and compared with a linear and a nonlinear solution in Ansys Workbench. The plot of the solutions is given in Figure 21.

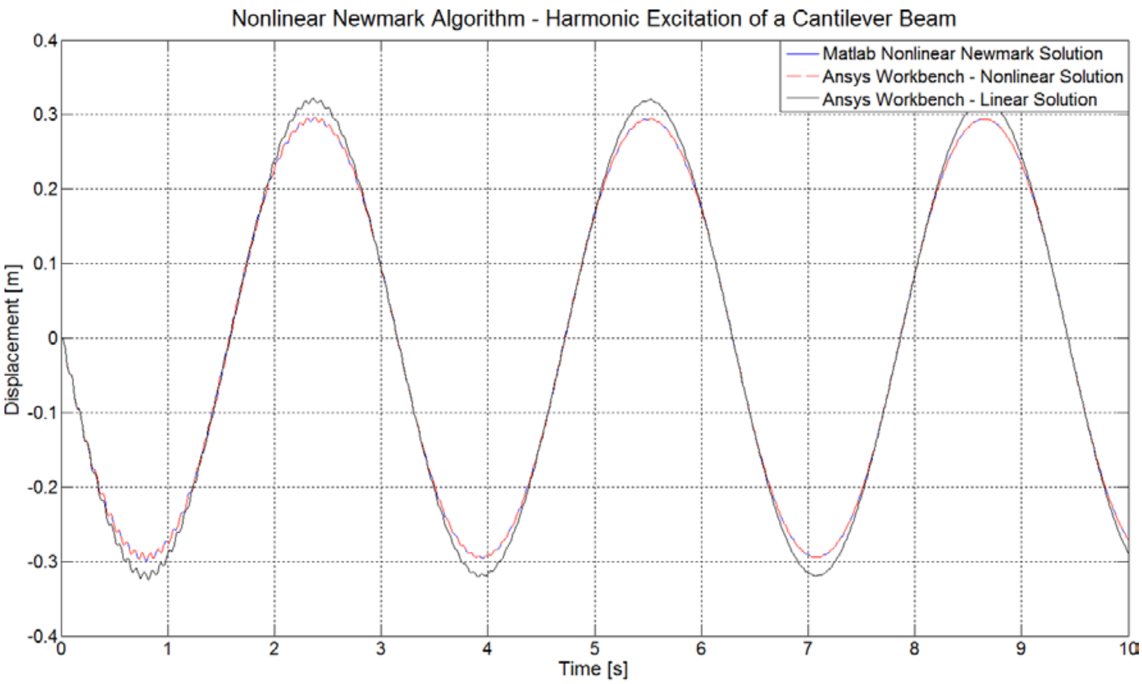

Figure 21: The dynamic response of the three solutions in Matlab and Ansys Workbench.

It is observed from Figure 21 that the nonlinear Newmark solution in the Nonlinear Wave Code agrees with the nonlinear solution in Ansys Workbench by which it can be concluded that the nonlinear Newmark algorithm is validated. The linear solution in Ansys is included to illustrate the difference between the linear and nonlinear solution.

The only sort of damping included in the analysis is a mass-proportional damping. In the following subsection 3.4 numerical damping is introduced and implemented in the Nonlinear Wave Code.

3.4 Algorithmic Damping

By introducing the algorithmic damping also referred to as the numerical damping, the Newmark integration scheme is stabilized by damping out the undesirable high frequency modes, i.e. algorithmic damping controls the numerical noise produced by the higher frequencies of a structure. The contributions of these high frequency modes are usually not accurate by which the numerical damping is preferred.

The algorithmic damping is already an optional option in the Ansys Workbench and has the default value of 0.1 for Transient Structural analysis. The amount of numerical damping α in the Nonlinear Wave Code is controlled by the following Newmark formulations of the γ and β parameters for an unconditional stable Newmark integration

$$\gamma = \frac{1}{2} + \alpha \qquad \beta = \frac{1}{4}(1+\alpha)^2 \tag{3.16}$$

in which the parameter $\alpha \geq 0$ serves to introduce algorithmic damping. It is remarked from Figure 22 that unconditional stability is obtained if $1/2 \leq \gamma \leq 2\beta$.

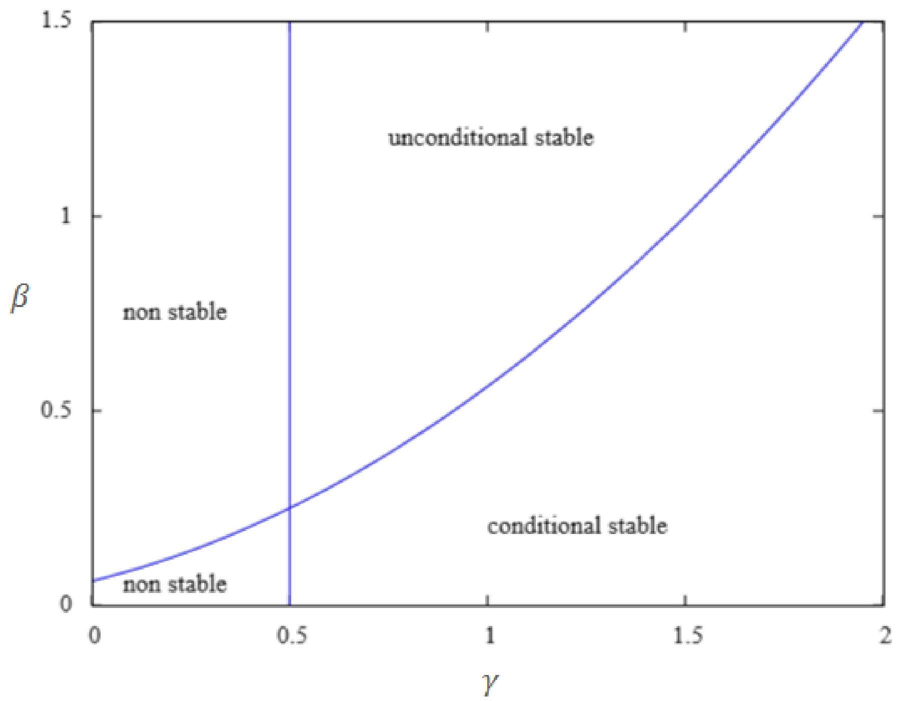

Figure 22: Stability scheme of the Newmark time integration algorithm.

The unconditional stable Newmark scheme is much preferable when the high-frequency vibrations related to the highest modes are of no interest. Stable results are obtained by this scheme but not necessarily accurate results. The algorithmic damping is implemented in the Nonlinear Wave Code file denoted *MainNonlinear.m*.

3.5 Summary of Corotational Beam Formulation

In this chapter a two-dimensional corotational beam formulation is implemented in the Nonlinear Wave Code to account for the geometric nonlinearities in consequence of the large displacements and rotations of the floating space frame structure. The corotational beam algorithm is performed implicit and uses Newton-Raphson iterations at the global level to achieve equilibrium during each incremental load step.

The Nonlinear Wave Code is validated by simple static and dynamic validation examples, in which a bar truss is considered. The static and dynamic nonlinear solutions obtained from the Nonlinear Wave Code are consistent with the nonlinear solutions performed analytically and in Ansys Workbench.

The Newmark algorithm is extended to account for dynamic nonlinear problems, in which iteration is performed at each time step in order to satisfy equilibrium. Furthermore for the preparation of the buoyancy and wave analyses, algorithmic damping is implemented in the Nonlinear Wave Code by which the Newmark integration scheme is stabilized by damping out the undesirable high frequency modes.

In the following Chapter 4 the wave theories and the method of modelling linear and higher order waves is introduced and described.

4 Method for Modelling of Wave Loads

The design of offshore structures is dominated by environmental loads which are caused by environmental phenomena such as wind, waves, current, earthquakes and ice. The most important environmental loading for the design basis of an offshore floating structure is the wave loading. The waves are generated due to the wind acting on the surface of the sea.

As aforementioned the wave kinematics are generated in the programmed Nonlinear Wave Code and subsequently used in the calculation of the hydrodynamic forces. In the following subsections 4.1 and 4.2, the theory behind the wave modelling is introduced, described and applied in simple validation examples of the Nonlinear Wave Code.

4.1 Basic Wave Mechanics

The ocean wave loads occurring on offshore floating structures are caused by the motion of the water due to the wind generated waves. The wind energy is partly transformed into waves by surface shear, and with increasing wave height the waves increases due to the larger roughness. Figure 23 illustrates the general definitions of the water wave mechanic parameters. These parameters are general for all types of water wave theories.

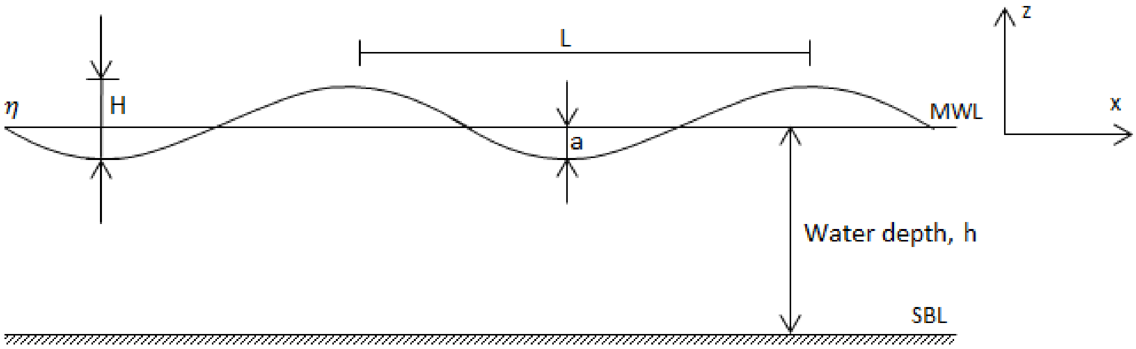

Figure 23: Water wave mechanic parameters. ***h*** is the water depth, *L* is the wave length and ***H*** the is wave height.

Waves are either classified as long-crested waves or short-crested waves. The short-crested are 3-dimensional waves travelling in different directions and have a relative short crest. Long-crested waves are 2-dimensional plane waves that travel in the same direction, perpendicular to the coast. Long-crested waves are a good approximation, although waves in reality are often short-crested and only long-crested near the coast. All waves in the present report are considered long-crested waves.

4.2 Wave Theories

The range of validity of different wave theories is determined by means of three important wave parameters, namely the wave height H, the wave period T and the water depth h. These wave parameters are used to define the non-dimensional wave steepness parameter $S = H/L$ that decides which wave theory to be applied. If $\frac{H}{L} \ll 0$ then the linear wave theory is used, and if $H/L > 0.01$ then higher order theories are applied.

The most common breaking wave/non-linear wave theories are the Stokes 2nd - 5th order or the Stream function theory. The classification of the waves is performed via the Le Mehaute diagram, shown in Figure 24, based on the wave height, water depth and the wave period.

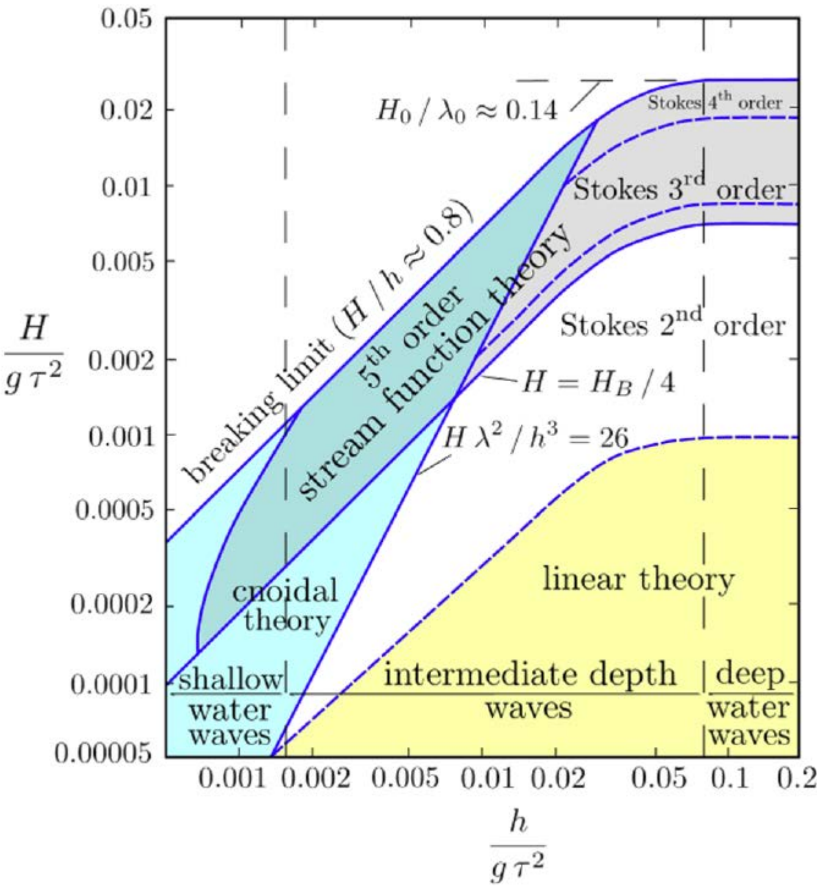

Figure 24: Le Mehaute diagram. ***h*** is the water depth, ***T*** is the period and ***H*** the is wave height. **[5]**

In engineering practice the linear theory is used in many cases, particularly when modelling irregular waves for the fatigue limit state. Regular waves for ultimate limit state design purposes are modelled by higher order theories.

The Linear Wave Theory

The simplest mathematical model of waves is the linear wave theory, referred to as Stokes 1st order wave theory or Airy wave theory. The mathematical solution of the linear wave theory is based on an exact solution of the Laplace equation with linearized boundary conditions. The theory is only valid for non-breaking waves with small amplitudes compared to the wave length and the water depth. The Laplace equation and the linearization of the boundary conditions at the free surface is not described and explained in the present, by which reference is made to [5].

The velocity potential for the linear wave theory is found by

$$\varphi = -\frac{a \cdot g}{\omega} \cdot \frac{\cosh\big(k(z+h)\big)}{\cosh(kh)} \sin(\omega t - kx) \tag{4.1}$$

while the surface elevation is given as

$$\eta = \frac{H}{2}\cos(\omega t - kx) = \mathrm{a}\cos(wt - kx) \tag{4.2}$$

in which the wave number k $[\mathrm{m}^{-1}]$ and the cyclic frequency ω $[\mathrm{rad/s}]$ is found as

$$k = \frac{2\pi}{L}, \qquad \omega = \frac{2\pi}{T} \tag{4.3}$$

H	Wave height [m]
a	Wave amplitude [m]
L	Wave length [m]
T	Wave period [s]
h	Water depth [m]
x	Horizontal coordinate [m]
z	Vertical coordinate [m]

The wave kinematic quantities, the velocity field and acceleration field, respectively are directly computed by differentiation of the velocity potential with respect to the horizontal and vertical direction given as

$$\begin{aligned} u &= \frac{\partial \varphi}{\partial x} = \frac{agk}{\omega} \cdot \frac{\cosh\big(k(z+h)\big)}{\sinh(k \cdot h)} \cdot \cos(\omega t - kx) && \text{for } z = 0 \\ w &= \frac{\partial \varphi}{\partial z} = -\frac{agk}{\omega} \cdot \frac{\sinh\big(k(z+h)\big)}{\sinh(k \cdot h)} \cdot \sin(\omega t - kx) && \text{for } z = 0 \end{aligned} \tag{4.4}$$

The acceleration field for the particles is determined with respect to time as

$$\begin{aligned} \dot{u} &= \frac{\partial u}{\partial t} = -agk \cdot \frac{\cosh\big(k(z+h)\big)}{\cosh(k \cdot h)} \cdot \sin(\omega t - kx) && \text{for } z = 0 \\ \dot{w} &= \frac{\partial w}{\partial t} = -agk \cdot \frac{\sinh\big(k(z+h)\big)}{\cosh(k \cdot h)} \cdot \cos(\omega t - kx) && \text{for } z = 0 \end{aligned} \tag{4.5}$$

In addition to the above-mentioned kinematic quantities, the wave length is found by iteration, as it cannot be computed explicitly. This is performed by means of the dispersion relation, which gives the relationship between wave period and wave length.

The dispersion relation is for linear waves in finite water depth given by

$$L = \frac{g \cdot T^2}{2 \cdot \pi} \cdot \tanh\left(\frac{2 \cdot \pi \cdot h}{L}\right) \tag{4.6}$$

The iterative procedure for the purpose of determining the wave length parameter is performed in the Nonlinear Wave Code in the script *WaveLength.m*, while the particle velocities and accelerations are generated in the file *ParticleVelandAccAiry.m* when the theory used is the linear wave theory.

A simple validation of the implementation of the surface elevation for the linear wave theory is given in Figure 25. The wave specifications are arbitrarily set to $H = 1m$, $T = 15s$ and $h = 40m$ in both the Nonlinear Wave Code and in the commercial wave program *WaveLab*.

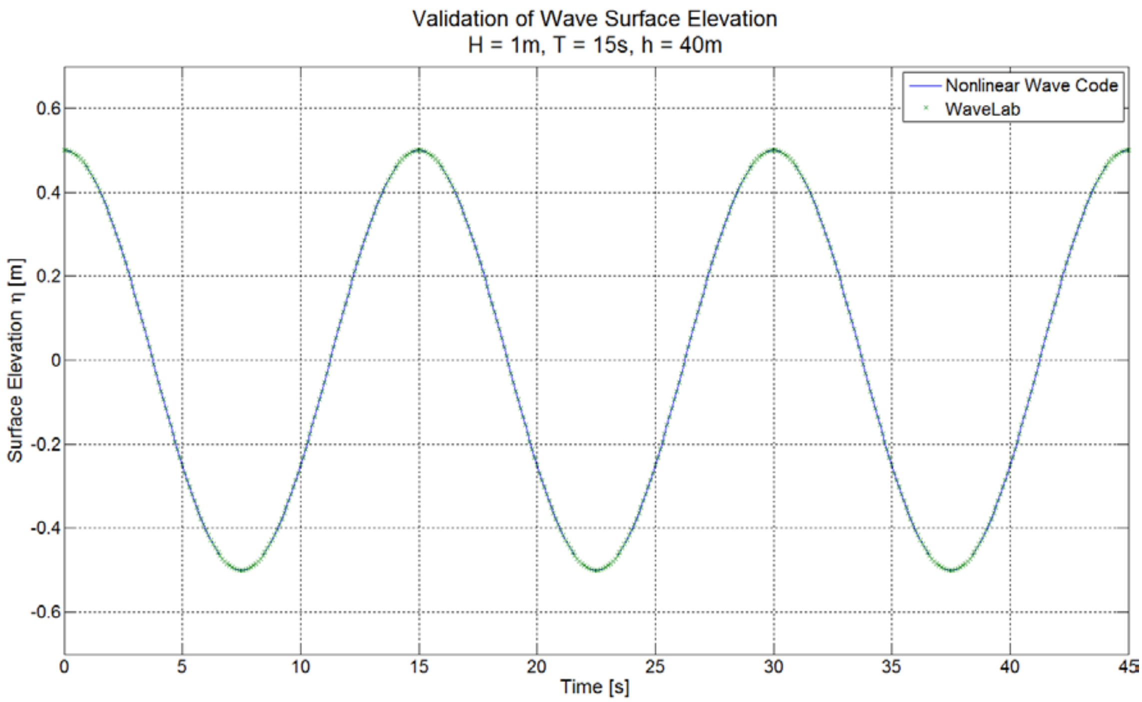

Figure 25: Comparison of wave surface elevation modelled in the Nonlinear Wave Code and WaveLab, respectively.

As illustrated in Figure 25, the surface elevation modelled by the Nonlinear Wave Code and *WaveLab* agrees.

In subsection 4.3 the application of the linear waves for the modelling of irregular waves is introduced and described, while the following subsection contains a description of the Stokes 5th order wave theory.

Higher Order Theory

Waves with large steepness imply that application of the Stokes 1st Order Wave theory is inaccurate as shown on Figure 26. It is remarked that both the wave crest and wave trough of the higher order wave modelled by Stokes 5th order theory are lifted compared to the linear wave.

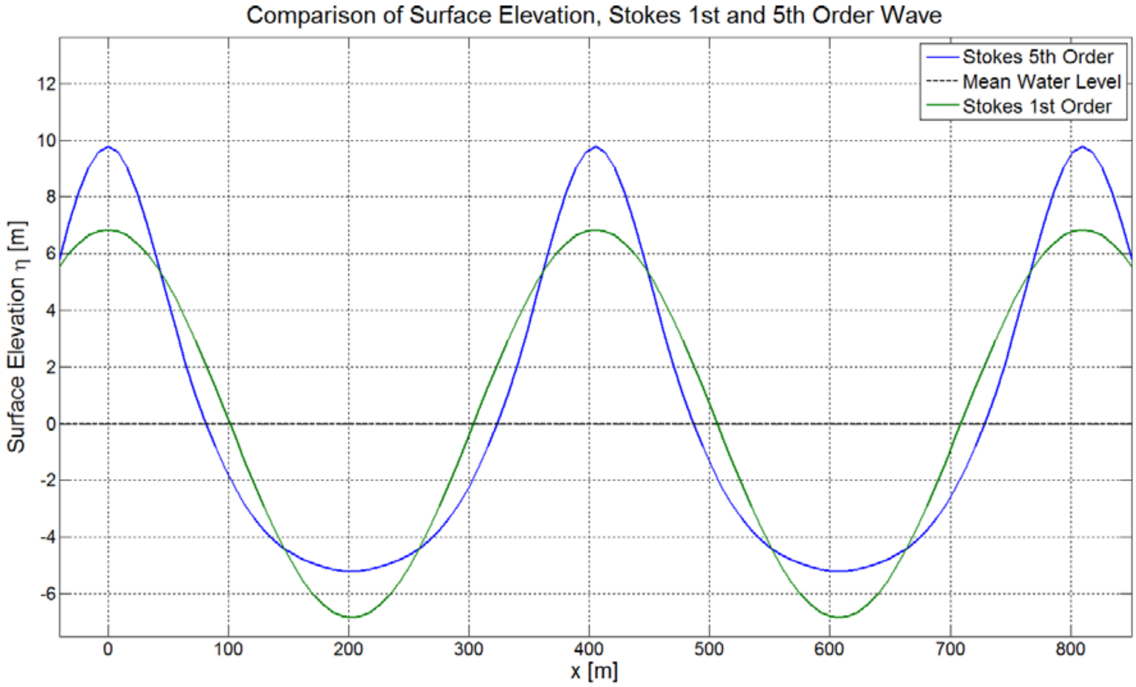

Figure 26: Wave comparison between Stokes 1st and 5th order wave.

The higher order wave crest is thus shorter and steeper than the linear wave crest, while the wave trough is longer and less steep. The ultimate limit state ULS waves can thus not be described validly by use of a linear wave theory, and it is instead necessary to implement the higher order wave theory, Stokes 5th order.

Using Stokes Theory, it is assumed that all variables can be expressed as a series expansion, in which the velocity potential and water surface elevation is given as

$$\begin{aligned} \varphi &= \varphi^1 + \varphi^2 + \ \dots\ \varphi^i + \ \dots \\ \eta &= \eta^1 + \eta^2 + \ \dots\ \eta^i + \ \dots \end{aligned} \tag{4.7}$$

in which i is Stokes order of theory. The Stokes 5th order is as aforementioned valid for waves with steepness $H/L > 0.01$, and likewise the linear wave theory, it is based on the Laplace equation. It is in the project assumed that the waves are periodic and long-crested, that there is no flow through the bottom of the sea and that the pressure is constant at the surface. The wave length L and the coefficient λ is determined by iteration of

$$\begin{aligned} L &= \frac{gT^2}{2\pi}\tanh(kh)\cdot(1+\lambda^2 C_1 + \lambda^2 C_2) \\ \pi H &= L\left(\lambda + \lambda^3 B_{33} + \lambda^5 (B_{35} + B_{55})\right) \end{aligned} \tag{4.8}$$

in which C_i and B_{ij} are variables dependent on the wave number $k = 2\pi/L$ and water depth. After the computation of the wave length and the λ coefficient, the velocity potential is found from

$$\varphi = -\frac{c}{k}\sum_{j=1}^{5} Dj \cdot \cosh(jk(z+h)) \cdot \sin j\theta \tag{4.9}$$

$c = \frac{L}{T}$	Phase velocity of wave [m/s]
θ	Phase angle of wave
z	Vertical coordinate [m]
D_j	Variables dependent on λ and A_{lm}, known function of kh

The velocity field can now be calculated by means of differentiation of the above-given velocity potential with respect to direction as

$$u = \frac{\partial \varphi}{\partial x} \qquad w = \frac{\partial \varphi}{\partial z} \tag{4.10}$$

The acceleration field is found by differentiation of the velocity field with respect to time

$$\begin{aligned}
\frac{du}{dt} &= \frac{\partial u}{\partial t} + u\frac{\partial u}{\partial x} + w\frac{\partial u}{\partial z} \\
\frac{\partial u}{\partial t} &= -c\omega \sum_{j=1}^{5} j^2 \cdot D_j \cosh jk(z+h) \cdot sin\, j\theta \\
\frac{\partial u}{\partial x} &= ck \sum_{j=1}^{5} j^2 \cdot D_j \cosh jk(z+h) \cdot sin\, j\theta \\
\frac{\partial u}{\partial z} &= ck \sum_{j=1}^{5} j^2 \cdot D_j \sinh jk(z+h) \cdot cos\, j\theta
\end{aligned} \tag{4.11}$$

Finally the water surface elevation η from mean water level MWL can be calculated by the following equation

$$\eta = \frac{1}{k}\sum_{j=1}^{5} E_j \cos j\theta \tag{4.12}$$

in which E_j are variables dependent on B_{ij} and λ. The above-mentioned Stokes 5th Order Wave theory is implemented in the Nonlinear Wave Code. In the present subsection the method for modelling of wave loads and determination of the hydrodynamic forces is given.

4.3 Modelling of Waves

The method of modeling the stochastic irregular FLS waves and the higher order ULS waves are described in the following subsections. The modelling of the waves is usually performed by means of either measured wave data from the location of the structure or on the basis of wind data, by which the waves are assumed to be wind generated. As a consequence of the objective of this project, no wave data are available and the wave specifications for the higher order and irregular waves are thus chosen arbitrarily.

Modelling of Higher Order Waves

The higher order waves are modelled for the purpose of the ultimate limit state analysis, ULS. A limit state is when the loads lead to an unfavourable situation e.g. a structural failure. The ULS is based on plausible combinations from the relevant DNV standard, and defines the maximum load bearing resistance, in which yielding of the materials and failure can occur. According to the DNV standard the characteristic load effect of the dominant environmental load must at least be based on a 50 years return period. [6] The deterministic ULS waves specification are as aforementioned obtained from measurements performed in the location of the structure, however in this project the specifications of the higher order waves are chosen arbitrarily based on the Le Mehaute diagram given in Figure 24.

Modelling of Irregular Waves

A real sea state is best described by a random wave model, as ocean waves are irregular in shape, length, phase and height. If recorded time series of the surface elevation of irregular waves are available, a time-domain or frequency-domain analysis is used to study the irregular waves. In the frequency-domain analysis, the irregular waves are modelled by superposition of *n* linear wave components, i.e.

$$\eta(t) = \sum_{i=1}^{N} \eta_i(t) = \sum_{i=1}^{N} a_i \cos(\omega_i t - k_i x + \delta_i) \tag{4.13}$$

in which δ_i is the phase angle of the i^{th} linear wave. The phase angles are assigned random numbers between 0 and 2π which makes the irregular waves certainly stochastic. The irregular waves are then generated by transforming data from the time-domain to the frequency-domain by describing the irregular sea state by means of a wave frequency spectrum, which is defined in terms of a significant wave height, the peak period and the wave direction. Two different wave spectrums are normally used, the Pierson-Moskowitz (PM) spectrum $S_{PM}(\omega)$ or the Joint North Sea Wave Observation Project, JONSWAP spectrum $S_J(\omega)$. The PM spectrum is only valid for a fully arisen sea while the JONSWAP spectrum is formulated as a modification of the PM spectrum for a developing sea state in a fetch limited situation, and is thus valid for non-fully arisen seas.

The JONSWAP spectrum, which is used in this project, is formulated as

$$S_f = \alpha \cdot H_s^2 \cdot f_p^4 \cdot f^{-5} \cdot e^{-\frac{5}{4}\left(\frac{f_p}{f}\right)^4} \cdot \gamma^\beta \tag{4.14}$$

In which S_f is the spectral density, f_p is the peak frequency calculated by taking the inverse of the peak periods

$$f_p = \frac{1}{T_p} \tag{4.15}$$

f is the frequency and γ is a peak factor between $1-7$. The parameters α and β are given by

$$\alpha = \frac{0.0624}{0.230 + 0.0336 \cdot \gamma - \left(\frac{0.185}{1.9+\gamma}\right)}$$
$$\beta = e^{-\frac{(f-f_p)^2}{2 \cdot \sigma^2 \cdot f_p^2}} \quad \text{where} \quad \sigma = \begin{Bmatrix} \sigma_a = 0.07 \;\; for\ f \le f_p \\ \sigma_b = 0.09\ for\ f > f_p \end{Bmatrix} \tag{4.16}$$

The averages values for the JONSWAP experiment data are $\gamma = 3.3$, $\sigma_a = 0.07$ and $\sigma_b = 0.09$. Setting $\gamma = 1$ reduces the JONSWAP spectrum to the PM spectrum. The effect of the peak shape parameter γ for JONSWAP spectrum for $H_s = 4m, T_p = 8s$ for $\gamma = 1, \gamma = 2$ and $\gamma = 5$ is illustrated in Figure 27.

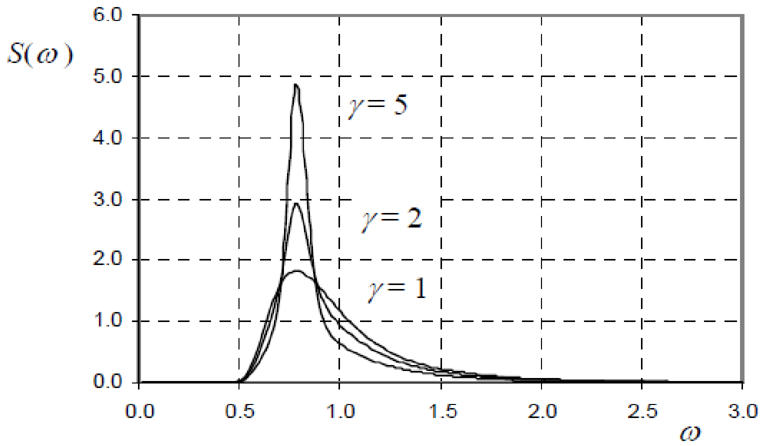

Figure 27: JONSWAP spectrum for Hs = 4m and Tp = 8s.

The influence of the peak shape parameter is shown in Figure 27, as it is observed that the size and sharpness of the spectrum is controlled by this parameter.

As aforementioned the average value of the parameter is $\gamma = 3.3$, however to obtain the exact value of the parameter, the following expression is used

$$\begin{aligned} &\gamma = 5 \; for \; \frac{T_p}{\sqrt{H_s}} \leq 3.6 \\ &\gamma = exp\left(5.75 - 1.15\frac{T_p}{\sqrt{H_s}}\right) \; for \; 3.6 < \frac{T_p}{\sqrt{H_s}} < 5 \\ &\gamma = 1 \; for \; 5 \leq \frac{T_p}{\sqrt{H_s}} \end{aligned} \tag{4.17}$$

where T_p is in seconds and the significant wave height H_s in meters. An example of a JONSWAP spectrum is shown in Figure 28, where the wave specifications arbitrarily are chosen to $H_s = 3m$ and $T_p = 10s$.

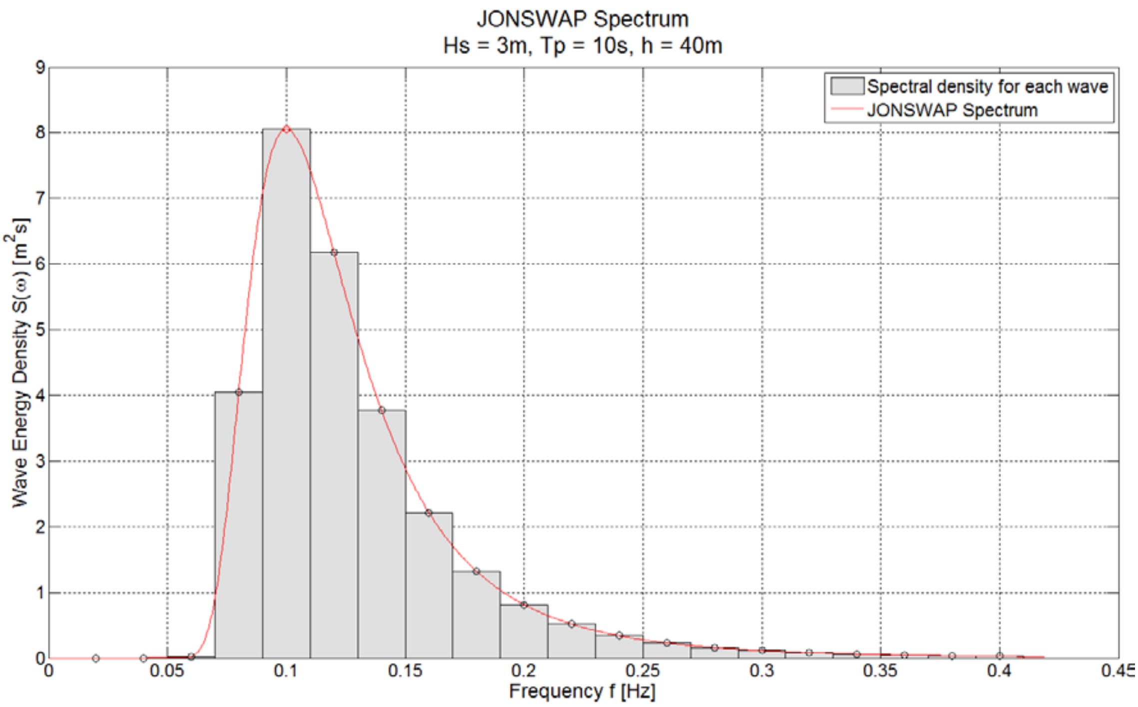

Figure 28: JONSWAP Spectrum for Hs = 3m, Tp = 10s and ocean depth h = 40m.

The JONSWAP spectrum is divided into 20 linear spaced frequency bins as illustrated in Figure 28. For each of these frequencies a regular wave is determined by taking the area beneath the frequency. The wave height is determined from

$$H_i = 2 \cdot \sqrt{2 \cdot S(f_i) \cdot \Delta f} \tag{4.18}$$

in which $S(f_i)$, is the spectral density for the frequency i and Δf is the width of frequency bin. The 20 linear waves with random phases are shown in Figure 29.

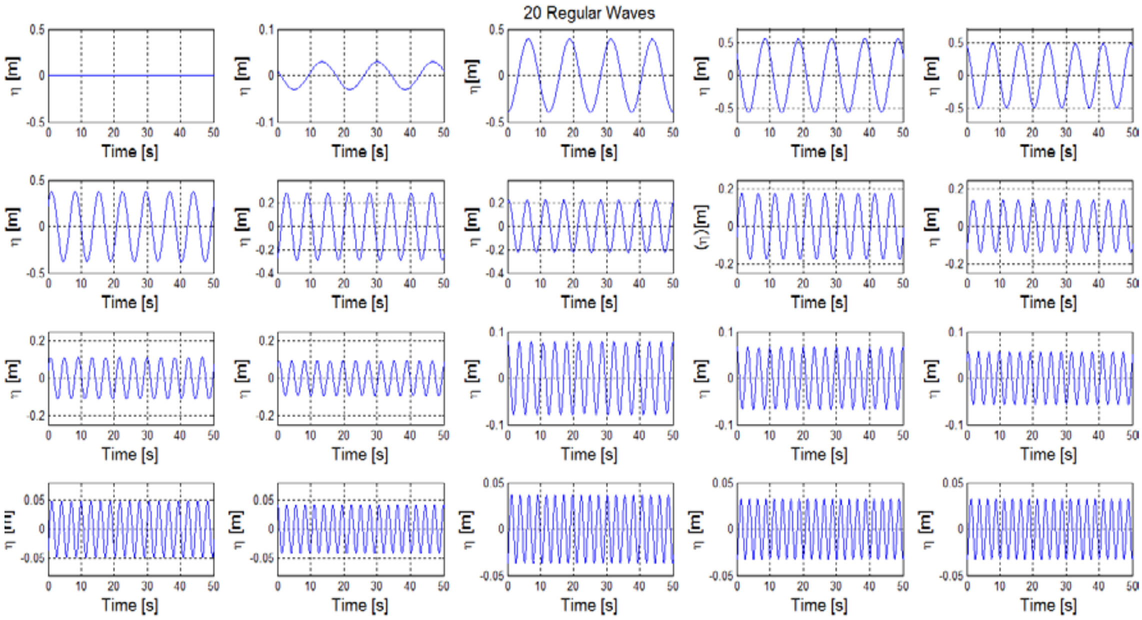

Figure 29: 20 regular waves generated from a JONSWAP spectrum.

Summation of all 20 regular waves by means of aforementioned formulation (4.13) leads to the irregular waves given in Figure 30.

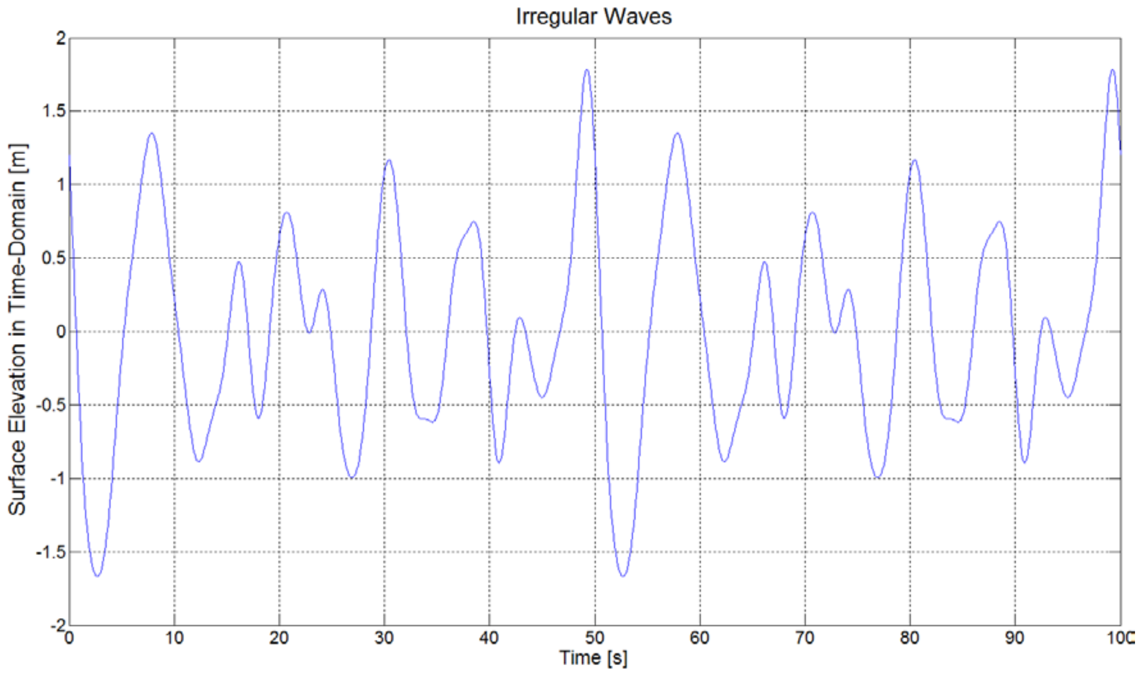

Figure 30: Irregular wave composed of 20 regular waves.

The duration and length of the irregular wave depends on the number of superimposed linear wave components. The generation of the irregular waves is programmed in the Nonlinear Wave Code by the script denoted *JonswapFLS.m*.

The Wheeler Stretching is often used when generating irregular waves, as it provides a more accurate approximation of the wave kinematics above mean water level. The Wheeler Stretching is introduced in the following subsection.

Wheeler Stretching

The linear wave theory is limited to small waves and does thus not yield valid wave kinematics for points above the mean water level as they are not in the fluid. This means that the theory does not yield valid description of the wave kinematics and needs thus to be stretched to include predictions of the fluid velocity and acceleration at points above the mean water level. The method of stretching applied is the so-called Wheeler Stretching which is implemented by substituting the vertical coordinates z with the stretched coordinate z' given as

$$z' = \frac{z - \eta}{1 + \frac{\eta}{h}} \quad for \quad -h \leq z' \leq \eta \tag{4.19}$$

where η is the surface elevation and h is the ocean depth. The wheeler stretching is valid for linear waves and irregular waves which are superposed by a number of linear waves as introduced in the previous subsection 4.3. As illustrated in Figure 31, the Wheeler Stretching modification stretches or compresses the velocity profile linearly into a height equivalent to the mean water depth.

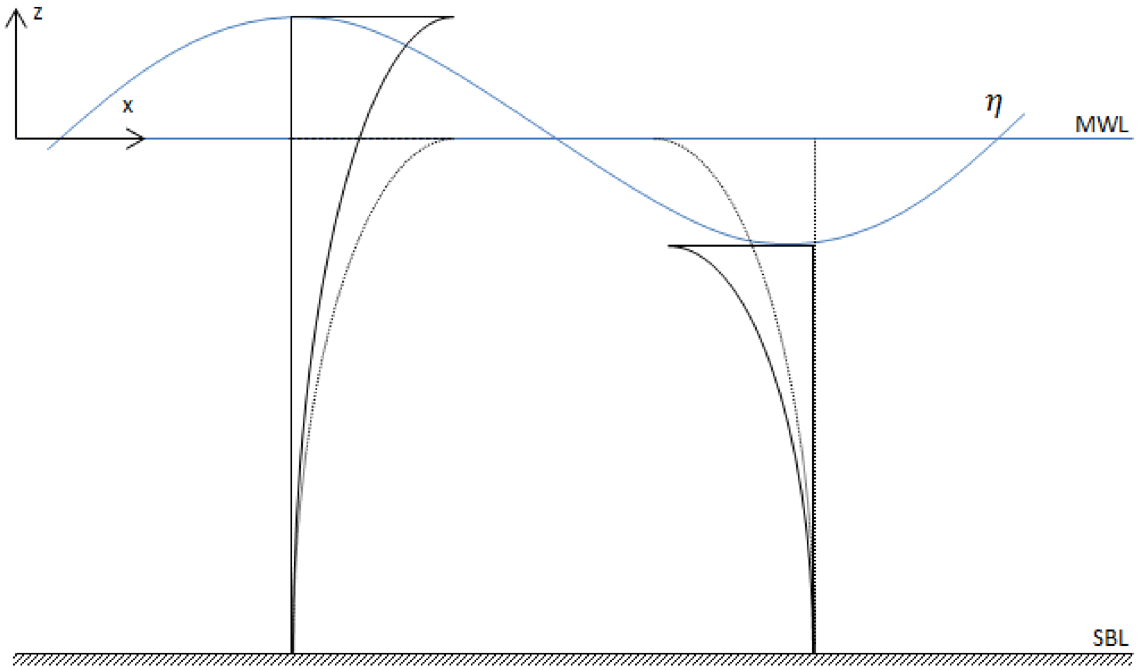

Figure 31: Wheeler stretching modification.

A comparison between the horizontal velocity of a linear wave and the horizontal velocity of a Wheeler stretched linear wave is given in Figure 31. The wave specifications are set to $H = 2$, $T = 8s$ and $h = 40m$.

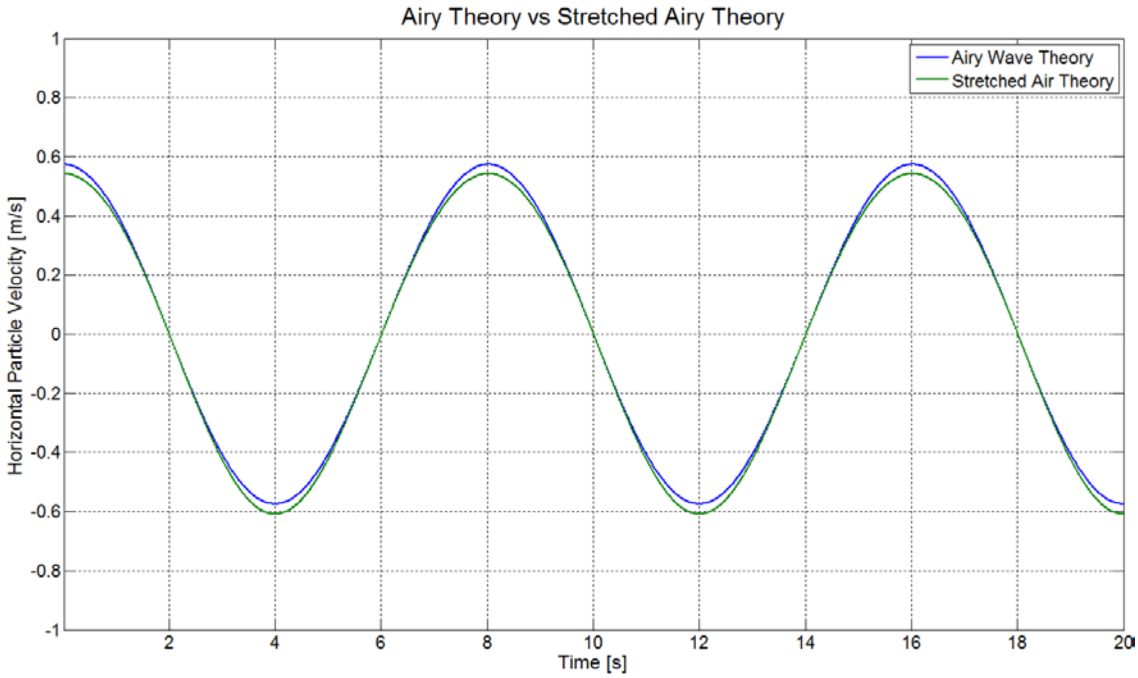

Figure 32: Comparison of the horizontal velocity for an Airy wave and a stretched Airy wave.

It is remarked that the Wheeler Stretching leads to larger kinematics quantities at the wave trough as the velocity profile is compressed, while the kinematic quantities are decreased at the wave crest as the velocity profile is stretched. The Wheeler Stretching is implemented in the Nonlinear Wave Code and can be applied instead of the linear wave theory as requested.

In the following subsection 4.4 the method of calculating the hydrodynamic forces by evaluating Morison's formula and the hydrodynamic coefficients is given.

4.4 Method of Hydrodynamic Forces

The determined kinematic quantities from the linear wave theory and Stokes 5th order wave theory respectively, are applied in the calculations of the hydrodynamic forces. In the present section the hydrodynamic forces due to incoming waves are implemented, in which a cylinder modelled by cylindrical beam elements is considered. An example of an incoming wave on a cylinder is illustrated in Figure 33.

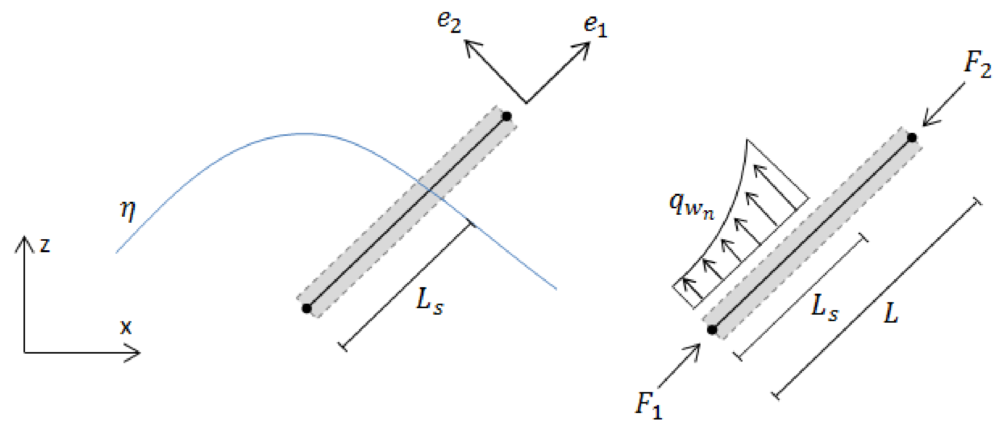

Figure 33: Distributed wave loading due to submerged cylinder.

Morison's load formula is only valid for non-breaking waves; however the formula is valid for breaking water if the structure members are fully covered by water. In deep water, waves break when $H/L > 0.14$ and in shallow the waves break as H/L exceeds 0.78. For non-breaking waves and slender structures, the general Morison's differential formulation is applicable and formulated as

$$dF = dF_{inertia} + dF_{drag} \tag{4.20}$$

consisting of a sum of an inertia force and a drag force in which the inertia force is proportional to the particle acceleration and the drag force is proportional to the square particle velocity. The Morison differential equation is only valid if the following ratio between the wave length L and the tube diameter D is obeyed

$$L > 5D \tag{4.21}$$

By satisfying the ratio, the use of the diffraction theory is ignored when computing the kinematic quantities as the diffraction is insignificant for slender members. This is the case in the present project and the application of the Morison's formulation to determine the hydrodynamic forces is valid. Considering restrained vertical members the Morison's formulation is defined as

$$dF = dF_{inertia} + dF_{drag} = (1 + C_A)\rho\frac{\pi D^2}{4}\dot{u} + \frac{1}{2}C_D\rho D u|u| \tag{4.22}$$

in which C_D and $(1 + C_A) = C_M$ is the dimensionless drag and inertia coefficients, respectively, D is the diameter of the member, ρ is the density of ocean water.

The above given Morison's load formula is as aforementioned valid for restrained structures in waves. Considering moving structures in waves, which is the case in this project, the Morison's equation is reformulated to account for the relative velocities and accelerations.

Considering Figure 33, the distributed wave force q_{w_n} is perpendicular to the beam axis and dependent on the orientation of the beam, the contribution to the wave force is divided into local components $q_w = \left[q_{w_t}\, ,\, q_{w_{n_z}}\right]$. The distributed wave loading is calculated by means of the relative Morison formulation given as

$$q_{w_{n_i}} = C_M \rho_w A_{s_i} \dot{u}_{Fn_i} - \rho_w C_A A_{s_i} \dot{u}_{Sn_i} + \frac{1}{2} \rho_w C_{D_n} H_{s_i} r_{n_i} |r_{n_i}| \tag{4.23}$$

where A_{s_i} is the submerged cross-sectional area, $\dot{u}_{Fn}$ is the fluid particle acceleration normal to the beam axis, $\dot{u}_{Sn}$ is the structural acceleration normal to thee beam axis, C_A is the added mass coefficient, r_n is the relative fluid-structure acceleration and r_n is the relative fluid-structure velocity. Additional hydrodynamic damping is not necessary to be included when using the relative Morison formula for the drag forces. The structure is damped due to the added mass coefficient C_A, which is described in the following subsection. The relative fluid-structure kinematics are defined and calculated as

$$\begin{aligned} r_n &= u_i - x_i \\ r_i &= \dot{u}_i - \dot{x}_i \end{aligned} \tag{4.24}$$

in which x_i and $\dot{x}_i$ are the velocities and accelerations, respectively. These are interpolated from the nodal velocities $\mathbf{x}$ and nodal accelerations $\dot{\mathbf{x}}$ by means of

$$x_i = \mathrm{N}^{\mathrm{T}}(x_i)\mathbf{x} \qquad \dot{x}_i = \mathrm{N}^{\mathrm{T}}(x_i)\dot{\mathbf{x}} \tag{4.25}$$

The wave load q_{w_t} is defined as the distributed wave loading tangential to the beam axis and is mainly due to skin friction. The tangential drag force is small compared to the normal drag force but with important impact for long slender elements. The contribution from the distributed wave loading tangential to the beam axis q_{w_t} is found by

$$q_{w_{t_i}} = \frac{1}{2} \rho_w C_{D_t} H_{s_i} r_{t_i} |r_{t_i}| \tag{4.26}$$

in which C_{D_t} is the tangential drag coefficient and r_t is the relative fluid-structure velocity tangential to the beam axis. The local distributed wave loads q_w are transformed into global nodal forces F_w by the method described in Chapter 5. The relative Morison formulation is implemented in the Nonlinear Wave Code script denoted *WaveForce.m*. The hydrodynamic coefficients of the structure are presented and described in the following subsection.

Hydrodynamic Coefficients

Before any dynamic analysis of the floating space frame structure is performed, it is necessary to determine the hydrodynamic coefficients as they are decisive for the motion of the structure. The total dynamic behavior of a floating body is described by the sum of two dynamic cases, namely the behavior of the body oscillating in still water and the behavior of a restrained body exposed to ocean waves as shown in Figure 34.

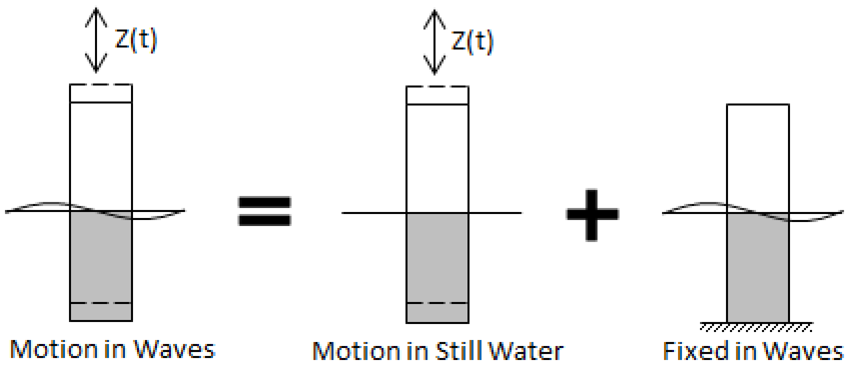

Figure 34: Illustration of the dynamic behaviour of a floating body in ocean waves.

The hydrodynamic coefficients that are to be included are the added mass and the drag and inertia coefficients. The importance and influence of the coefficients in the further analyses are described in the following subsection.

Added Mass

An additional force resulting from the fluid acting on a body under water has to be included in the analysis of a body's motion in waves. As a body moves in fluid, an amount of fluid moves with it, i.e. when the body accelerates the fluid does too. More force is required to accelerate the body in fluid than in vacuum. The additional force is given by the added mass and is for a cylinder calculated by the following formulation

$$m_a = \rho \pi r^2 L \tag{4.27}$$

where ρ is the fluid density, r is the radius of the cylinder and L is the length. The non-dimensional added mass coefficient C_A is found by

$$C_A = \frac{m_a}{\rho A_s} \tag{4.28}$$

in which A is the amount of submerged cross-sectional area. A good approximation of the amount of added mass is given by equation (4.28) as the Nonlinear Wave Code knows the approximate amount of submerged cross-sectional area in every time step. The calculation of the added mass coefficient is implemented in the script *WaveForce.m*.

Drag and Inertia Coefficients

Offshore floating structures are divided into structures which are either drag or inertia-dominated. A structure with large cross-sections is inertia-dominated due to wave diffraction and the global forces are thus significantly larger than the drag induced global loads as described in the introduction of the project. The drag coefficient C_D is most accurately derived by experimental test in which a restrained cylinder is subjected to waves.

The drag- and inertia coefficients are functions of Reynolds number R_e, the Keulegan-Carpenter number K_C and the non-dimensional roughness Δ. These parameters are defined as following.

$$R_e = \frac{uD}{v} \qquad K_C = \frac{u_m T}{D} \qquad \Delta = \frac{k}{D} \tag{4.29}$$

Where:

D	Diameter [m]
T	Wave period [s]
k	Roughness height [m]
u	Total flow velocity [m/s]
v	Fluid kinematic viscosity [m^2/s]
u_m	Maximum orbital particle velocity [m/s]

The inertia coefficient is defined by the following expression

$$C_M = \begin{Bmatrix} 2.0 & for\ KC < 3 \\ \max[2.0 - 0.044(KC-3)\ ;\ 1.6 - (C_{DS} - 0.65)] & for\ KC > 3 \end{Bmatrix} \tag{4.30}$$

while the drag coefficient is found by

$$C_D = C_{DS} \cdot \psi(C_{DS}, K_C) \tag{4.31}$$

where C_{DS} is the drag coefficient for steady-state given by equation (4.32) and ψ is the wake amplification factor given by Figure 35. The drag coefficient for steady state is given by

$$C_{DS} = \begin{Bmatrix} 0.65 & for\ \ k/D < 10^{-4}\ (Smooth) \\ \dfrac{29 + 4 \cdot \log(k/D)}{20} & for\ \ 10^{-4} < k/D < 10^{-2} \\ 1.05 & for\ k/D > 10^{-2}\ (Rough) \end{Bmatrix} \tag{4.32}$$

In which k is the surface roughness, which for painted and uncoated steel is smooth, and if the structure is covered by marine growth then k is chosen to be $0.005 - 0.05\ m$. It is assumed that the floating space frame structure is made of painted steel by which the wake amplification factor ψ is found by Figure 35.

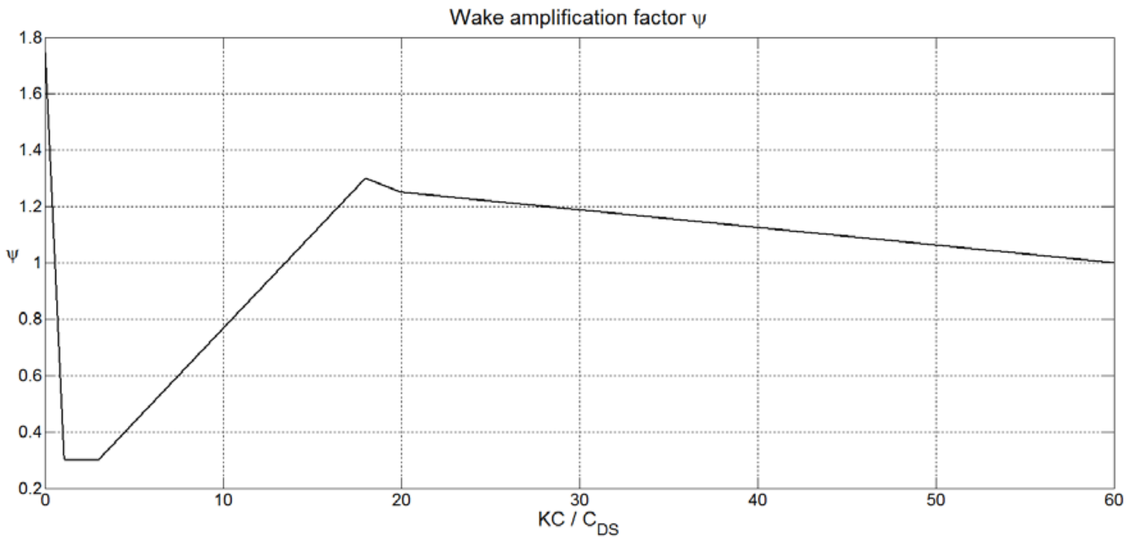

Figure 35: The diagram for determination of the wake amplification factor.

The calculation of the drag coefficient is automated in the Nonlinear Wave Code file *WaveForce.m* while the user has the option to specify the values as requested. The drag and inertia coefficients are obtained at each node and extraction point throughout every time step.

However, as aforementioned the drag and inertia coefficients are best represented by experimental studies. It is thus chosen to use constant drag and inertia coefficients in the project for the sake of simplification. Considering the slender structures used in the project and the recommendation of the DNV, the drag coefficient is set to $C_D = 0.5$ and $C_M = 2$ in all calculations performed in the project.

In the following subsection the influence of the drag and inertia coefficients on large and small volume structures is described.

The Influence of the Drag and Inertia Coefficients

The influence of the drag and inertia-coefficients on large and slender cylinders is studied in the following by analyzing two wave cases on a restrained cylinder. The influence of the coefficients is firstly tested on a restrained cylinder with a large cross-sectional diameter of $5m$ as illustrated in Figure 36. The wave specifications are set to $H = 1m$, $T = 15s$ and $h = 40m$.

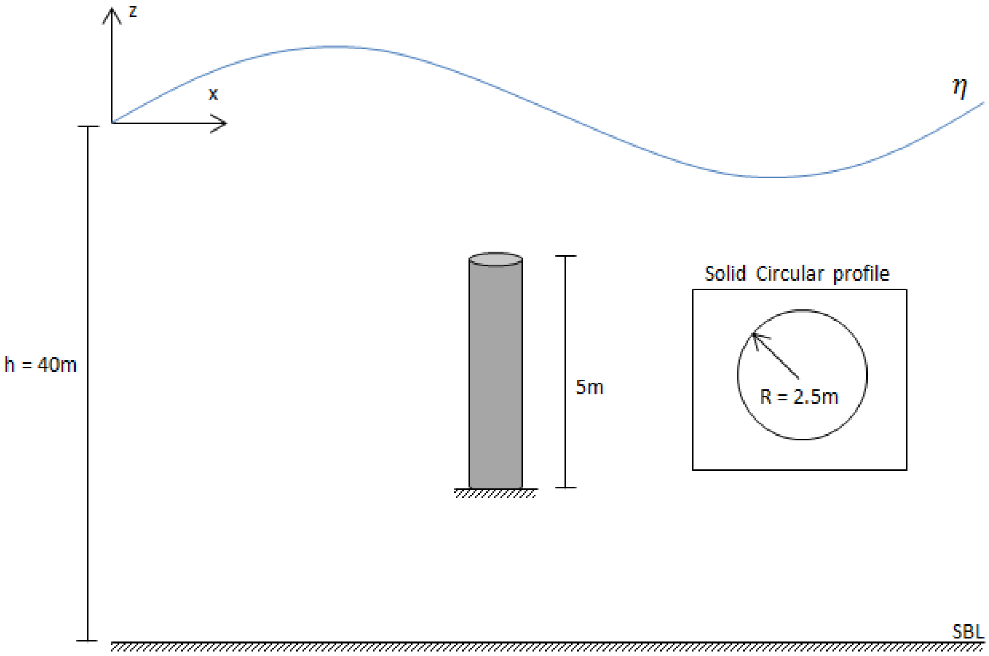

Figure 36: Restrained cylinder of L = 5m and r = 2.5m.

Considering the large diameter of the fixed cylinder, the drag and inertia coefficients are set to $C_D = 1.2$ and $C_M = 2$, respectively. The drag and inertia forces and the total Morison force is executed and plotted in Figure 37.

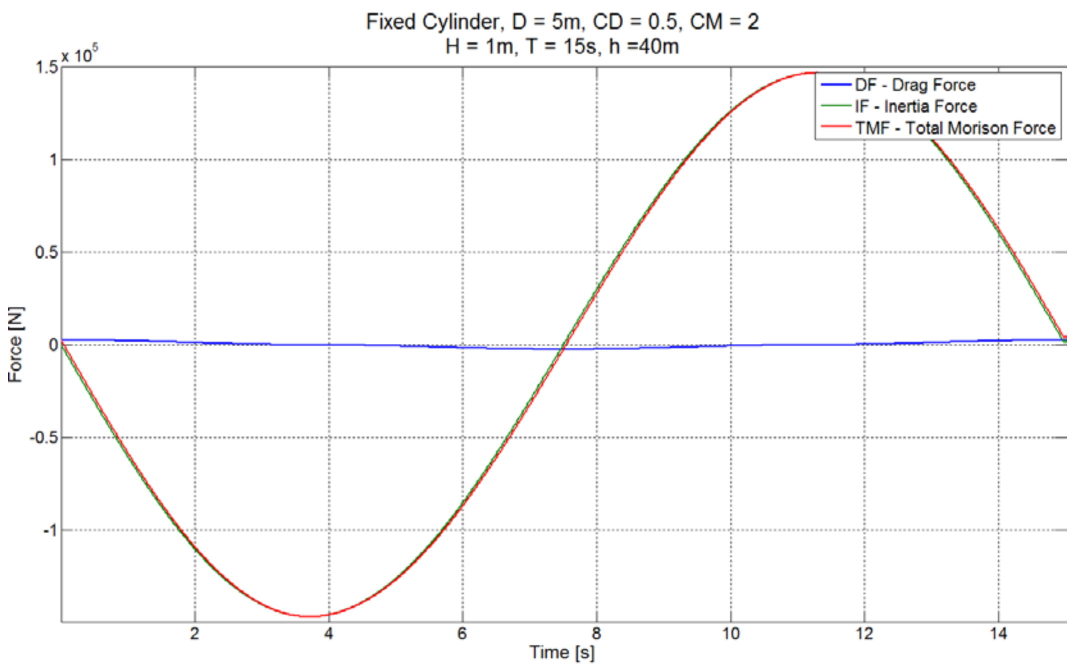

Figure 37: The influence of the drag- and inertia coefficients on a restrained cylinder with large cross-section.

It is remarked from Figure 37 that the structure is clearly inertia-dominated due to the large volume structure. The influence of the drag force on the structure is as observed almost of no importance compared with the inertia force. By replacing the large volume structure with a small volume structure of $D = 0.01m$ with drag and inertia coefficients of $C_D = 0.5$ and $C_M = 2$ respectively, the force results are illustrated in Figure 38.

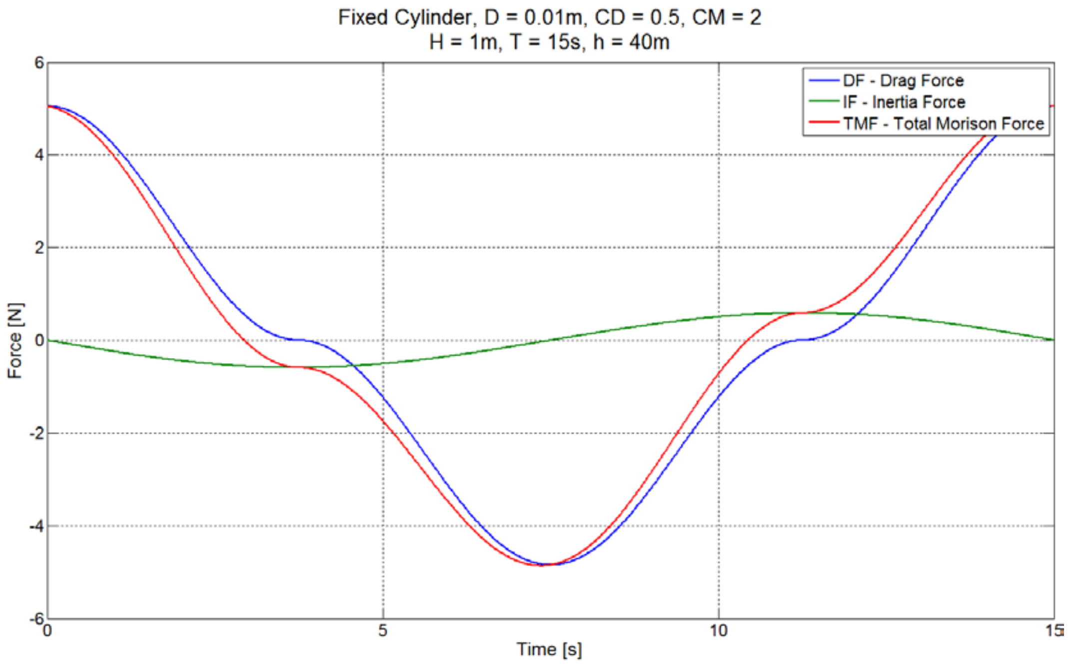

Figure 38: The influence of the drag- and inertia coefficients on a restrained cylinder with small cross-section.

The force results obtained in Figure 38 confirms as aforementioned that the structure is drag-dominated when the structure consists of slender members. As this project considers slender cylinders, it is further confirmed that the drag-coefficient has the most significant influence on the hydrodynamic forces exposed to the structure.

4.5 Summary of Wave Modelling Methods

The basic wave mechanics, linear waves and higher order waves are in this chapter described and implemented in the Nonlinear Wave Code. More specific the wave kinematics is in this chapter generated in the programmed Nonlinear Wave Code and subsequently used in the calculation of the hydrodynamic forces. As the objective of the project is to predict the dynamic response of the floating space frame structure, the hydrodynamic forces are represented by the relative Morison formula which is expressed in terms of the relative fluid-structure velocities and accelerations.

The drag and inertia coefficients are best represented by experimental studies. The drag and inertia are however in this project assumed to be constant, and are thus by the recommendation of the DNV set to $C_D = 0.5$ and $C_M = 2$ in all wave analyses performed in the project.

The wave modelling in Ansys Workbench is introduced and described in Appendix A.

5 Modelling of Wave Loads

The impact of the wave loads on the floating space frame structure is obtained from the kinematic quantities and by application of the relative Morison formulation to obtain the hydrodynamic forces. As the hydrodynamic forces are given in differential form as a force per unit length, a transformation of the differential hydrodynamic forces into nodal loads is needed. This is accomplished by the following two approaches.

- The differential hydrodynamic forces are represented by a higher order polynomial regression. The forces are subsequently transformed into consistent beam loads by the interpolation functions.
- The hydrodynamic forces are transformed into nodal forces by introducing numerical integration, based on the trapezoidal rule, and by means of interpolation functions.

In the present chapter the projection of the kinematic quantities is described, and the implementation of the two abovementioned methods of representing the hydrodynamic forces is introduced. The methods are implemented in the Nonlinear Wave Code and validated by simple examples in which a restrained slender cylinder is subjected to wave loading.

5.1 Projection of Kinematic Quantities

The kinematic quantities induce a transverse and a tangential force contribution for each member of the floating space frame structure. The transverse and tangential force contribution is obtained either by the difference or the sum of the projected horizontal and vertical components of the kinematic quantities, depending on the angle of the member. The orientation of each member is represented by the transformation matrix given as following

$$\begin{bmatrix} x_l \\ z_l \end{bmatrix} = \begin{bmatrix} \cos\theta & \sin\theta \\ -\sin\theta & \cos\theta \end{bmatrix} \begin{bmatrix} X \\ Z \end{bmatrix} \qquad \begin{bmatrix} X \\ Z \end{bmatrix} = \begin{bmatrix} \cos\theta & -\sin\theta \\ \sin\theta & \cos\theta \end{bmatrix} \begin{bmatrix} x_l \\ z_l \end{bmatrix} \tag{5.1}$$

The projection of the kinematic quantities is implemented in the Nonlinear Wave Code in the script *WaveForce.m* and is illustrated in Figure 39.

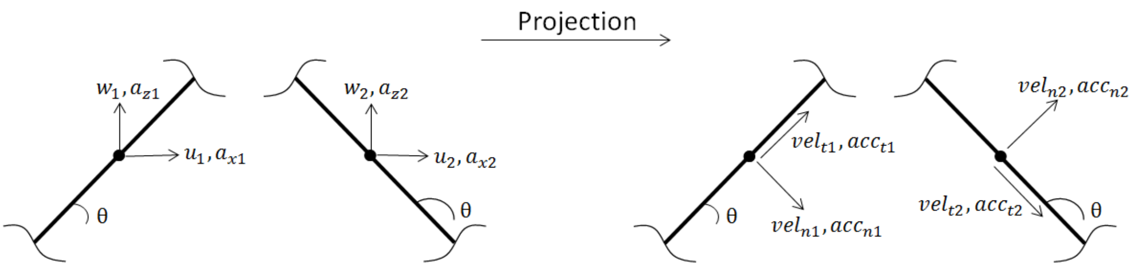

Figure 39: Projection of the kinematic quantities.

The transverse and tangential contributions of the kinematic quantities are applied in the calculation of the differential hydrodynamic forces by means of the relative Morison's formula and the hydrodynamic forces are subsequently transformed into nodal loads. To obtain an accurate transformation of the hydrodynamic forces into nodal loads, a satisfactory distribution of the hydrodynamic forces is needed and achieved by a sufficient beam discretization. To avoid a large discretisation of the structure and thereby a demanding computational effort, extractions points are introduced in the subsequent subsection.

5.2 Extraction Points

To ensure that a given structure has a sufficient number of nodes, extra subnodes are generated between the main nodes. These nodes are referred as extraction points and implemented in the Nonlinear Wave Code by *ExtractionPoints.m*. An illustration of a beam element with two extraction points is given in Figure 40.

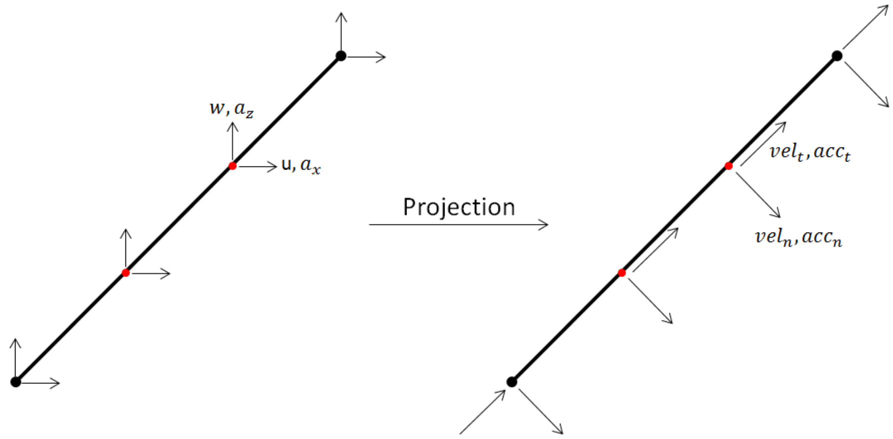

Figure 40: An element with 2 generated subnodes marked with red.

The number of extraction points needed to obtain a sufficient representation of the hydrodynamic forces depends on which method is used to transform the forces into consistent nodal loads. The two methods are described in subsection 5.3 and 5.8.

5.3 Polynomial Regression of Hydrodynamic Forces

The differential hydrodynamic forces are in this subsection represented by a mathematic regression. In Figure 41 a solid cylinder of $r = 0.01m$ and length $L = 40m$ restrained at seabed level is illustrated. The purpose of this configuration is to represent the hydrodynamic force distribution over the depth of the ocean. The differential hydrodynamic forces are determined at each node at time step $t = 0s$ for the wave specifications set as $h = 40m$, $H = 1m$ and $T = 15s$.

The cylinder is initially vertical at this time step and only the normal force contribution f_n from Morison's formula is acting on the cylinder as the tangential force contribution f_t is set to zero. With a sufficient number of nodes, a relatively accurate polynomial can be drawn as illustrated in Figure 41.

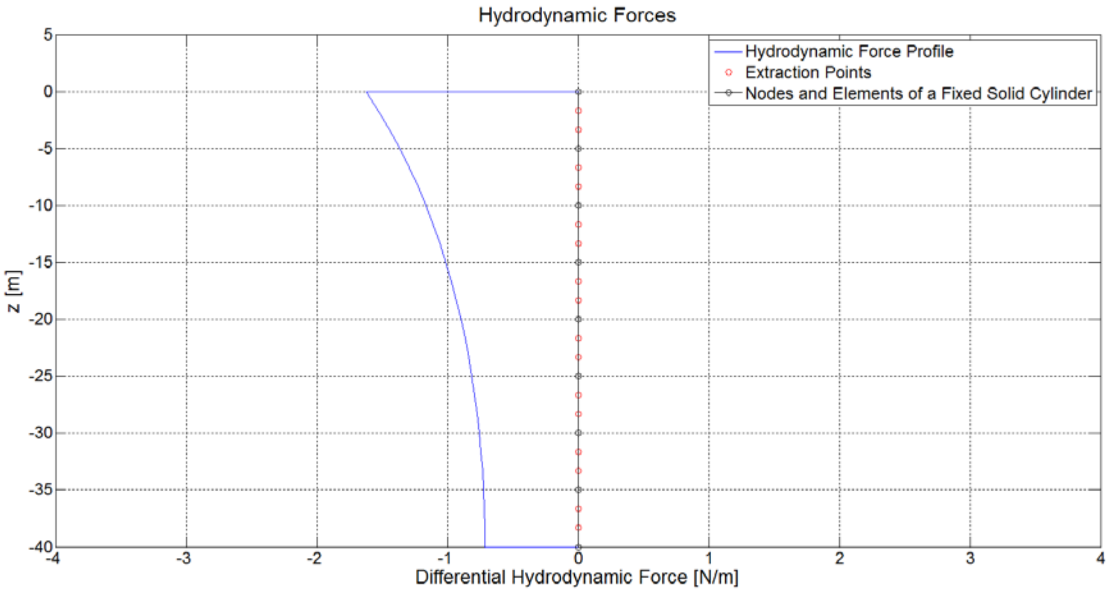

Figure 41: Differential hydrodynamic forces determined for a restrained solid cylinder.

As remarked from Figure 41 the hydrodynamic force profile must be represented by a higher order polynomial regression. A 3rd order polynomial regression gives a decent representation of the hydrodynamic forces. A quadratic regression over 4 and 25 points representing the differential hydrodynamic forces are illustrated in Figure 42 together with the hydrodynamic forces at each node.

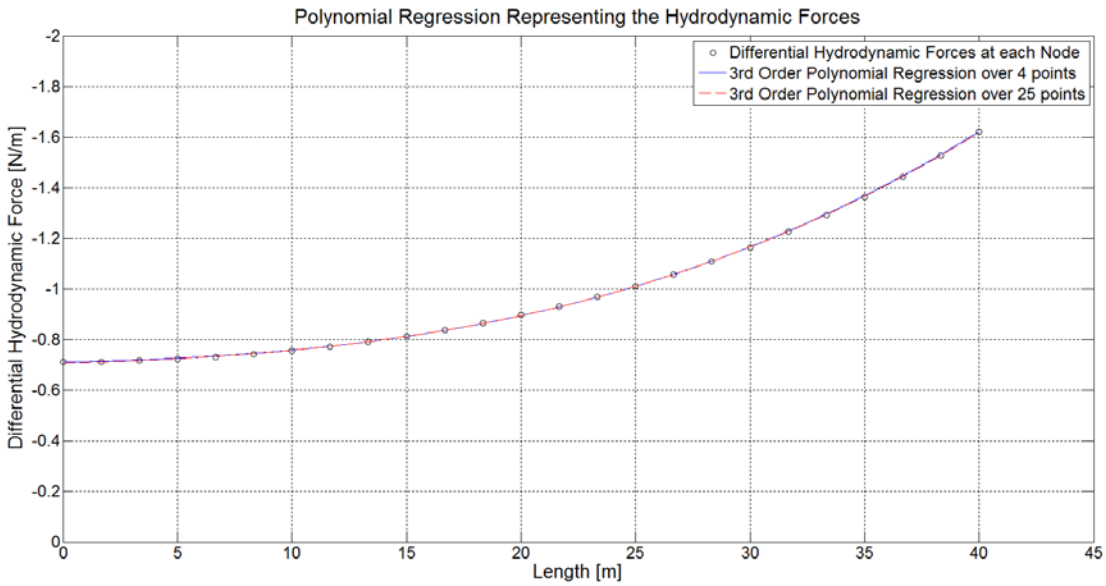

Figure 42: Polynomial regression representing the differential hydrodynamic forces acting on the solid cylinder.

It should be noted that Figure 42 is rotated 90 degrees in comparison with Figure 41. It is however remarked from Figure 42 that the polynomial regression is relatively accurate even with few points. A decent rule of thumb is that the number of known points of a polynomial must be one more than the order of the polynomial. For example, to achieve a quadratic regression, four points are needed to obtain reasonable results. This can either be done by dividing the solid cylinder into 3 elements with 4 nodes or one element with two nodes and two extraction points.

The degree of polynomial depends on which type of load the structure is exposed to. For 1st order waves, a quadratic regression provides a decent fit to the hydrodynamic forces. The quadratic regression takes form as

$$p(x) = p_1 \cdot x^3 + p_2 \cdot x^2 + p_3 \cdot x + p_4 \tag{5.2}$$

The coefficients p_1 to p_4 are obtained by using the Matlab function *Polyfit*, where the input parameters are the differential hydrodynamic forces in the nodes and in the extraxtion points for each element, the distance between the nodes and the extraction points and the degree of polynomial. The calculations are executed in the Nonlinear Wave Code in the Matlab script denoted *WaveForce.m*.

5.4 Transformation of Hydrodynamic Forces into Beam Loads

With the quadratic regression describing the distributed forces over the elements, the forces are now transformed into beam loads by means of the consistent load vectors. The consistent load vectors are defined via integration of the product of the transposed shape functions N^T and the polynomial loads p over the length of the elements L.

$$r = \int N^T p \, dL \tag{5.3}$$

The consistent load vector contains a transverse load, a tangential load and a bending moment at each node of each element as illustrated in Figure 43.

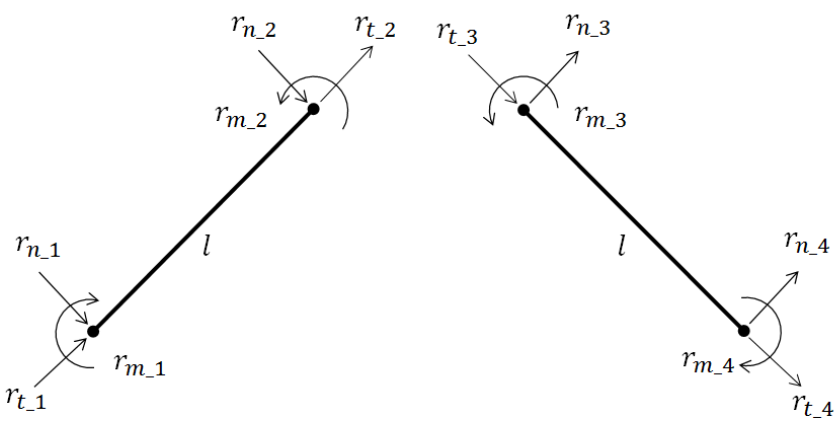

Figure 43: Transverse and tangential loads and bending moments acting on two beam elements.

The last step of the transformation is the projection of the local loads to global loads by means of the transformation matrix. The transformation of the differential hydrodynamic forces into nodal loads is implemented in the Nonlinear Wave Code in the script *WaveForce.m* and the consistent load vectors are implemented in the script denoted *ConsistentLoadVectors.m*.

5.5 Modelling of Self-weight

The loading obtained from the mass due to the gravity acceleration has likewise the wave loading an impact on the floating space frame structure. The self-weight is implemented in the same manner as the hydrodynamic forces, namely by projection and transformation of the distributed self-weight load to nodal loads. The self-weight load of the structure is separated into a transverse load and a tangential load by projection as shown in Figure 45.

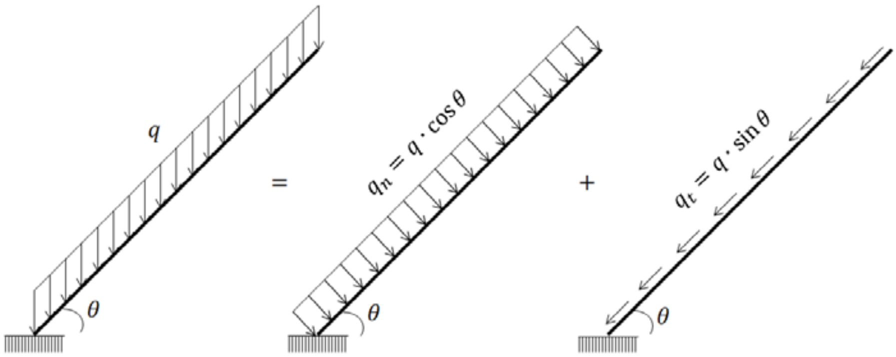

Figure 44: The loading obtained by the mass due to the acceleration acting on the structure.

By application of the consistent load vectors, the distributed loads are transformed into beam loads and subsequently projected to global loads. The self-weight is included in all wave analyses performed in the report.

5.6 Validation of Hydrodynamic Forces by Polynomial Regression

In the present subsections two analyses of a solid cylinder are performed to validate the method of representing the hydrodynamic forces by means of polynomial regression in the Nonlinear Wave Code. In the first example the cylinder is restrained and fully submerged, while the cylinder is partially submerged in the second example. Furthermore a convergence study is performed to clarify the accuracy of the Nonlinear Wave Code compared to Ansys Workbench.

Validation of Fully Submerged Cylinder

The method of determining the hydrodynamic forces in the Nonlinear Wave Code is below validated by means of Ansys Workbench. An example consisting of a restrained solid cylinder is exposed to linear waves as illustrated in Figure 45.

The structure has the dimensions $L = 5m$, $r = 0.01m$ and the wave specifications are set to $H = 1m$, $T_p = 15s$, $h = 40m$ while the hydrodynamic coefficients are set to $C_D = 0.5$, $C_M = 2$ and $C_A = 1$. The cylinder is modelled relatively slender to obtain large displacements and thus to validate the fluid-structure interaction.

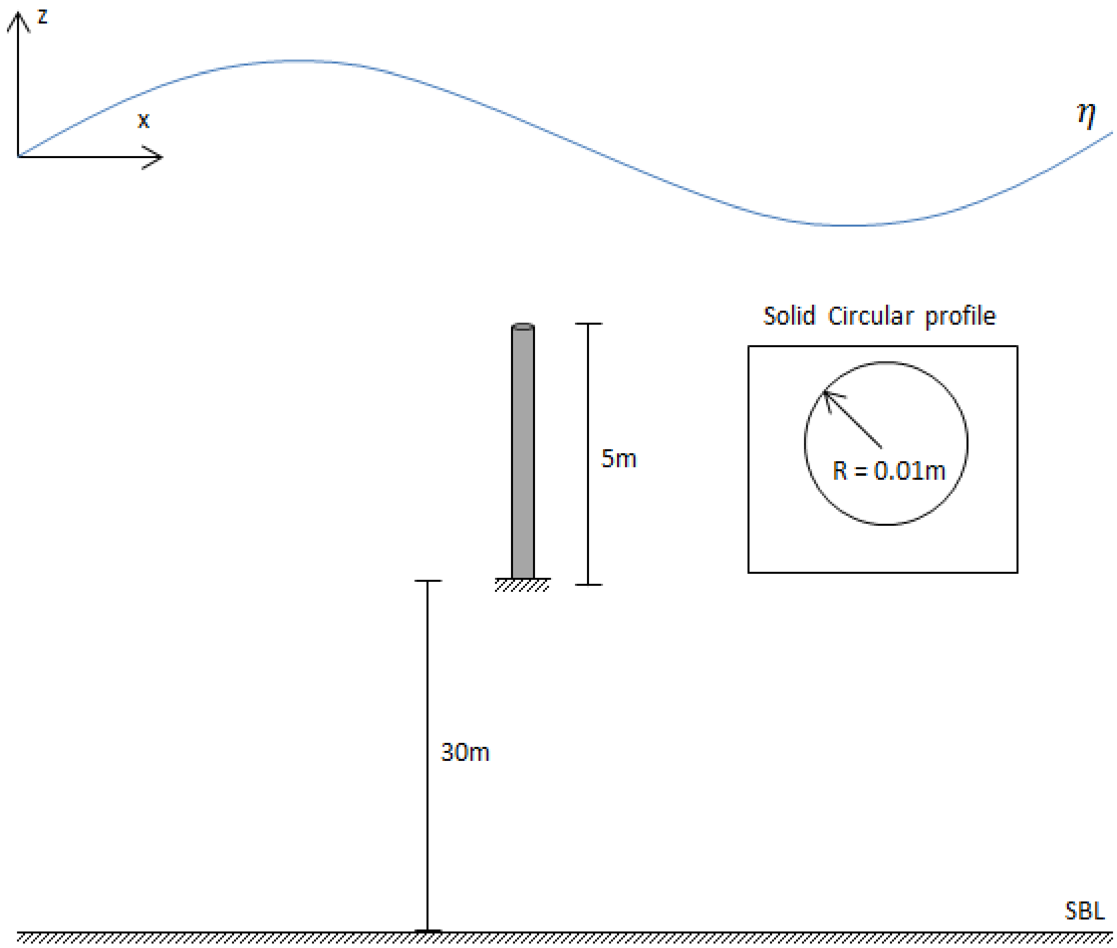

Figure 45: Validation example of the implemented hydrodynamic forces by a restrained solid cylinder.

The cylinder is modelled by 10 beam elements and 10 extraction points for each element. The horizontal displacement, velocity and acceleration responses in both programs are extracted from the end node and compared in Figure 46.

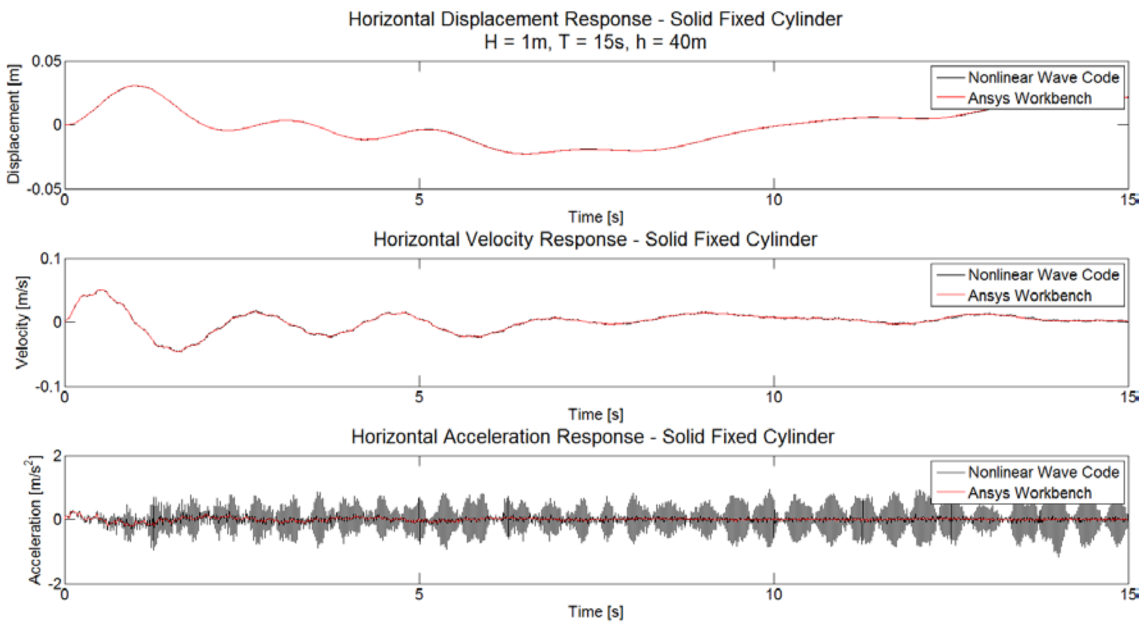

Figure 46: Comparison of the displacement, velocity and acceleration responses extracted from Ansys and Matlab.

The interaction between the method of determining the hydrodynamic forces by polynomial regression in the Nonlinear Wave Code and Ansys Workbench given in the above example, confirms that both programs are agrees with each other. The deviation between the two results is determined to 2.6%. Representing the hydrodynamic loads by polynomial regression on a fully submerged structure is thus a good approximation, and by a finer mesh the deviation is reduced.

However, as remarked in Figure 46, the acceleration response obtained by the Nonlinear Wave Code and Ansys Workbench both are dominated by high-frequency peaks. An explanation of the origin of the high-frequency peaks is given in subsection 5.9. It is furthermore remarked that the displacements of the cylinder is relatively small which is due to the small amplitude linear waves. In the following subsection the response of a partially submerged cylinder is predicted.

Validation of Partially Submerged Cylinder

An additional validation example is performed by the Nonlinear Wave Code to confirm that the method can deal with a structure that is partially submerged as illustrated in Figure 47. The purpose of this example is to validate that the method is able to deal with the interaction between the structure and the nature of the ocean water surface. The same cylinder is applied with the length $L = 5m$ and ocean wave specifications $H = 1m$, $T = 15s$ and $h = 40m$. The hydrodynamic coefficients are set to $C_D = 0.5$, $C_M = 2$ and $C_A = 1$.

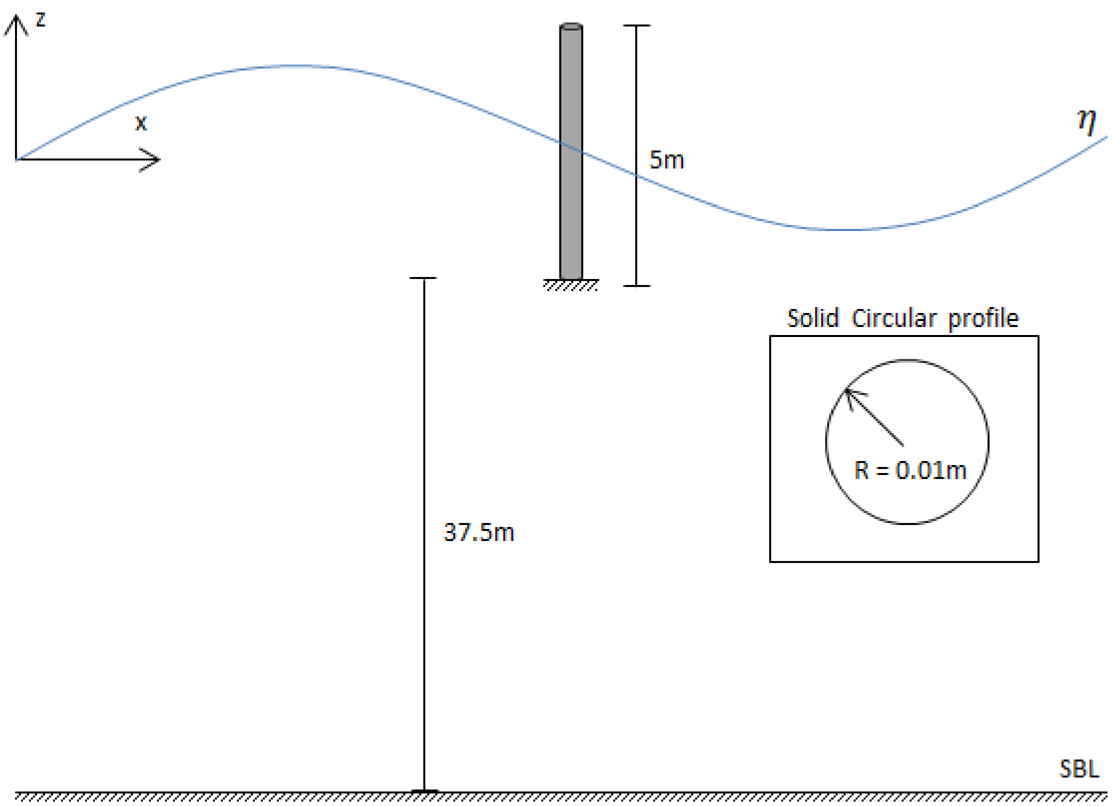

Figure 47: Validation example for a restrained solid circular cross-section positioned partly above MWL.

The cylinder is modelled by 10 beam elements and 10 extraction points for each element. The comparison of the horizontal displacement, velocity and acceleration is given in Figure 48.

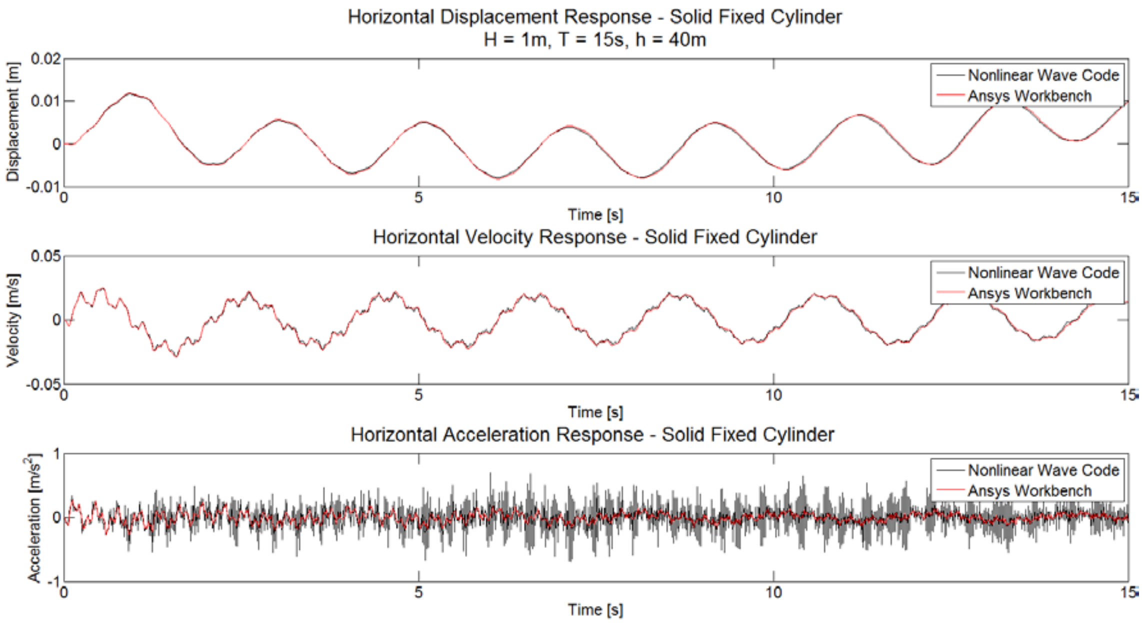

Figure 48: Comparison of the displacement, velocity and acceleration responses extracted from Ansys and Matlab.

Besides the accelerations, which are discussed in subsection 5.9, the displacement and velocity plot results confirm that the implemented method is consistent with Ansys Workbench, and that the present method is able to represent the interaction at the ocean water surface.

For partially submerged elements, this approach of evaluating the hydrodynamic forces by polynomial regression has some limitations. The method has difficulties describing the wave load distribution along the part of the element which is above the ocean water surface, as the load distribution goes rapidly from values to zero values. This is a gab that makes it impossible to find an exact polynomial regression to fit the load distribution along the length of element.

To illustrate the polynomial fit for a partially submerged element, a solid cylinder is modelled by two elements, in which *Element 1* is fully submerged and *Element 2* is partially submerged as illustrated in Figure 49.

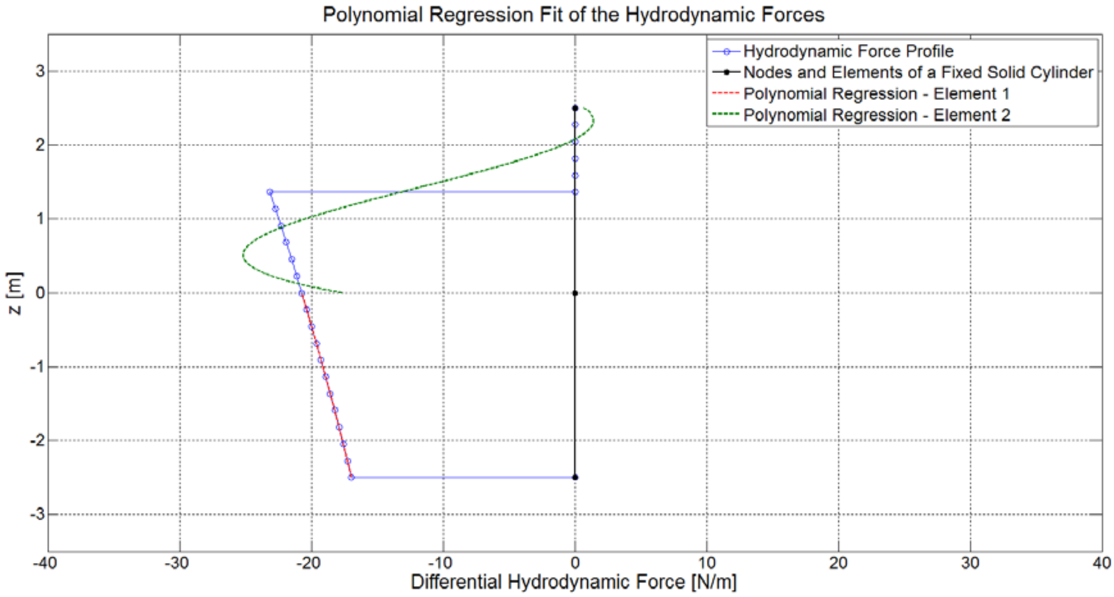

Figure 49: The polynomial regression fits over the two elements of the solid cylinder.

It is remarked from Figure 49 that the polynomial regression fits perfectly for the fully submerged *Element 1*, whereas the polynomial regression fits badly for the partially submerged *Element 2*.

Convergence Study of Structure Discretization

It is crucial to impose the necessary amount of structure discretization to obtain a satisfactorily balanced accuracy and computing resources. The purpose of the convergence study is thus to obtain a sufficient accurate solution with a beam discretization that is sufficient and not overly demanding of computing resources. The convergence study is performed so that the mesh firstly is created using the fewest, reasonable number of elements, after which the beam discretization is increased and compared to both those of the previous mesh and Ansys Workbench until the results converge satisfactorily.

Two convergence studies are thus performed to evaluate the influence of the number of extraction points and elements. Both convergence studies are performed on the partially submerged restrained cylinder shown in Figure 47, in which the first convergence study clarifies the influence of the extraction points, while the second convergence study confirms the importance of the element division of the structure. The mean percentage difference of the horizontal displacement of the partially submerged cylinder over a period of 15s between the Nonlinear Wave Code and Ansys Workbench is stated in Figure 50. The cylinder is modelled by two beam elements and the number of applied extraction points is gradually increased until convergence is satisfied.

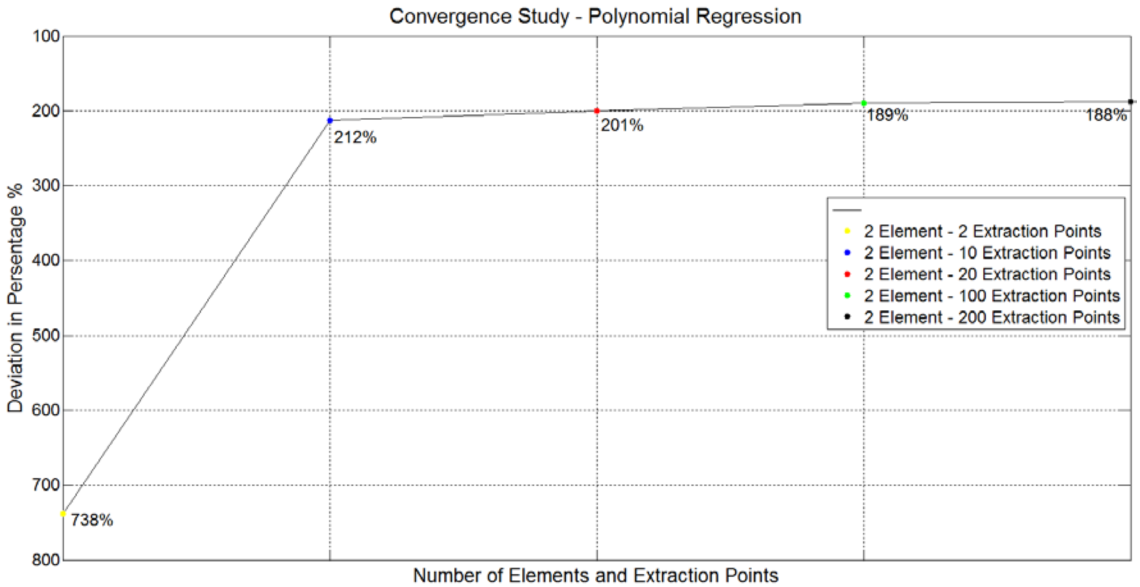

Figure 50: Convergence study of the cylinder modelled with only two elements and a different number of extraction points.

As remarked from Figure 50, the results are significantly more accurate by increasing the number of extraction points from 2 points per element to 10 points. However, the analyses converge at a deviation of 188 %, which is due to a phase shift that occurs between the results from the Nonlinear Wave Code and Ansys Workbench. Representing the hydrodynamic forces by only two beam elements is thus not sufficient, by which a convergence study of the necessary number of element division is given in the following.

In the present convergence study, the number of extraction points is set to 10 while the number of element division is gradually increased from 2 to 100 beam elements as illustrated in Figure 51.

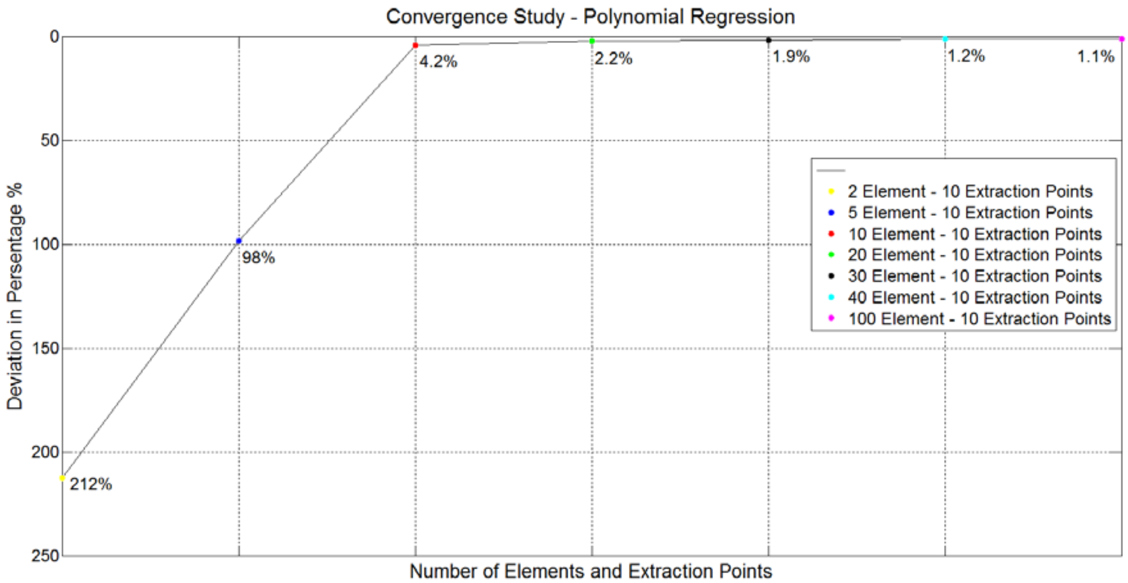

Figure 51: Convergence study of the cylinder modelled with a different number of elements and 10 extraction points.

As observed from Figure 51, the results become significantly better as the number of elements is increased. With 100 beam elements and 10 extraction points for each element, the deviation is reduced to 1.1 %. The convergence study is not continued with further elements because of the increasing demand of computational time and effort.

The reason why the results are more accurate by increasing the number of elements and not by increasing the number of extraction points is that the incorrect polynomial fit near the ocean water surface now is limited to a small element. The more elements used the smaller the elements become and the more insignificant the error at the water surface becomes.

5.7 Summary of Wave Loads by Polynomial Regression

The representation of the hydrodynamic forces by a polynomial regression in the Nonlinear Wave Code is proven to be a consistent approximation for fully submerged structures in comparison with Ansys Workbench. It is remarked that the polynomial fit provides a good representation of the wave loading by few nodes and extraction points.

However, considering partially submerged elements the polynomial regression is not capable of providing a sufficient representation of the wave distribution along the partially submerged elements. A convergence study shows that a large number of beam discretization is needed to obtain reasonable results for the partially submerged cylinder.

An approach to avoid the above-mentioned problem at the water surface is by representing the hydrodynamic forces by numerical integration. In the present subsection 5.8 a new approach of evaluating the hydrodynamic forces is introduced.

5.8 Numerical Integration of Hydrodynamic Forces

The distributed wave loading is in the same manner as in the method using polynomial regression, converted into nodal forces by introducing interpolation functions $N(x)$ and integrating the dot product along the local beam axis as

$$\mathrm{F} = \int_L \mathrm{N}^{\mathrm{T}} q \, dx = \int_L f(x) \, dx \tag{5.4}$$

However, the representation of the ocean loads near the free surface is performed by introducing numerical integration in the Nonlinear Wave Code. The numerical integration is based on the trapezoidal rule which works by approximating the region under the graph of the function $f(x)$ as a trapezoid and determining its area as illustrated in Figure 52.

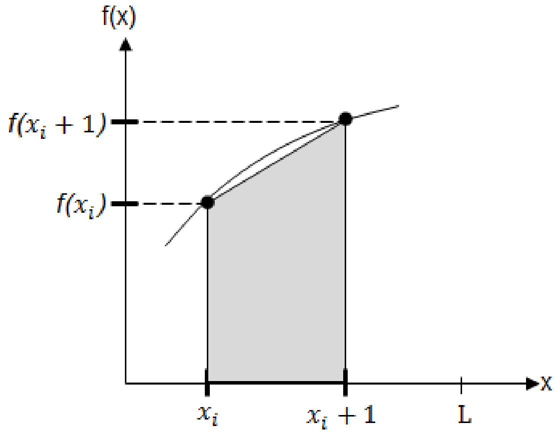

Figure 52: Trapezoidal Rule

The area of $f(x)$ considered in Figure 52 can be approximated by N trapezoidals as

$$\int_L \mathrm{f(x)}dx \approx \sum_{i=1}^{N} (x_{i+1} - x_i) \frac{f(x_i) + f(x_i + 1)}{2} \tag{5.5}$$

which is simplified to the following expression as the discretization $(x_{i+1} - x_i)$ is constant along the length L

$$\int_L \mathrm{f(x)}dx \approx (x_{i+1} - x_i) \left(\frac{f(x_i)}{2} + f(x_{i+1}) + f(x_{i+2)} \dots \frac{f(x_n)}{2} \right) \tag{5.6}$$

More trapezoids give a better approximation of the area under the curve, i.e. using an appropriate number of points along the beam length provides a sufficient simulation of the global system response. In the following subsection 5.9 the validation of using numerical integration to describe the ocean waves is given.

5.9 Validation of Hydrodynamic Forces by Numerical Integration

In the same manner as for the polynomial regression method, two validation examples are performed to validate the method of representing the hydrodynamic forces by numerical integration. As a matter of form, the illustration of the validation examples is recalled and shown in Figure 53 for the fully submerged cylinder and in Figure 55 for the partially submerged cylinder.

Validation of Fully Submerged Cylinder

The structure has the dimensions $L = 5m$, $r = 0.01m$ and the wave specifications are for linear waves set to $H = 1m$, $T_p = 15s$, $h = 40m$. The hydrodynamic coefficients are set to $C_D = 0.5$, $C_M = 2$ and $C_A = 1$.

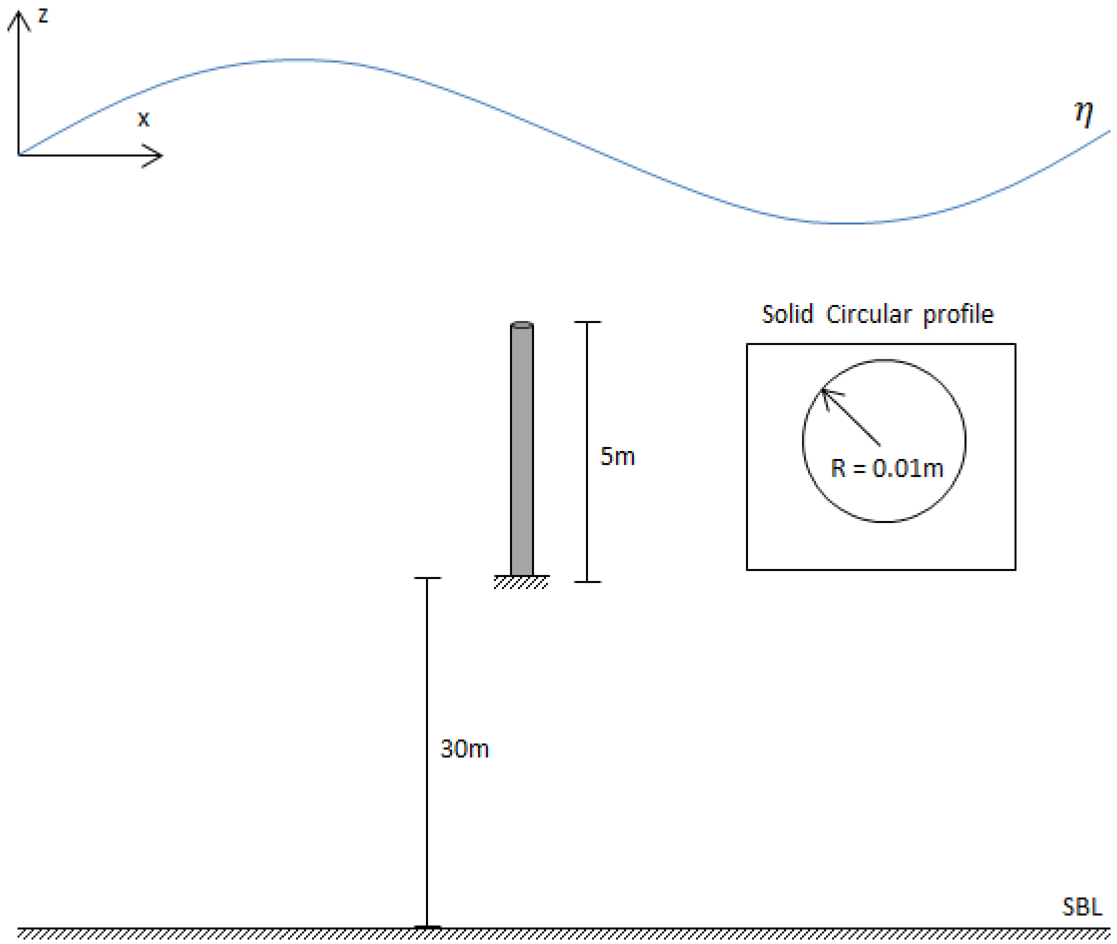

Figure 53: Validation example of the implemented hydrodynamic forces by a restrained solid circular cross-section.

The horizontal displacement, velocity and acceleration responses in both programs are extracted at the end node and compared in Figure 54.

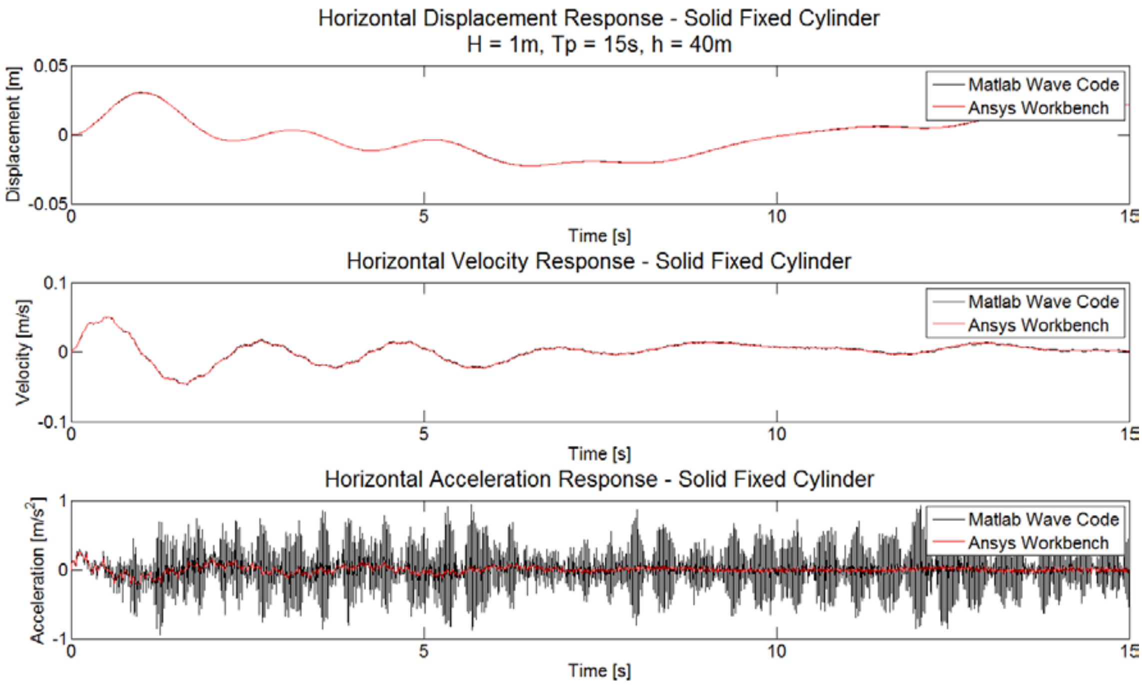

Figure 54: Comparison of the displacement, velocity and acceleration responses extracted from Ansys and Matlab.

The interaction between the method of determining the hydrodynamic forces by numerical integration in the Nonlinear Wave Code and Ansys Workbench, confirms that both programs are consistent when considering fully submerged restrained structures. The deviation of the results between the two programs is estimated to 2.5%, which is significantly reduced by applying a finer mesh. It is remarked that the deviation approximately agrees with the deviation obtained by the polynomial fit for a fully submerged cylinder.

However, as remarked in Figure 54, the acceleration response obtained by the Nonlinear Wave Code and Ansys Workbench both is dominated by high-frequency peaks. An explanation of the origin of the high-frequency peaks is given in the following subsection.

Validation of Partially Submerged Cylinder

An additional simple validation example is performed by the Nonlinear Wave Code to validate that the method is able to deal with the interaction between the structure and the nature of the ocean water surface. The cylinder has the length $L = 5m$ while the ocean wave specifications are set to $H = 1m$, $T = 15s$ and $h = 40m$. The hydrodynamic coefficients are set to $C_D = 0.5$, $C_M = 2$ and $C_A = 1$.

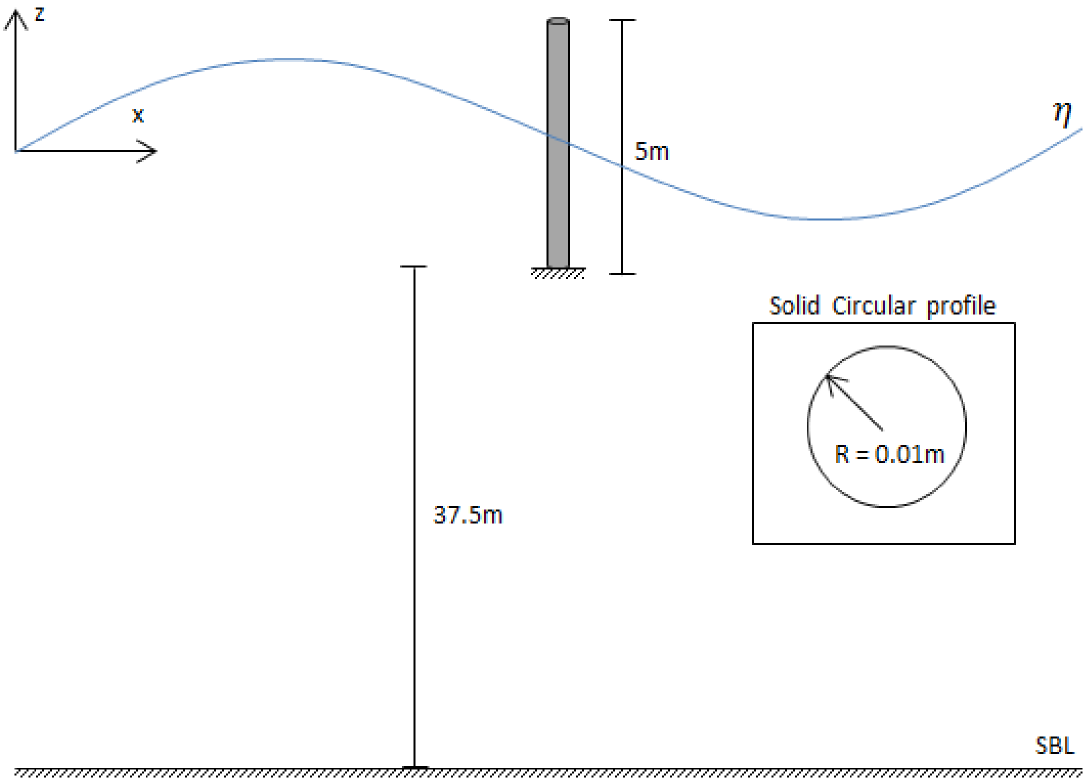

Figure 55: Validation example for a restrained solid circular cross-section positioned partly above MWL.

The comparison of the horizontal dynamic response is given in Figure 56.

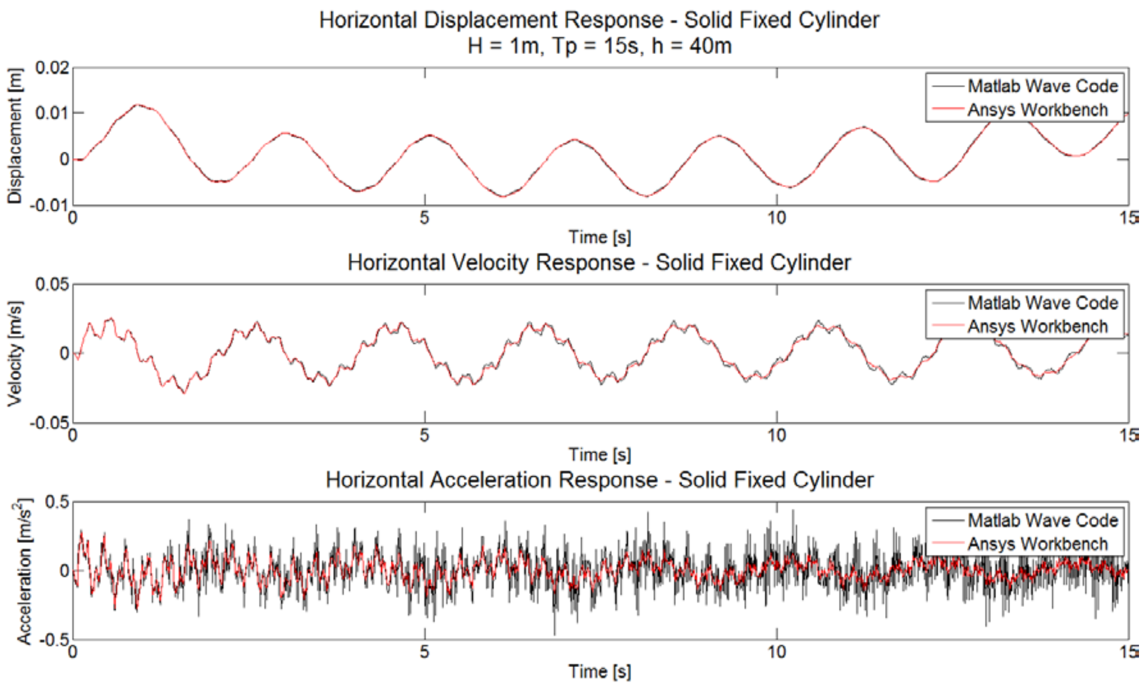

Figure 56: Comparison of the displacement, velocity and acceleration responses extracted from Ansys and Matlab.

The displacement and velocity plot results confirm that the implemented method of calculating the hydrodynamic forces is consistent with Ansys Workbench, and that the method can handle the variation and nature of the water surface.

However, it is remarked that the acceleration signal is dominated by high-frequency peaks as aforementioned. The high-frequency peaks can be reduced by introducing numerical damping described in subsection 3.4. By performing a Fast Fourier Transform (FFT) analysis using the acceleration time-domain signal, the acceleration response is transformed from the time-domain to the frequency-domain by which the frequencies of the signal are clarified. Performing a FFT analysis on the acceleration response introduced in Figure 56 in which no algorithmic damping is included, the following frequency spectrum is obtained in Figure 57.

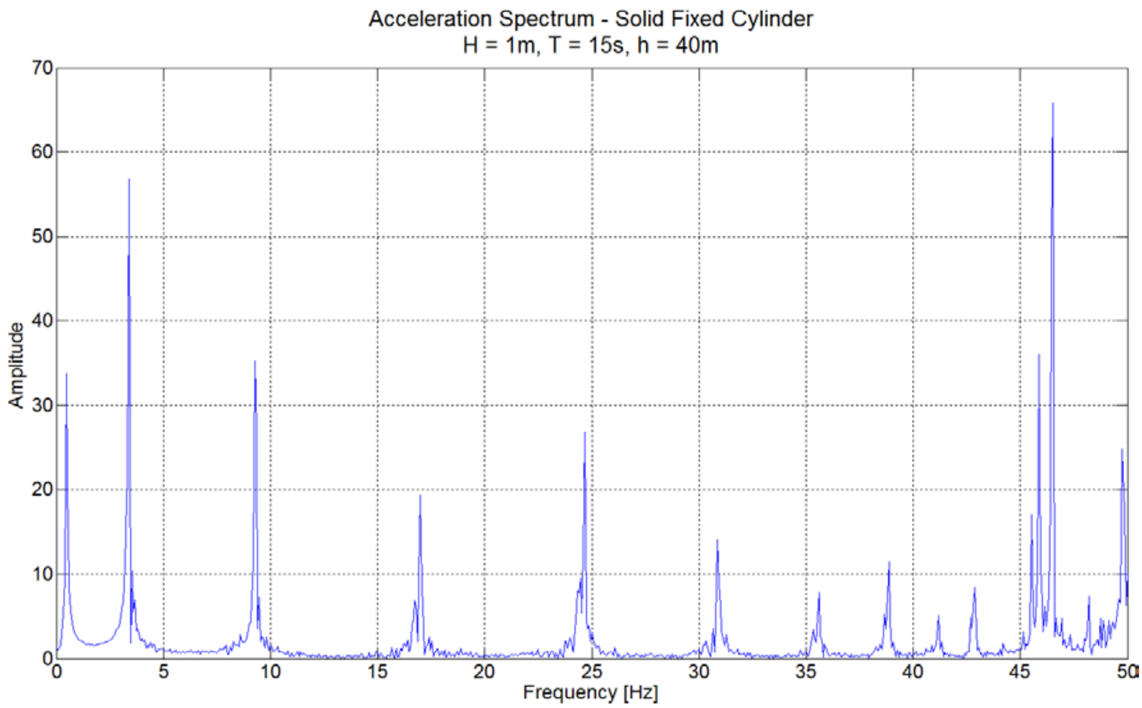

Figure 57: FFT-analysis of the acceleration response to identify the frequencies of the response. No Algorithmic damping is introduced.

It is observed from Figure 57 that the FFT-analysis of the acceleration response reveals that frequencies with large amplitudes occur when no numerical damping is included. By introducing numerical damping of 0.1 in the analysis, the following acceleration response in Figure 58 is given.

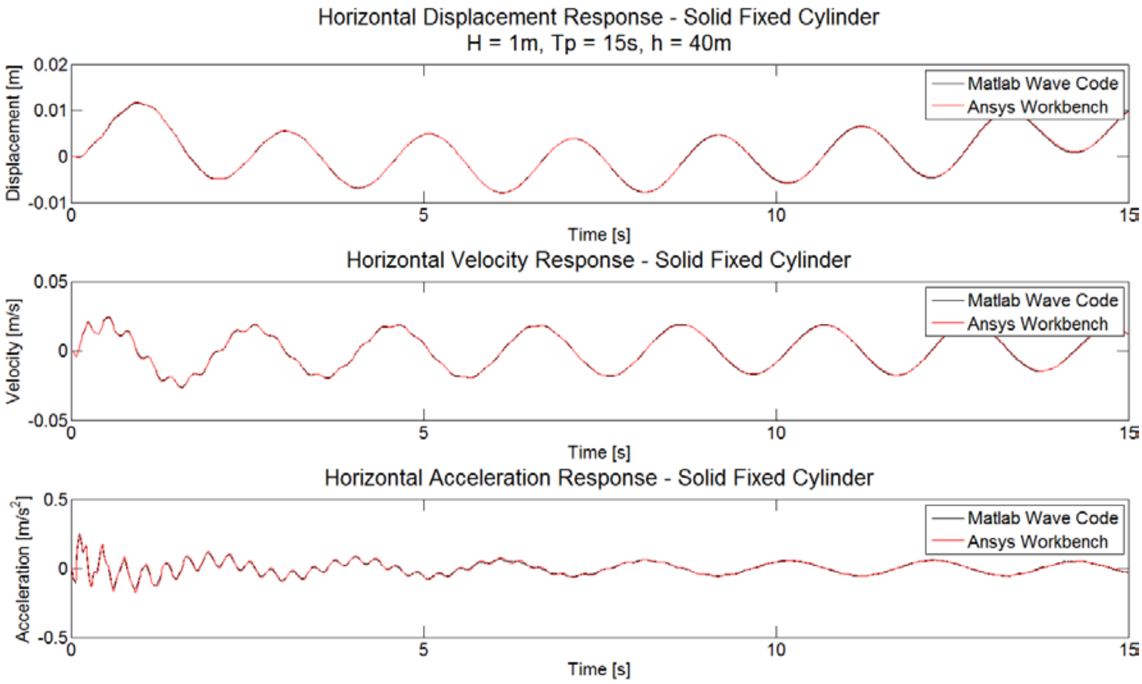

Figure 58: Displacement, velocity and acceleration response when algorithmic damping is included.

It is remarked that the high-frequency peaks are significantly reduced when algorithmic damping is introduced. The accelerations are thus damped and by performing a FFT on the acceleration signal the following acceleration spectrum is obtained.

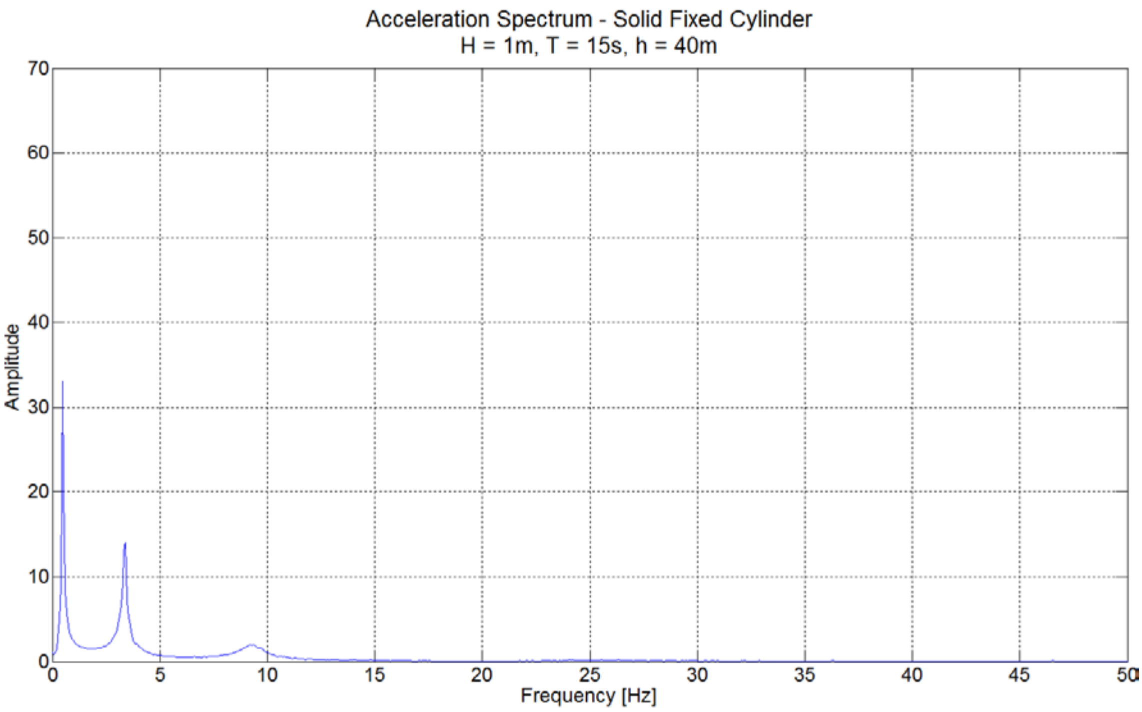

Figure 59: FFT-analysis of the acceleration response to identify the frequencies of the response. Algorithmic damping of 0.1 is included.

To verify that the global response of the structure is not damped by introducing the numerical damping, the eigenfrequencies of the structure is determined and compared with the acceleration spectrum. A modal analysis shows that the first three eigenfrequencies of the system are approximately $0.5\ Hz$, $3.5\ Hz$ and $9\ Hz$ which are consistent with the clarified frequencies obtained by the FFT analysis given in Figure 59. The amount of algorithmic damping implemented is thus valid as it has no impact on the global response of the structure.

In the following subsection a convergence study of the necessary number of structure discretization is introduced.

Convergence Study of Structure Discretization

The study is performed on the aforementioned solid cylinder illustrated in Figure 55 in the same manner as in subsection 5.6. The difference of the displacement at the end node of the cylinder in the Nonlinear Wave Code and Ansys Workbench is determined at each time step where after the mean value over the total time of 15 seconds is calculated.

Firstly, the cylinder is modelled by two beam elements while the number of extraction points is gradually increased until convergence is satisfied as illustrated in Figure 62.

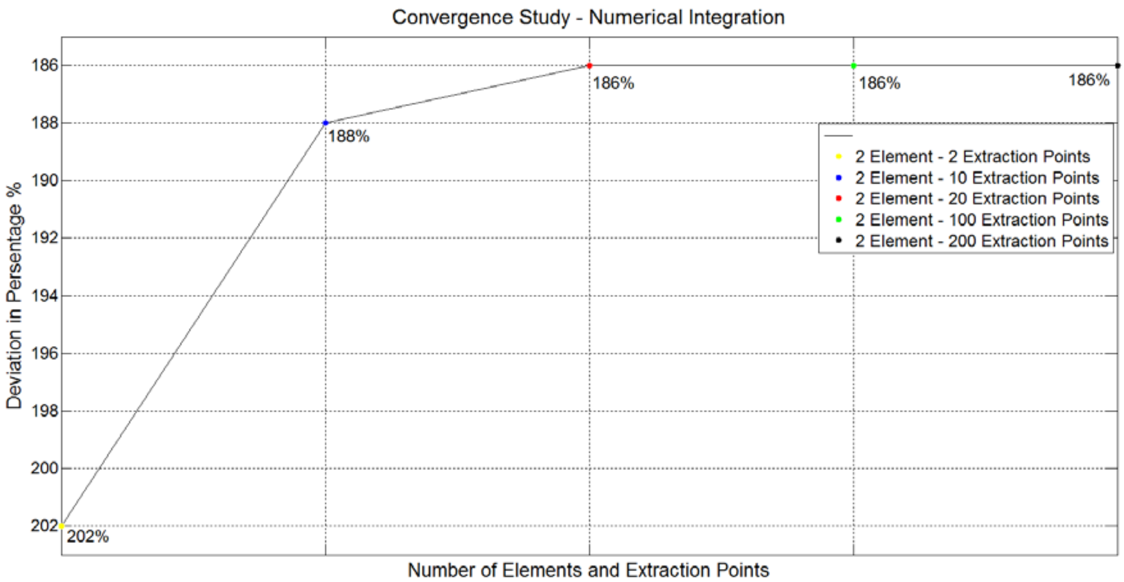

Figure 60: Convergence study of the cylinder modelled with only two elements and a different number of extraction points.

As remarked, the results only become relatively little more accurate than the results obtained in subsection 5.6 by the polynomial regression method. This confirms that the element division of the structure is of significant importance both to obtain a sufficient representation of the hydrodynamic forces and the dynamic response of the structure.

With both methods a phase shift occurs by a small number of structure discretization and consequently, the deviation is large even with many extraction points. However, it is remarked that with the numerical integration method, the results converges faster than the polynomial regression method.

In Figure 61, the number of elements is increased and the number of extraction points remains 10 and as remarked, the results are marginally more accurate in comparison with the results from Figure 51. Similar as the result in Figure 61 and Figure 51, the deviation between the Nonlinear Wave Code and Ansys Workbench is large for a low number of element divisions and becomes relatively accurate for a large number of element divisions.

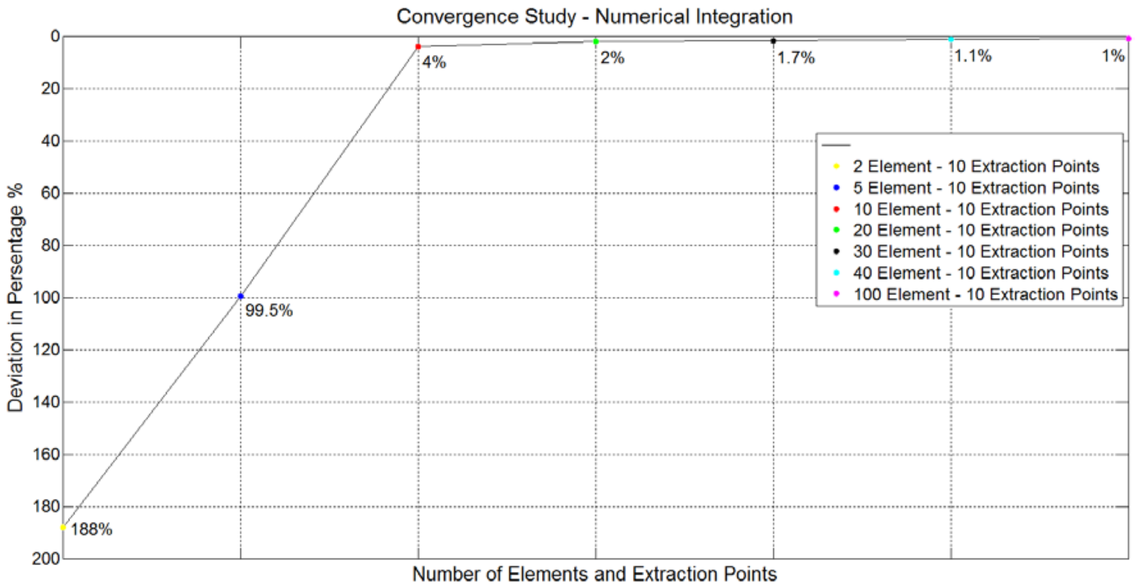

Figure 61: Convergence study of the cylinder modelled with a different number of elements and 10 extraction points.

The hydrodynamic forces are thus not accurately represented according to Ansys Workbench when using few elements. The agreement is highly increased when using 10 or more beam elements; however the finer discretization the more time-consuming the calculation becomes.

Given that the wave loads are implemented and validated in the Nonlinear Wave Code, the modelling of the buoyancy forces is brought into focus in the following Chapter 6 in which two different approaches of evaluating the hydrostatics is introduced.

5.10 **Summary of Wave Loads by Numerical Integration**

The representation of the hydrodynamic forces by a numerical integration in the Nonlinear Wave Code is proven to be a consistent approximation for fully submerged structures in comparison with Ansys Workbench. It is further remarked that the present method provides an improved representation of the hydrodynamic forces for a partially submerged cylinder in comparison with the method of polynomial regression.

As the method of numerical integration provides a better approximation of the wave distribution along the partially submerged elements, the method is used for the prediction of the ocean loads subjected to the floating space frame structure. However, as observed from the convergence studies, a fine mesh is necessary to obtain a sufficient representation of the hydrodynamic forces for partially submerged elements.

6 Modelling of Hydrostatics

The Nonlinear Wave Code is in the present modified to include the hydrostatic forces. As aforementioned in the introduction of the project, two methods of evaluating the hydrostatics of a floating structure is evaluated.

- The first method is based on a paper formulated by A. Yazdchi [4], in which the buoyancy forces appears as a consequence of two contributions, a distributed pressure and a buoyancy term existing as the ends of the cylinder are capped. The buoyancy forces are calculated as a function of the submerged element length.
- In the second method, the buoyancy forces are determined as a function of the amount of submerged cross-sectional area, and subsequently transformed into global nodal forces by introducing numerical integration.

Both methods are implemented in the Nonlinear Wave Code and compared with the buoyancy formulation in Ansys Workbench. The most accurate method is subsequently applied for the prediction of the buoyancy forces on the floating space frame structure.

6.1 Buoyancy Forces as Function of the Submerged Element Length

To add the effects of buoyancy for the analysis of offshore marine systems a paper produced by A. Yazdchi [4] concerning modern formulations for the nonlinear analysis of flexible beams and pipes, modified to include the appropriate hydrostatic forces, is considered. The paper considers only the axial effects, bending effects and effects due to shear deformation and do thus not among other things account for ovalization effects which may be important for pipes in some cases.

The contribution to the buoyancy force is divided into three effects, namely the distributed excess buoyancy $\{qe\}_d$ related to the external pressure from the seawater density, the curvature of the cylinder and a final buoyancy term $\{\boldsymbol{q}_e\}_e$ which only exist if the ends of an element are capped as illustrated in Figure 62. The effect from the curvature of the cylinder is omitted in this project and the element is thus idealized as a line element acting about its centre-line.

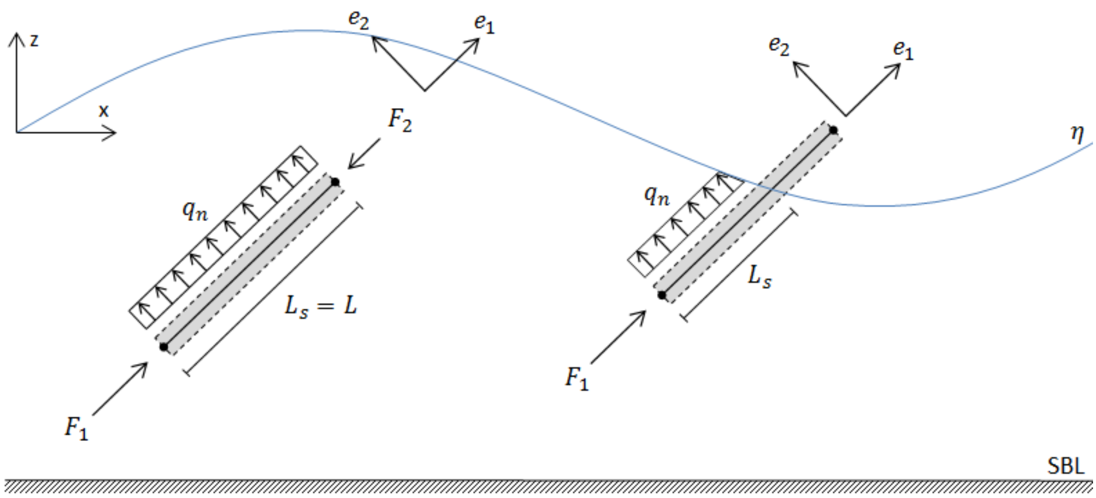

Figure 62: Distributed excess buoyancy force.

The distributed excess buoyancy force vector $\{qe\}_d$ is calculated at the nodes of the element by evaluating

$$\{qe\}_d = A_0 \gamma_w l_n e_2^T j \begin{Bmatrix} k_A e_2 \\ 0 \\ k_B e_2 \\ 0 \end{Bmatrix} \tag{6.1}$$

In which:

A_0	The cross-sectional area of the cylinder [m^2]
γ_w	The seawater density [1025 kg/m^3]
l_n	The length of the cylinder [m]
e^2	The orthogonal unit vector [-]
j	Unit vector [-]

The dimensionless coefficients k_A and k_B are used to transform the buoyancy forces to the nodes of the element, and these coefficients are dependent of the position of the element in the seawater. These are namely set to 0.5 for a fully submerged element and for a partially submerged element calculated by the following expressions

$$k_A = \frac{l_s}{l_n}\left(1 - \frac{l_s}{2l_n}\right) \qquad k_A = \frac{l_s}{l_n}\left(1 - \frac{l_s}{2l_n}\right) \qquad l_s = \frac{H_A}{H_A - H_B} l_n \tag{6.2}$$

Where l_s is the submerged length of the element. These formulations are relevant if only end A of the element is submerged as illustrated in Figure 63.

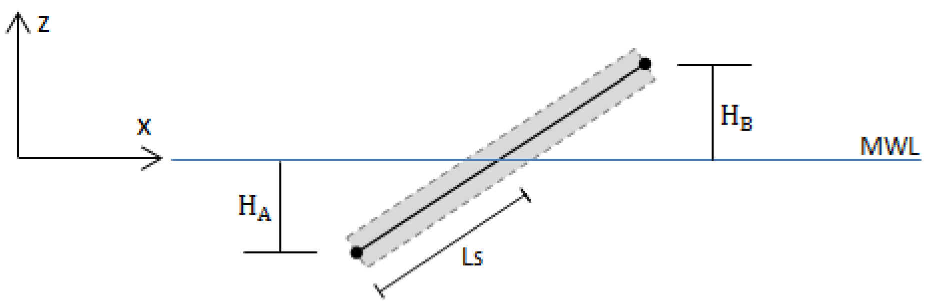

Figure 63: Partially submerged cylinder.

The values of H_A and H_B are given by the following formulations

$$H_A = h - x_A^T \mathbf{j} \qquad H_B = h - x_B^T \mathbf{j} \tag{6.3}$$

In which h is the height of the water surface above the ocean sea bed level. The current position vectors of the nodes, A and B, are given by x_A and x_B. It is easily observed that these coefficients are zero when both ends, A and B, are out of the water.

The last effect contributing to the buoyancy forces is as mentioned previously only existing if the ends of the cylinder are capped. The buoyancy term is given as

$$\{\boldsymbol{q}_e\}_e = A_0\gamma_w \begin{Bmatrix} (H - x_A^T\mathbf{j})\mathrm{e}_1 \\ 0 \\ (H - x_B^T\mathbf{j})\mathrm{e}_1 \\ 0 \end{Bmatrix} = A_0\gamma_w\{q_{e1}\}_e \tag{6.4}$$

The total final buoyancy force is thus formulated as following

$$F_B = \{\boldsymbol{q}_e\}_d + \{\boldsymbol{q}_e\}_e \tag{6.5}$$

These buoyancy force formulations are implemented in the Nonlinear Wave Code and in the present subsection 6.2 the method is validated in which the limitations of the method are assessed and discussed.

6.2 Validation of Buoyancy Forces

To validate the method of determining the buoyancy forces formulated as function of the submerged element length, two simple validation examples are performed in the Nonlinear Wave Code and Ansys Workbench. The first example concerns a vertical hollow cylinder dropped in still water, followed by an example in which a horizontal hollow cylinder is dropped in still water. The dimensions of the cylinders are chosen so that the subjected buoyancy force is twice the magnitude of the self-weight, in which the state of equilibrium is obtained when half of the cylinders are submerged.

Validation of Buoyancy Forces for Vertical Cylinder

The first validation example includes a vertical cylinder initially positioned at the water surface and subsequently dropped in still water as illustrated in Figure 64.

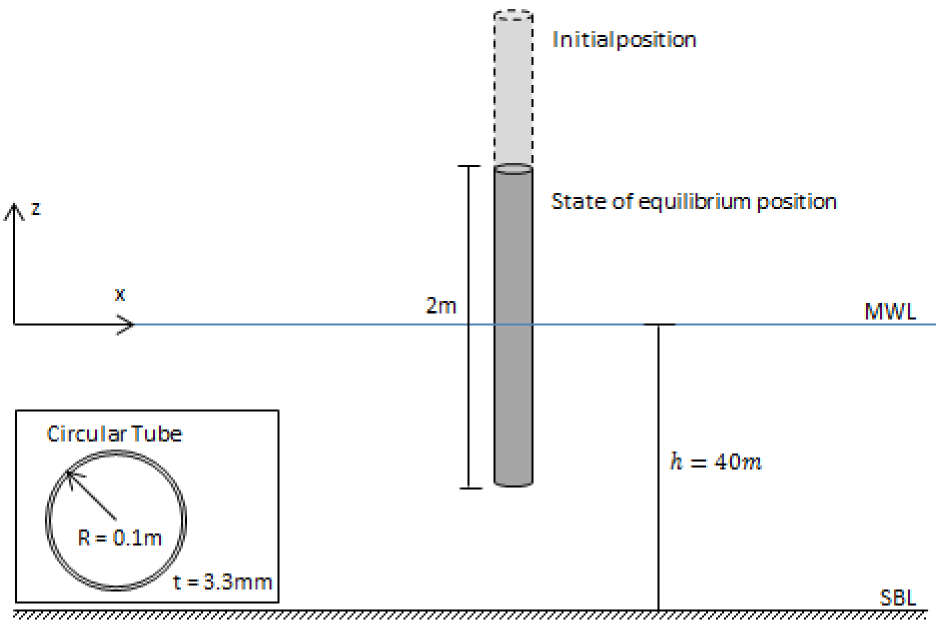

Figure 64: Validation of buoyancy formulation by a vertical cylinder.

The buoyancy test is executed by dropping the cylinder from its initial position, as illustrated in Figure 65, which by some time finds its state of equilibrium position. The displacement, velocity and acceleration response from both the Nonlinear Wave Code and Ansys Workbench are shown in Figure 65.

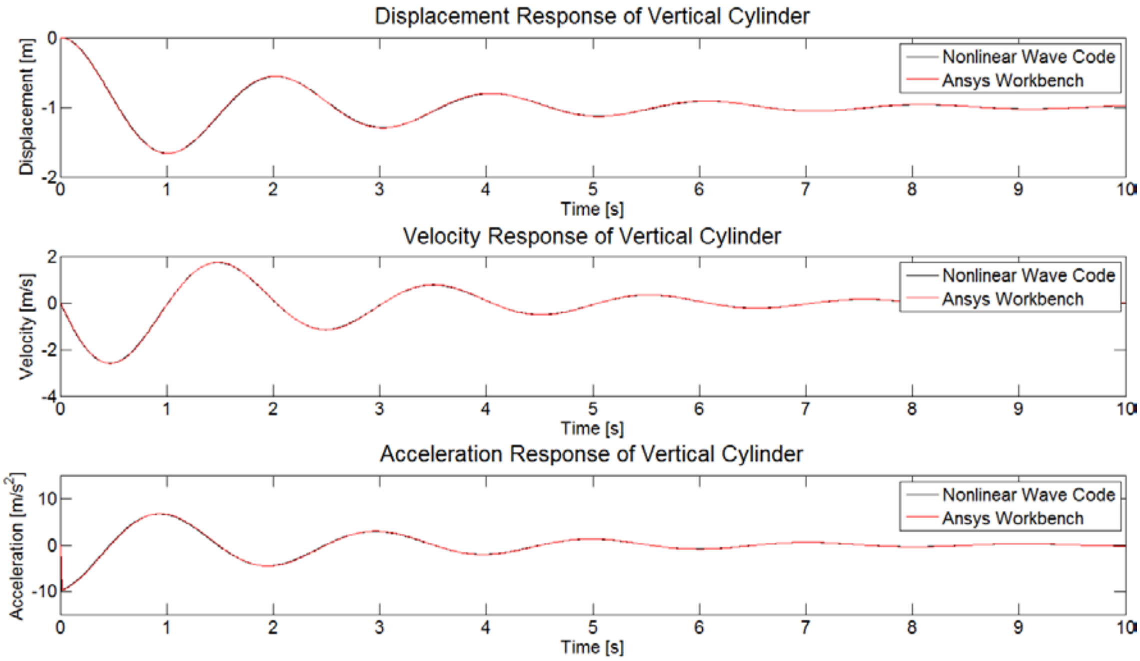

Figure 65: Buoyancy test on a vertical cylinder.

It is observed that the results of the buoyancy test from the Nonlinear Wave Code and Ansys Workbench are consistent and it is thus validated that the programmed Nonlinear Wave Code and the applied theory is able to represent the buoyancy effect on vertical cylinders.

The deviation between the two results is determined to be 0.8% by which confirms that the buoyancy formulation in the Nonlinear Wave Code for vertical cylinders compared to Ansys Workbench is valid.

Validation of Buoyancy Forces for Horizontal Cylinder

An additional buoyancy test has been performed on a horizontal hollow cylinder. The initial configuration of the horizontal cylinder is shown in Figure 66.

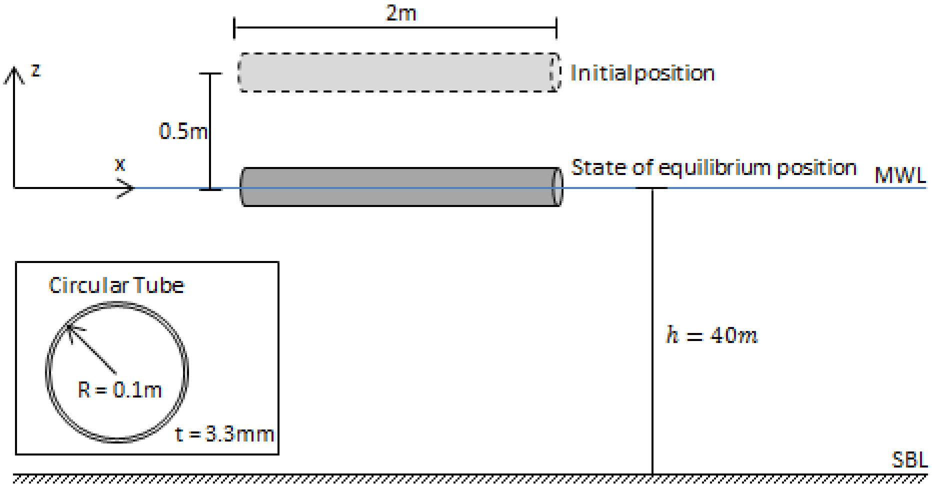

Figure 66: Buoyancy test on a horizontal cylinder.

The buoyancy test is performed in the same manner by dropping the cylinder from its initial position, which by some time finds its state of equilibrium position. A comparison of the displacement, velocity and acceleration response of the buoyancy test is illustrated in Figure 67.

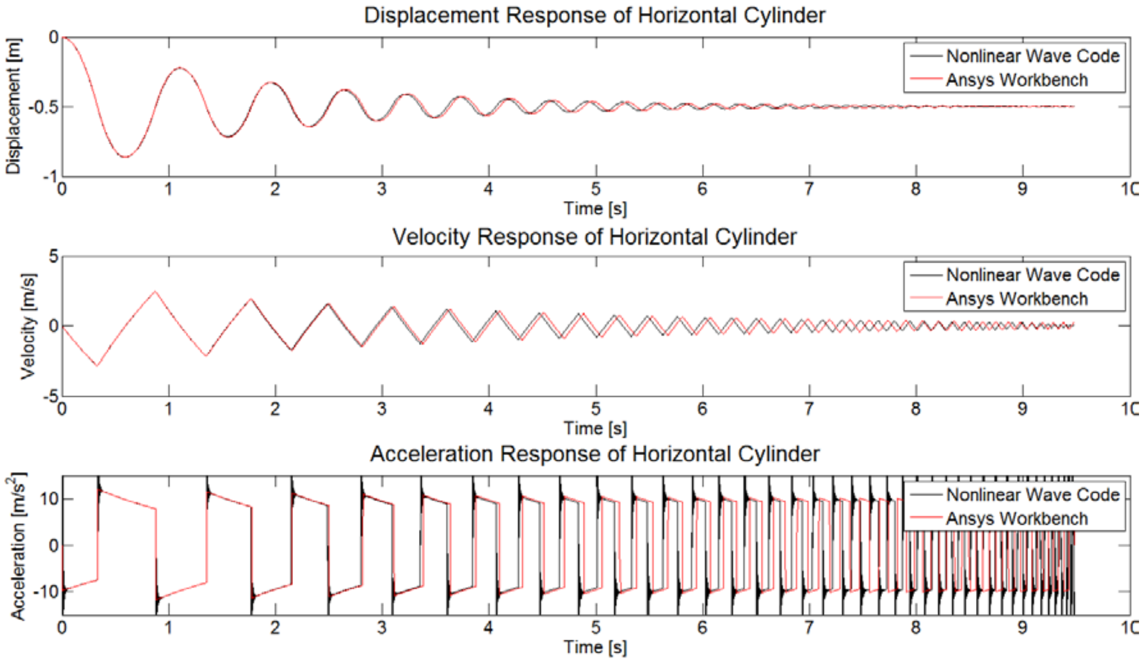

Figure 67: Comparison of displacement plot from Matlab Code and Ansys Workbench.

The responses from the Nonlinear Wave Code agree with Ansys Workbench in the first part of the response. However, it is observed that the results start to deviate in consequence of a shifting between the responses. This can be solved by applying a smaller time step of $0.0001s$ contrary to the applied time step of $0.001s$. The finer time step the better fit is given between the responses.

However, a critical limitation of this method is that convergence difficulties appears when reaching the state of equilibrium as seen from Figure 67. The method is not able to handle a single horizontal cylinder positioned near the water surface. It is assumed that the Ansys Workbench uses the present formulation implemented in Nonlinear Wave Code as the responses are consistent with each other and the convergence of both keeps up with each other.

An additional limitation of the present method of evaluating the buoyancy forces is that the method does not account for the varying amount of submerged area which especially for horizontal cylinders does not imply an accurate representation of the buoyancy forces. The buoyancy forces are thus subjected once the center-line of the horizontal cylinder is in contiguity with the ocean water surface.

This buoyancy force formulation given as function of the submerged length is implemented in the Nonlinear Wave Code, given as *BuoyoncyForceVector.m*. However, these significant limitations of the present buoyancy force formulation imply that a different method of evaluating the buoyancy forces is used. In the present subsection 6.3 the hydrostatics of a single cylinder is determined by introducing numerical integration.

6.3 Buoyancy Forces as Function of the Submerged Area

In the present subsection a different approach of calculating the buoyancy forces of a submerged cylinder is introduced and implemented in the Nonlinear Wave Code.

The distributed excess buoyancy q_n of a cylindrical beam element is found by introducing numerical integration based on the trapezoidal rule. The distributed excess buoyancy q_n, acting normal to the beam axis as shown in Figure 68, is calculated as a function of the submerged area.

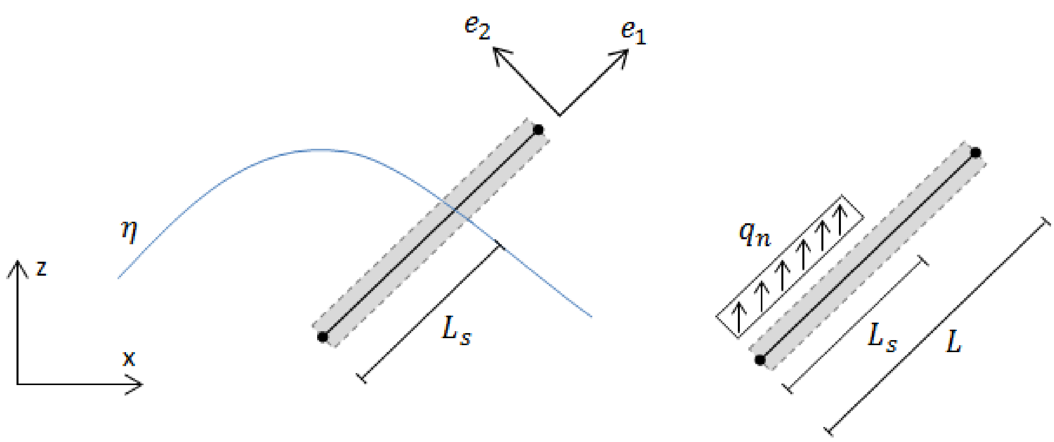

Figure 68: The distributed excess buoyancy of the submerged beam element.

The excess buoyancy of the submerged body is determined by the given formulation

$$q_n = \rho_w g A_s \tag{6.6}$$

in which A_s is the submerged cross-sectional area.

One major consideration regarding the buoyancy forces is the amount of submerged area of the structure. The challenge of using beam elements is defining the amount of submerged cross-sectional area when the structure is near the water surface. By implementation of beam elements, the shape of the structure is not fully described and therefor, the position of the beam elements does not specify the exact submerged volume of the structure.

An example of a cylinder with capped ends floating on the water surface is illustrated in Figure 69 and as seen a large volume is submerged.

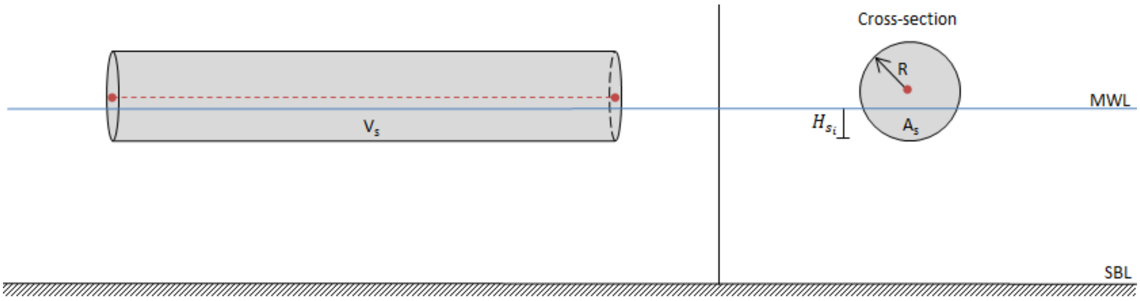

Figure 69: A cylinder with capped ends floating on still water. The beam element of the cylinder is marked with red.

Considering the cylinder as a beam element acting about its centre-line, the position of the beam is thus above the water surface as illustrated in Figure 69. Defining the water surface as the blue line, the submerged area is either zero (above the water surface) or the fully submerged area of the structure (under the water surface). This definition gives a large error for large volume structures.

A definition of the submerged cross-sectional area is implemented by considering the position of the beam element and the radius of the cylinder. For a horizontal cylinder, the submerged area is constant along the length of the cylinder by which the following expression of the submerged cross-sectional area is given by

$$A_s = R^2 \cdot \cos^{-1}\left(\frac{R - H_{s_i}}{R}\right) - (R - H_{s_i}) \cdot \sqrt{2R \cdot H_{s_i} - {H_{s_i}}^2} \tag{6.7}$$

For inclined beam elements the submerged area of a given cross-section varies along the beam element and the method of how to determine the submerged area at a given extraction point i is illustrated in Figure 70.

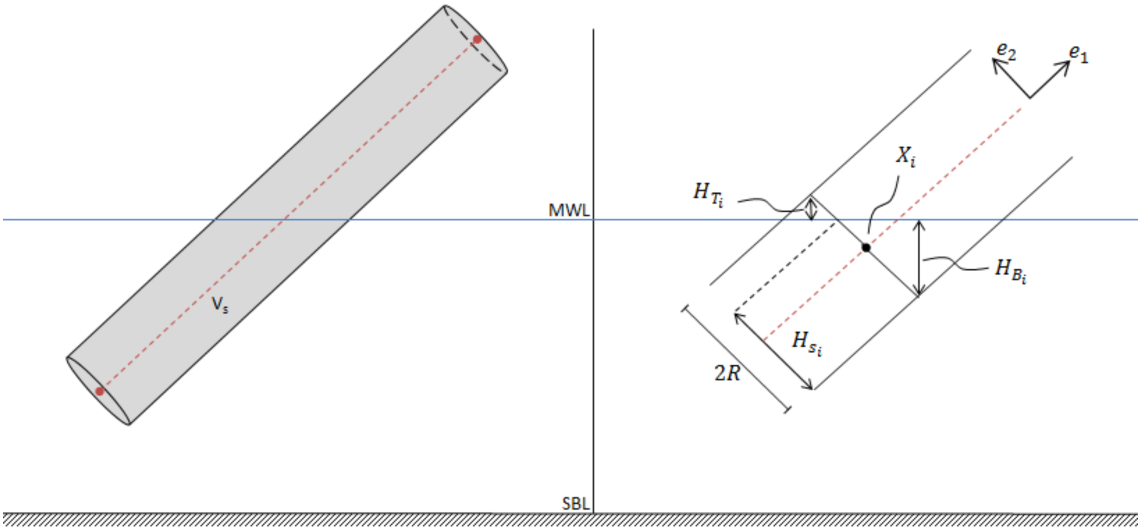

Figure 70: Floating inclined cylinder on still water. The principle of the calculation of the submerged area is illustrated on the right side of the figure. The beam element of the cylinder is marked with red.

As remarked from Figure 70, H_{s_i} is the only variable and is calculated in the following for a given extraction point X_i of the beam element. The distances H_{T_i} and H_{B_i} are obtained by

$$\begin{aligned} H_{T_i} &= \eta - (X_i + e_2 R)^T \cdot j \\ H_{B_i} &= \eta - (X_i - e_2 R)^T \cdot j \end{aligned} \tag{6.8}$$

where $X_i = [x_i, y_i]$ is the coordinate set for the extraction point i and $j = [0\ 1]^T$ is a unit vector directed vertically. e_2 is the unit vector perpendicular to the local beam axis. The submerged height H_{s_i} is obtained by

$$H_{s_i} = \begin{cases} 2R & if \quad H_{T_i} \geq 0 \\ \dfrac{2R}{\left(H_{B_i} - H_{T_i}\right)} H_{B_i} & if \quad H_{B_i} > 0 \ \wedge \ H_{T_i} < 0 \\ 0 & if \quad H_{B_i} \leq 0 \end{cases} \tag{6.9}$$

When the submerged height H_{s_i} is calculated the submerged area at extraction point i is obtained by (6.10). This definition of the submerged cross-sectional area is only valid when assuming a constant free surface elevation η at each extraction point i.

The total buoyancy effect is in contrary to the method formulated by A. Yazdchi not found by adding the two contributions: the distributed excess buoyancy q_n and the forces F_1 and F_2 due to hydrostatic pressures at the capped ends as illustrated in Figure 62. The total buoyancy effect is on the other hand as illustrated in Figure 68 determined by adding a transverse and tangential contribution given as

$$\begin{aligned} F_{qn1} &= \rho_w g A_s e_1\, j \\ F_{qn2} &= \rho_w g A_s e_2\, j \end{aligned} \tag{6.11}$$

The distributed excess buoyancy is subsequently transformed into global nodal forces by evaluating the product of the transposed interpolation functions $N(x)$ and the distributed excess buoyancy by introducing numerical integration as described in subsection 5.8. In the following subsections this present method of evaluating the buoyancy forces is validated.

6.4 Validation of Buoyancy Forces

In the same manner as for the buoyancy force formulation given by A. Yazdchi, validation examples are performed in the Nonlinear Wave Code and Ansys Workbench for the purpose of validating the buoyancy force formulation given as function of the amount of submerged cross-sectional area.

Validation of Buoyancy Forces for Vertical Cylinder

Recalling Figure 71, the first part of the validation is based on a vertical cylinder dropped in still water in which the initial position and state of equilibrium is illustrated.

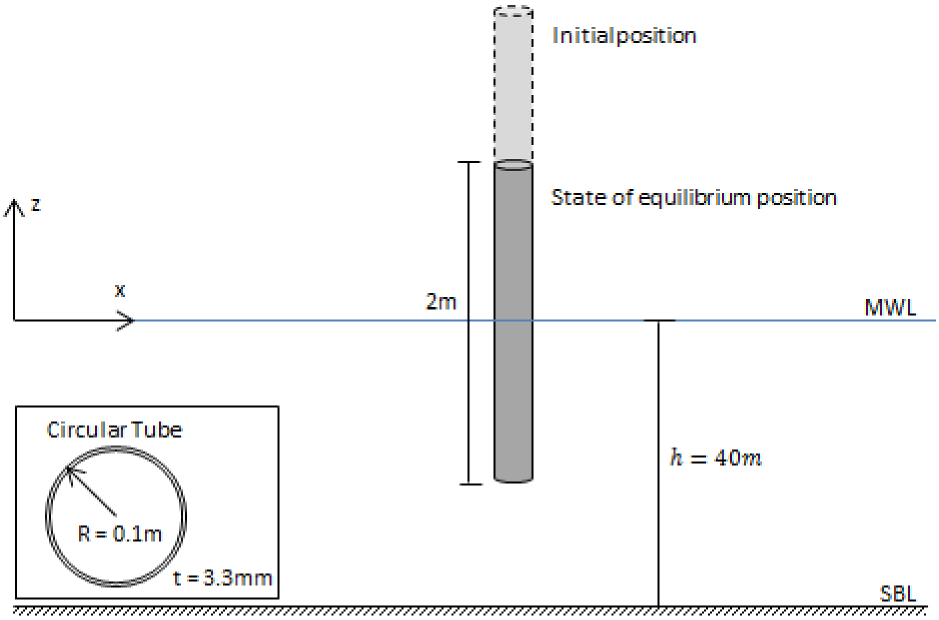

Figure 71: Validation of buoyancy formulation by a vertical cylinder.

The displacement, velocity and acceleration responses are extracted from the Nonlinear Wave Code and compared with the responses obtained by Ansys Workbench as shown in Figure 72.

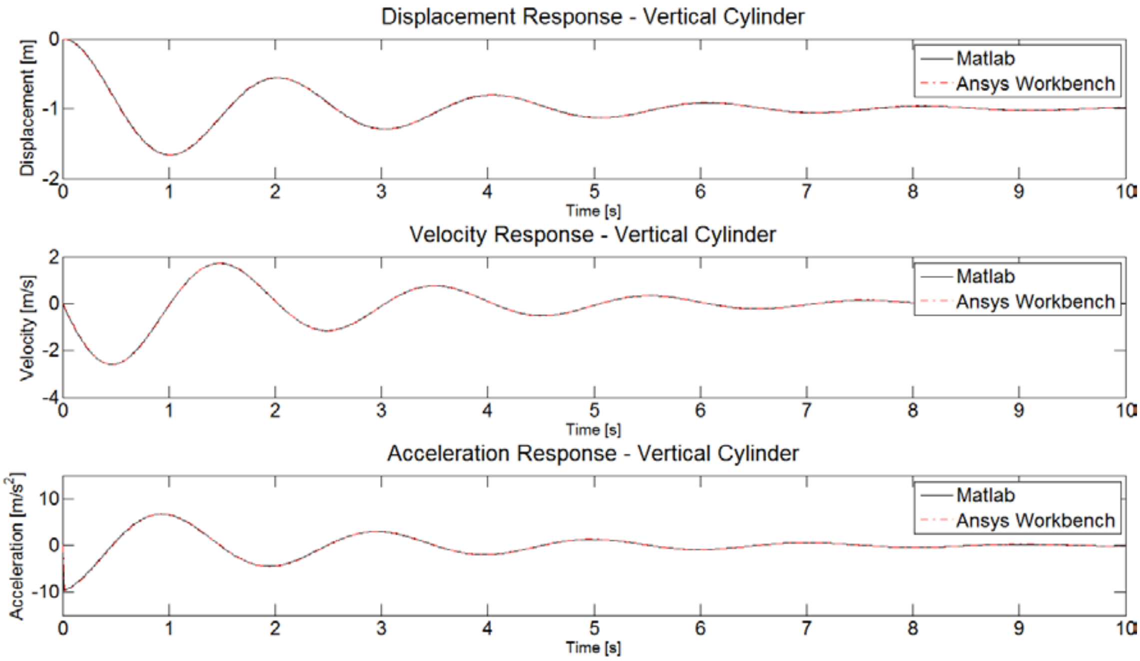

Figure 72: Buoyancy test performed on a vertical cylinder by numerical integration.

The responses are completely consistent with each other as observed. The deviation between the two results is found to be 0.8% which is consistent with the deviation obtained by the previous buoyancy force formulation of A. Yazdchi. This is due to that the buoyancy forces are subjected as function of the submerged element length for vertical cylinders, i.e. both method formulations are identical for vertical elements as long as the element discretization of the cylinder is identical.

Validation of Buoyancy Forces for Horizontal Cylinder

Recalling Figure 73, the second part of the validation is based on a horizontal cylinder dropped in still water in which the initial position and state of equilibrium is illustrated.

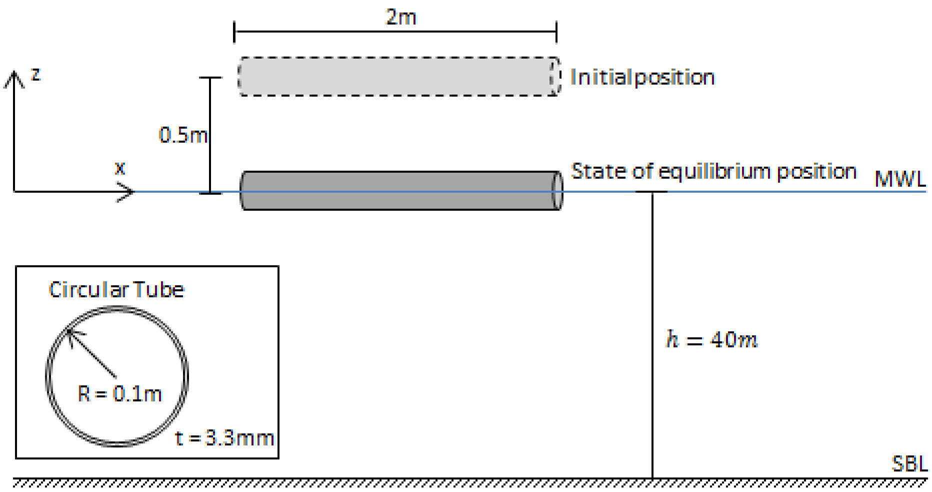

Figure 73: Buoyancy test on a horizontal cylinder.

It is not possible to validate the present method for a horizontal cylinder with Ansys Workbench as the buoyancy formulation used in Ansys does not as aforementioned consider the amount of submerged cross-sectional area. The predicted dynamic response of the horizontal cylinder is shown in Figure 74.

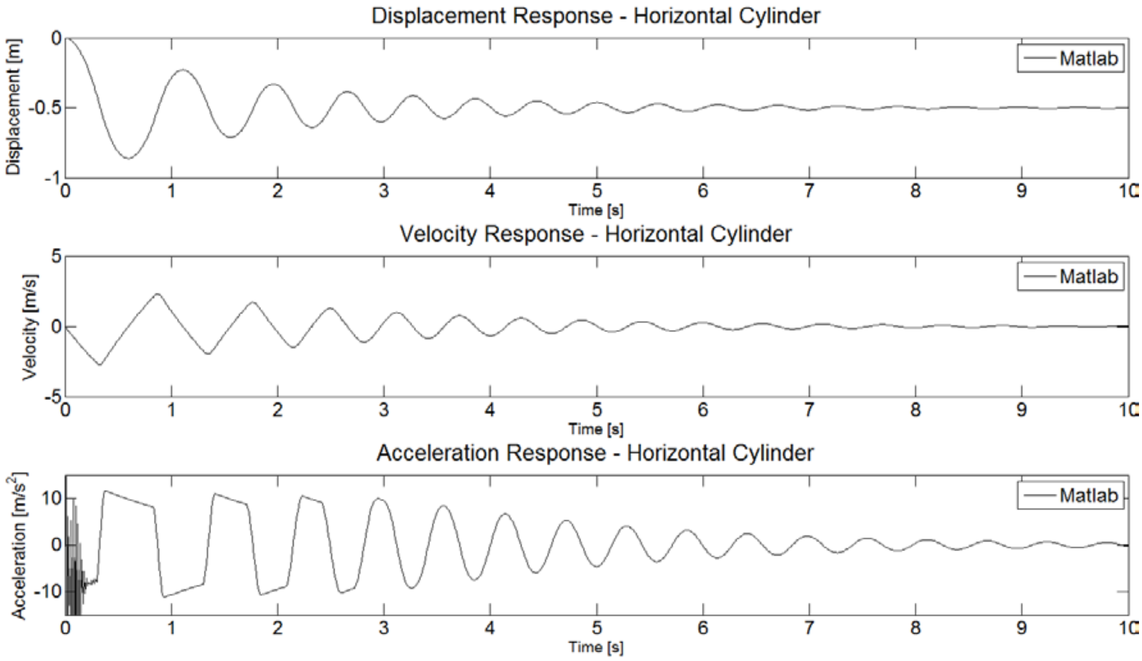

Figure 74: Buoyancy test performed on a horizontal cylinder by numerical integration.

As opposed to the previous buoyancy force method by A. Yazdchi, it is observed that the present method, in which the buoyancy forces are calculated as function of the submerged cross-sectional area, is able to represent the response of a horizontal cylinder in motion near the free water surface. This buoyancy force formulation is implemented in the Nonlinear Wave Code, given as *BuoyoncyForceVector.m*, and applied for the prediction of the loads and the response of the floating space frame structure.

6.5 Summary of Buoyancy Force Formulations

Two buoyancy force formulations are introduced and implemented in the Nonlinear Wave Code. The method given by A. Yazdchi determines the buoyancy forces as a function the submerged length of a cylinder while the buoyancy forces in the second method are determined as a function of the submerged cross-sectional area.

Comparing with the buoyancy force formulation in Ansys Workbench, the two methods provide identical results when considering vertical elements, while both Ansys Workbench and the method by A. Yazdchi has convergence difficulties when considering horizontal elements at the ocean water surface. The buoyancy forces are thus calculated as function of the submerged cross-sectional area for the prediction of the buoyancy forces subjected to the floating space frame in the project.

In preparation for the dynamic analysis of the floating space frame structure, the interaction between the buoyancy and wave loads is verified in the following Chapter 7.

7 Interaction between Buoyancy and Wave Loading

For the present the contribution from the buoyancy and the contribution from the wave loading has been introduced and validated independently. In this chapter the interaction between the buoyancy forces and the wave forces is validated for the purpose of predicting the response of a floating cylinder exposed to the nature of the ocean.

Firstly a simple example is investigated, in which a vertical cylinder is subjected to linear waves with the wave specifications given as $H = 1m$, $T = 15s$ and $h = 40m$, while the structural coefficients are set to $C_D = 0.5$, $C_M = 2$ and $C_A = 0$. The cylinder is structural supported so that it is able of moving vertically and horizontally, while the rotational degree of freedom is restrained. The objective of this example is to validate that the Nonlinear Wave Code is able to represent an accurate dynamic response of the interaction between buoyancy and wave loading for a floating vertical cylinder. The configuration of the example is illustrated in Figure 75.

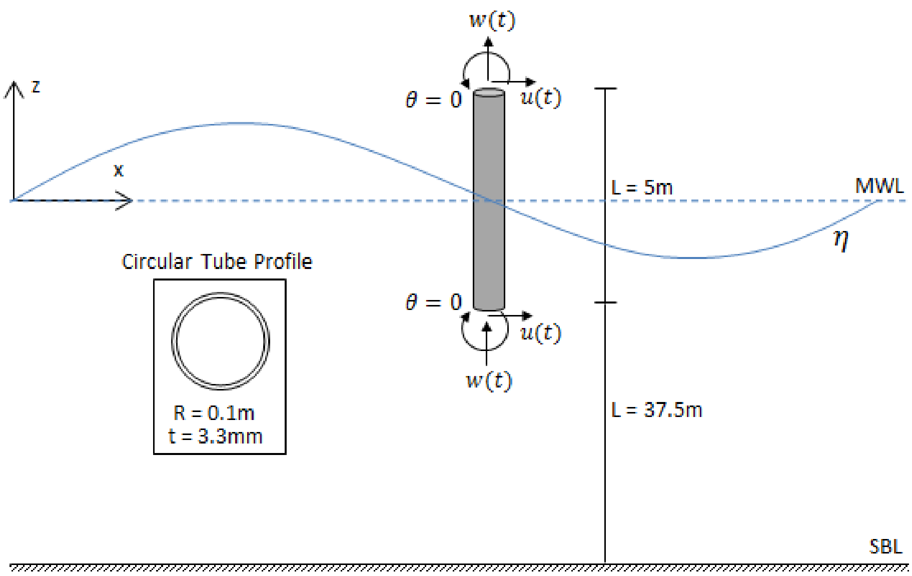

Figure 75: Cylinder tube exposed to both wave loads and buoyancy force simultaneously.

It is remarked that the added mass coefficient C_A is assumed to equal zero, which in the project for the purpose of improving the calculation time and simultaneous to prevent possible convergence difficulties. As confirmed in the project, the contribution from the inertia force is insignificant when considering slender cylinders, by which it is assumed to be valid to neglect the inertia force contribution obtained by the relative Morison formulation in the further calculations performed in the project.

The vertical cylinder is discretised into 20 beam elements while 10 extractions points are evaluated for each beam element obtain an sufficient representation of the wave and buoyancy forces. The response of the system is shown in Figure 76.

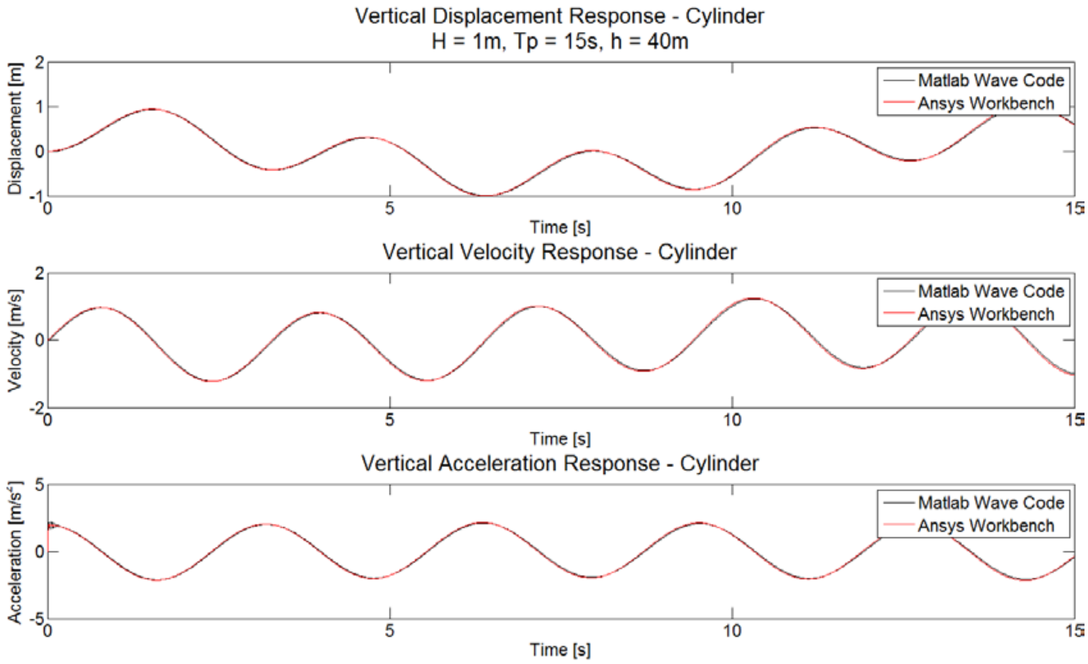

Figure 76: Vertical response of the cylinder tube subjected to both waves and buoyancy simultaneously.

The vertical response of the cylinder is consistent with Ansys Workbench. However, a deviation of approximately 10% exist between the results, which is reduced by dividing the cylinder into a sufficient number of elements. Figure 77 illustrates the horizontal response of the cylinder.

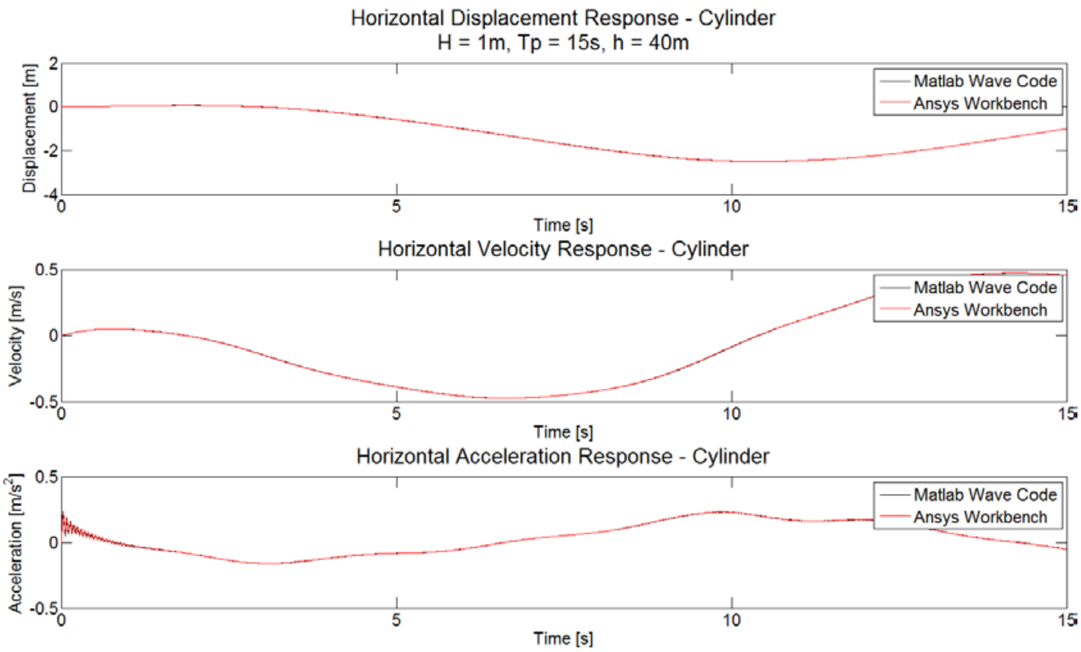

Figure 77: Horizontal response of the cylinder tube subjected to both waves and buoyancy simultaneously.

It is remarked that the horizontal response of the cylinder as well agrees with Ansys Workbench, by which it is verified that the Nonlinear Wave programme is able to represent vertical floating cylinders subjected to waves and buoyancy simultaneously. The deviation is found to be 2.5% which a significant smaller deviation compared to deviation obtained from the results of the vertical response of the cylinder.

It is additionally desirable to validate that the Nonlinear Wave Code is capable of predicting the response of a floating horizontal cylinder. However, it is recalled from subsection 6.2 that the Ansys Workbench is not able to represent the buoyancy effect on floating horizontal cylinders positioned near the free ocean water surface. In the following simple validation example the initial position of the horizontal cylinder is $5m$ under the water surface, i.e. the cylinder is initially fully submerged. The cylinder is likewise the previous example able to move in the vertical and horizontal direction, while the rotational degree of freedom is restrained. The configuration of the example is given in Figure 78.

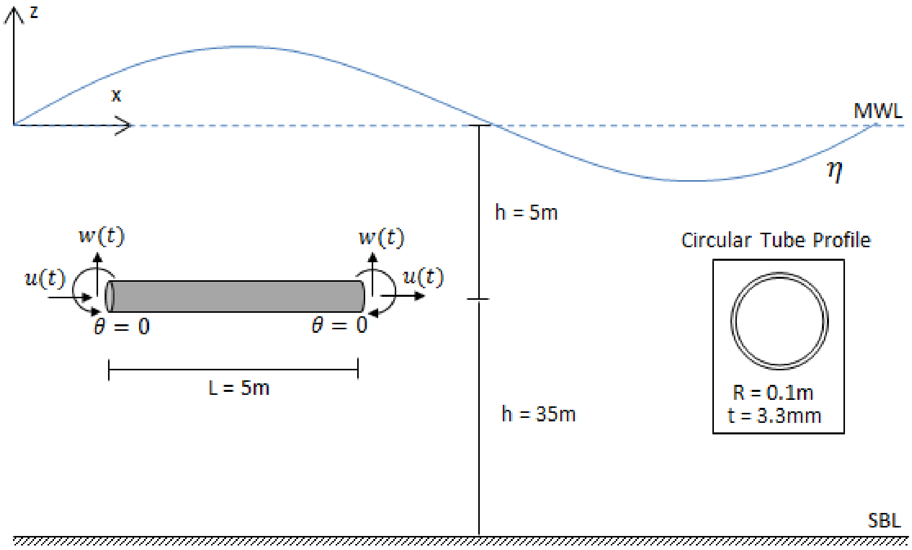

Figure 78: Initial position of the horizontal cylinder subjected to wave forces and buoyancy.

The horizontal cylinder is subjected to a linear wave with the same ocean specifications as given in the previous validation example. The dynamic response is shown in Figure 79.

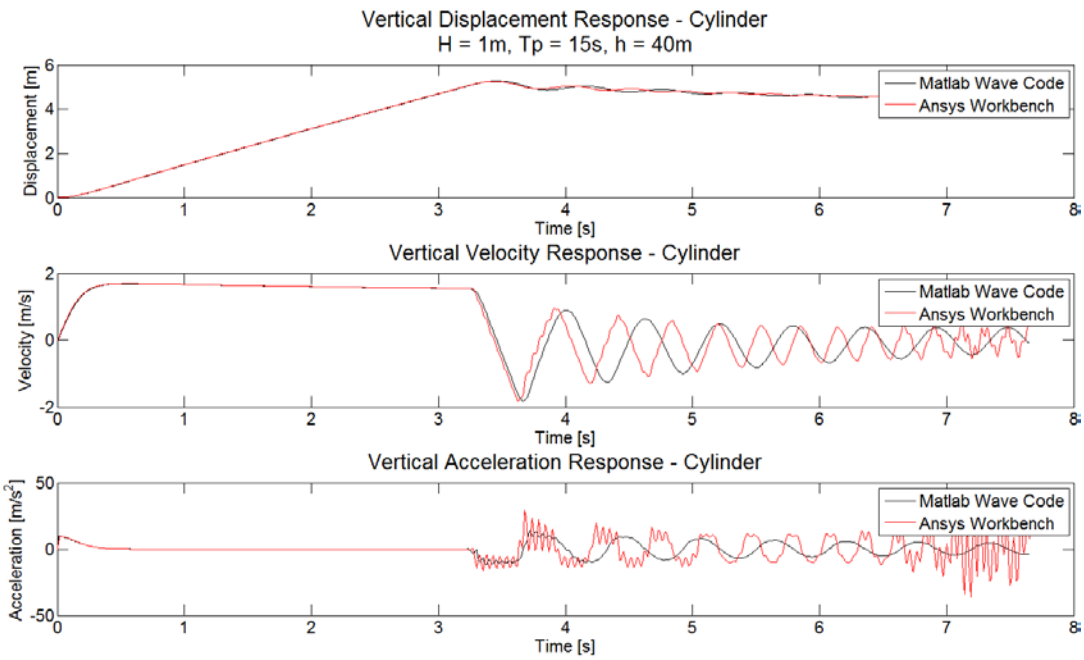

Figure 79: Vertical response of the horizontal cylinder tube which initially is fully submerged.

As expected the dynamic response of the floating horizontal cylinder represented by the Nonlinear Wave Code deviates in proportion to the results from Ansys Workbench. It is observed that the responses are consistent with each other during the first 3 seconds, which is because the horizontal cylinder still is fully submerged in that duration. As soon as the cylinder nears the ocean surface the deviation starts. As seen in Figure 79 the acceleration response becomes uncontrolled as the Ansys Workbench is not capable of representing the response of the cylinder near the free surface.

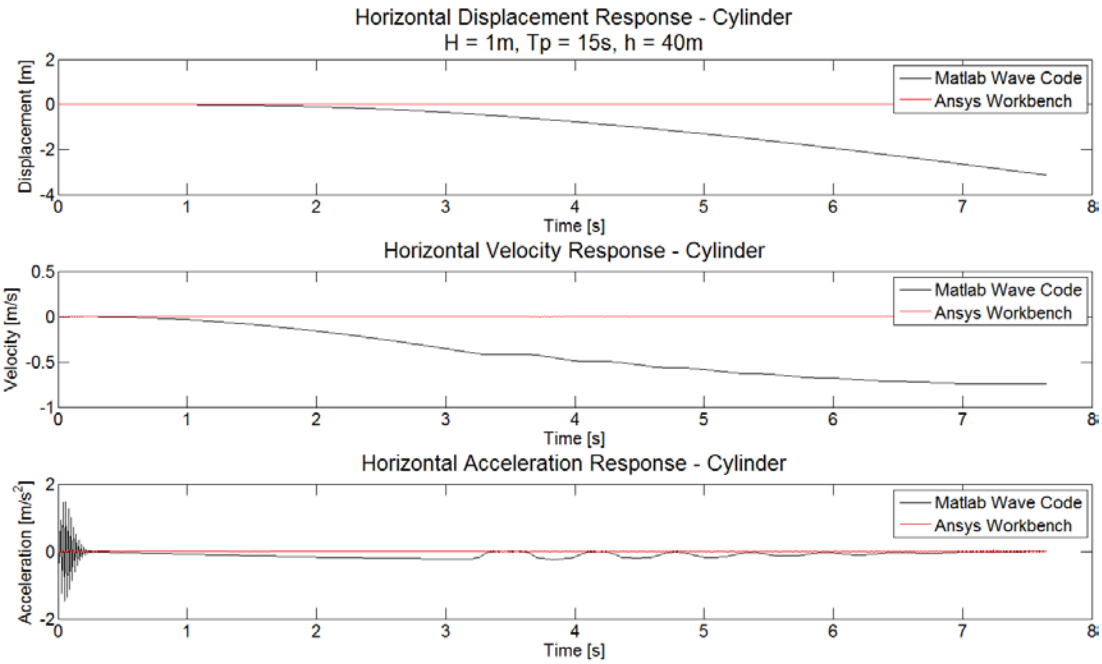

Figure 80: Horizontal response of the horizontal cylinder tube which initially is fully submerged.

Observing the horizontal response of the cylinder given in Figure 80, yet again no agreement is obtained between the two numerical programs. These deviations due to the formulation of the buoyancy and wave forces near the free ocean surface in Ansys Workbench give rise to a possible disagreement of the responses between the Nonlinear Wave Code and Ansys Workbench when analysing the floating space framed structure which is introduced in the following Chapter 8.

8 Floating Space Frame Structure

In this present chapter the time-domain dynamic response of the floating space frame structure is predicted by the Nonlinear Wave Code and compared with a response obtained from Ansys Workbench. The floating structure is as described in the introduction of the project constructed by offshore marine cables, a buoy and a space frame structure as shown in Figure 81.

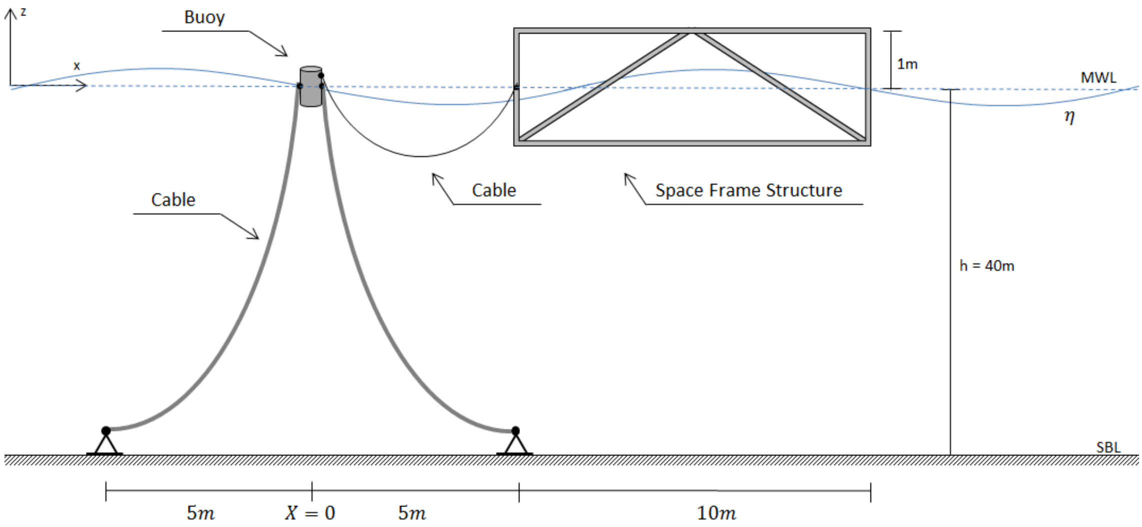

Figure 81: Floating structure consisting of offshore cables, a buoy and a space framed structure.

The dimensions are set in proportion to the mean water level while the surface elevation is only considered as an illustration. In reality the wave length is very long compared to the dimensions of the space frame structure and is thus not possible to illustrate correctly. Both the space frame and the buoy are initially subjected to a wave crest.

It has not been possible to model the anchoring ropes with cable specifications in Ansys Workbench by which no comparison of the predicted dynamic response of the floating space frame structure with anchoring cables is performed between the Nonlinear Wave Code and Ansys Workbench. Instead two analyses are performed

- In the first analysis the predicted dynamic response of the floating space frame structure with anchoring cables is only performed in the Nonlinear Wave Code.
- For the purpose of validating that the Nonlinear Wave Code is able to predict the response of the coupled floating structure the cables are in both Ansys Workbench and in the Nonlinear Wave Code modelled by cylindrical beam elements without cable specifications.

In the following subsections the modelling of the cables in the Nonlinear Wave Code is introduced and described, followed by an introduction to the modelling of the boundary conditions of the structure including charnier in both the Nonlinear Wave Code and in Ansys Workbench.

8.1 Modelling of Anchoring Cables

The modelling of the anchoring cables supporting the floating space frame structure and the buoy is based on a product information catalogue given by the manufacturer Phillystran. [7] The cables are modelled in the Nonlinear Wave Code as circular solid cross-sections in which the moment of inertia is reduced so that the cables are assumed to be flexible in bending, in which they only possess transvers stiffness. The cables used in the project are an approximation of realistic offshore anchoring cables.

The cable used as anchor line for the space frame structure is a wire rope manufactured in a 6x36 wire lay construction. The rope is designed for applications such as mooring lines and deep water buoy anchor lines. The diameter of the rope wire is $D_W = 32mm$ while the weight is given as $4.19kg/m$.

As regards the anchoring of the buoy, polyester fibre ropes manufactured in a 7x19 wire lay construction are used. These ropes are usually designed for applications such as mooring lines and deep water buoy anchor lines. The diameter of the rope is $D_W = 0.127m$ while the weight is given as $10.4kg/m$, and the length of these ropes is set to $L = 41m$.

8.2 Modelling of Charnier

Among other things, the connection between the cable and the floating structure is modelled by a charnier, as the beam ends between the cable and the floating structure not necessarily has the same rotation. This means that an extra rotation degree of freedom is introduced, hence one for each of the two elements. An example of a charnier in Node 2 of a beam appears in Figure 82.

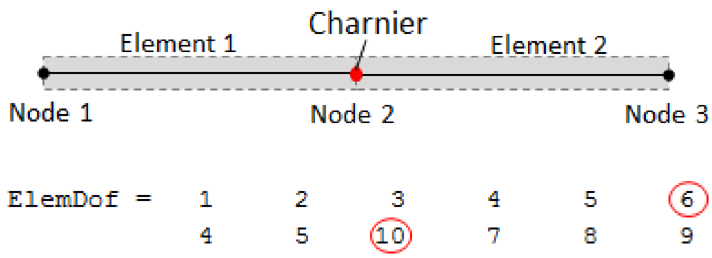

Figure 82: Charnier in Node 2 by which the rotation degree of freedom is not the same for both elements.

It is remarked that by implementation of a charnier in Node 2, the rotation degree of freedom is not identical for Element 1 and 2, although the node is shared between the two elements.

Validation of Charnier

The implementation of charnier is validated by creating a similar case as the single bar truss subjected to a transverse force in subsection 3.1 and compare the results of the two cases. The structure is simple supported and modelled with two bar trusses connected by a charnier as illustrated in Figure 83. The two bar trusses have the same length and cross-section as the single bar truss in the previous case but the subjected lateral force is doubled as the structure has two bar trusses.

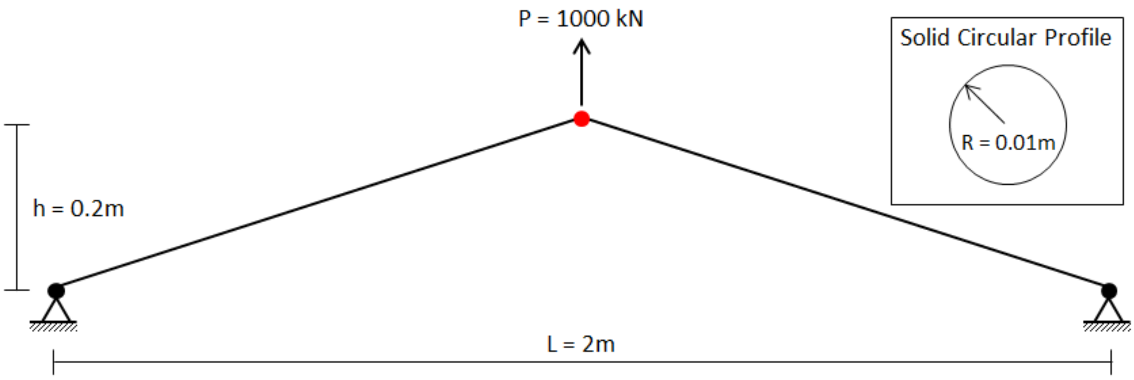

Figure 83: Two bar trusses subjected to a transverse force. The two trusses are held together by a charnier (red dot).

The initial configuration and deformed state of the structure is shown in Figure 84 and as remarked, the height h increases from $0.2m$ to $0.311m$ exactly as in the previous case in subsection 3.1.

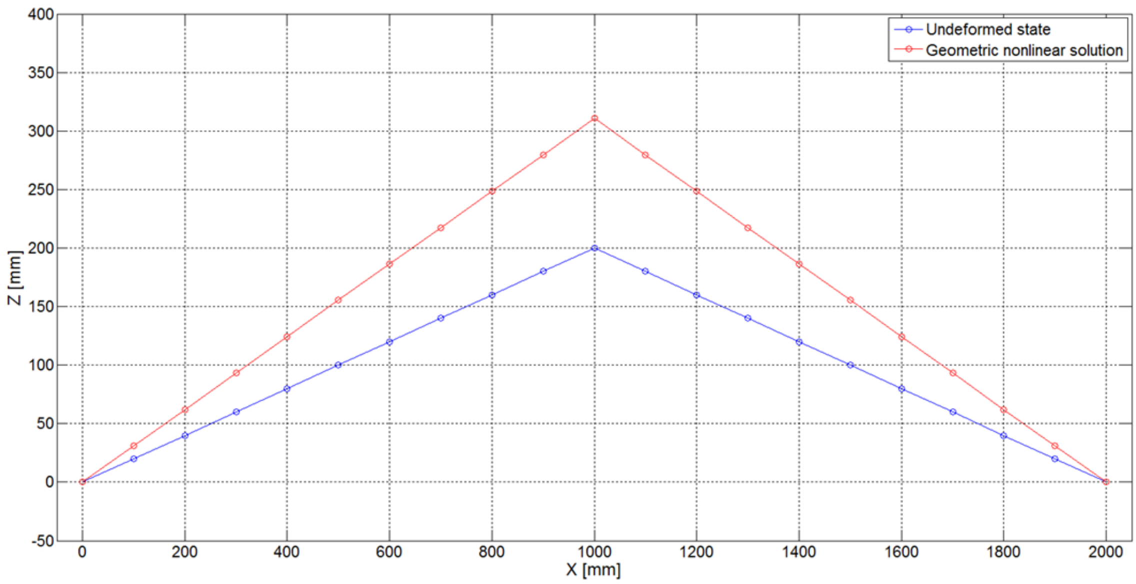

Figure 84: The initial configuration (blue line) and deformed state (red line) of the structure.

For further validation the load displacement results are compared for the two cases in Figure 85. The structure with charnier is denoted Charnier model.

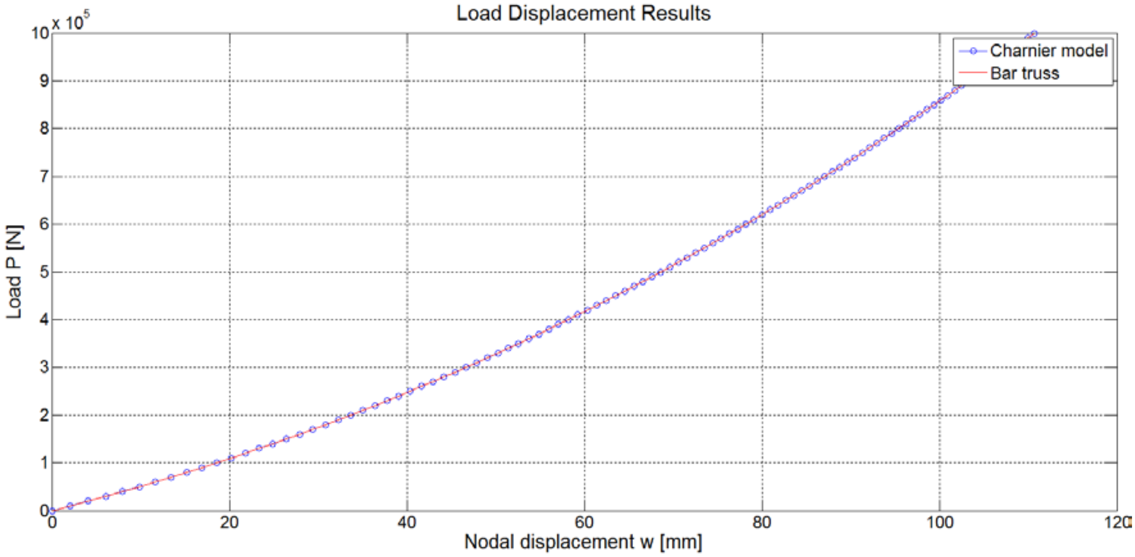

Figure 85: Load Displacement results of the structure (blue circles) and the bar truss (red line).

The structure with charnier responds in the same manner as the single bar truss in subsection 3.1, which is expected, as the two cases in principle are the same when subjected to a transverse force at the same point. The implementation of the charnier is thus validated.

8.3 Modelling of Buoy and Space Frame Structure

Both the buoy and the space frame structure are modelled by cylinders and the floating of these elements is ensured by modelling them so that the buoyancy is twice the self-weight of the elements. The design specifications of the buoy and the space frame structure are stated in Figure 86 below.

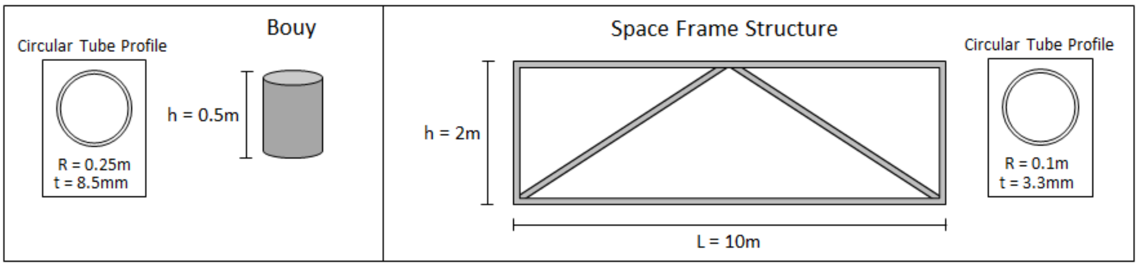

Figure 86: Design of buoy and space frame structure.

As remarked from Figure 86 the length of the space frame structure is five times the height of the structure. This design is chosen to avoid that the structure tilts while the height is set to $2m$ as far as possible to avoid that the horizontal cylinders get in contiguity with the ocean water surface as Ansys Workbench is not able to give a sufficient representations of the elements near the water surface. The design of the buoy is chosen with a view to ensure that the anchoring sea bed level ropes connected to the buoy, is not submerged due to the weight of the ropes.

8.4 Modelling of Boundary Conditions

The connection between the cables and the space frame structure and the buoy is modelled by charnier by which an extra rotational degree of freedom is introduced, one for each element. The charnier is thus an important boundary condition for the global dynamic response of the floating space frame structure. The insertion of the charnier marked with a red colored sphere is illustrated in Figure 87.

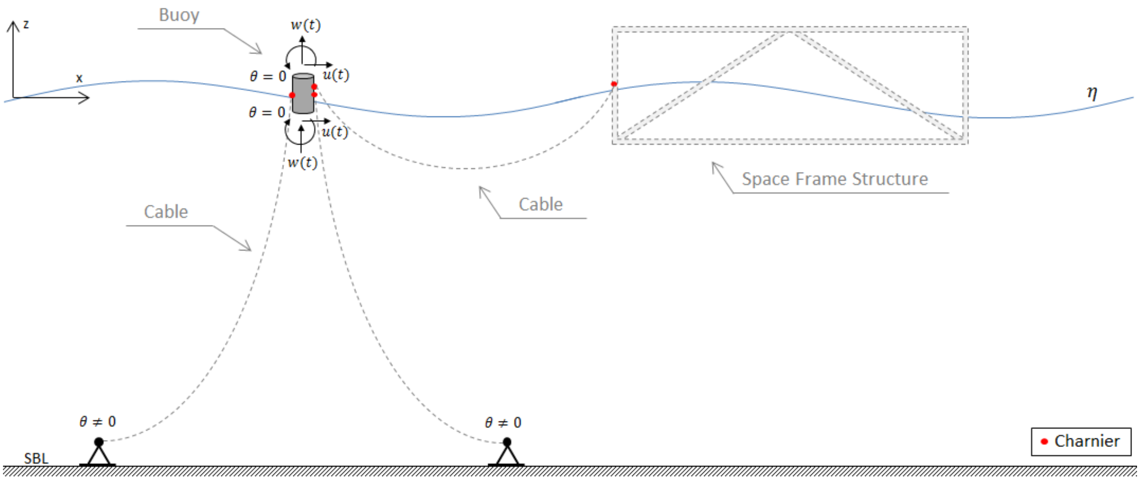

Figure 87: Boundary conditions of the floating space frame structure. The charnier is illustrated by a red sphere.

The buoy is free to follow the movement of the ocean waves, while the rotation of the buoy is restrained. The anchoring ropes are simply supported at the sea bed level, in which they are only able to rotate. This is done to avoid large moment forces and to obtain proper cable conditions.

In Ansys Workbench the charnier has been modelled by creating a body-to-body connection between two elements in the node connecting the elements, in which the rotation in the y-direction is set to free. The supports of the buoy and the ropes are modelled by means of *Remote Displacement* by which it is possible to control all the degree of freedoms in the considered node.

8.5 Dynamic Response of Floating Space Frame Structure

With implementation of the anchoring ropes and the boundary conditions, the dynamic response of the floating space frame structure is in the present subsection predicted in the Nonlinear Wave Code.

A time-domain analysis with simulation duration of $15s$ and a time step of $0.01s$ is performed. The structure is subjected to a linear wave with the wave specifications set to $H = 1m$, $T_p = 15s$ and ocean depth $h = 40m$. Both the horizontal and vertical displacement responses are extracted from the model with the appertaining velocity and acceleration responses. The dynamic response is predicted for both the buoy and the space frame structure at the node locations stated in Figure 88.

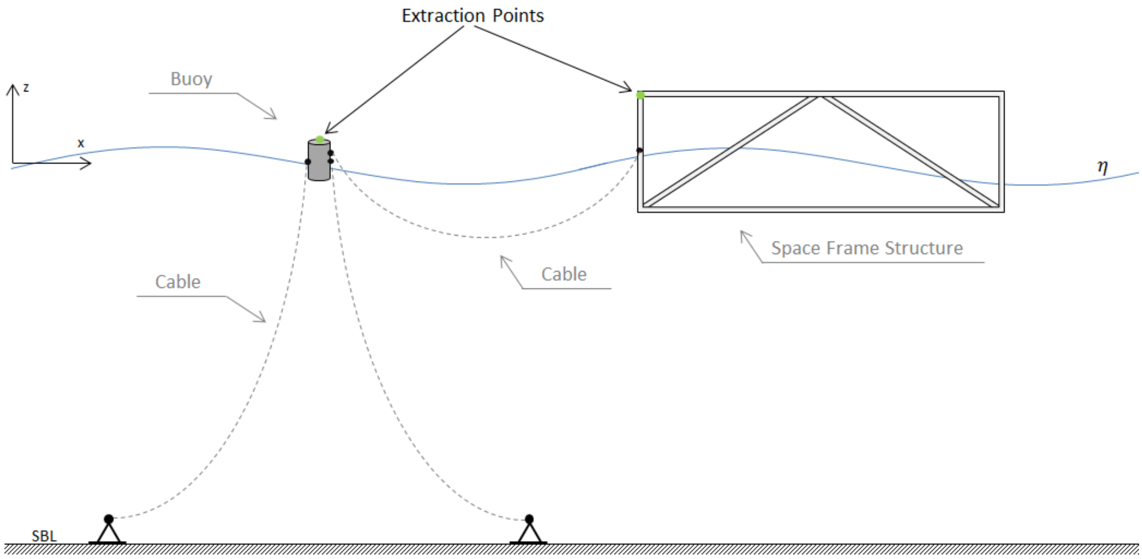

Figure 88: Extraction points for the global dynamic response of the floating space frame structure.

As determined through the convergence study performed in subsection 5.9, a large number of beam element divisions are needed to obtain an accurate representation of the hydrodynamic forces and buoyancy forces. In this simulation the total number of beam elements is 212 while 10 extraction points are applied for each beam element. The horizontal displacement, velocity and acceleration response for the buoy is extracted and given in Figure 89 below.

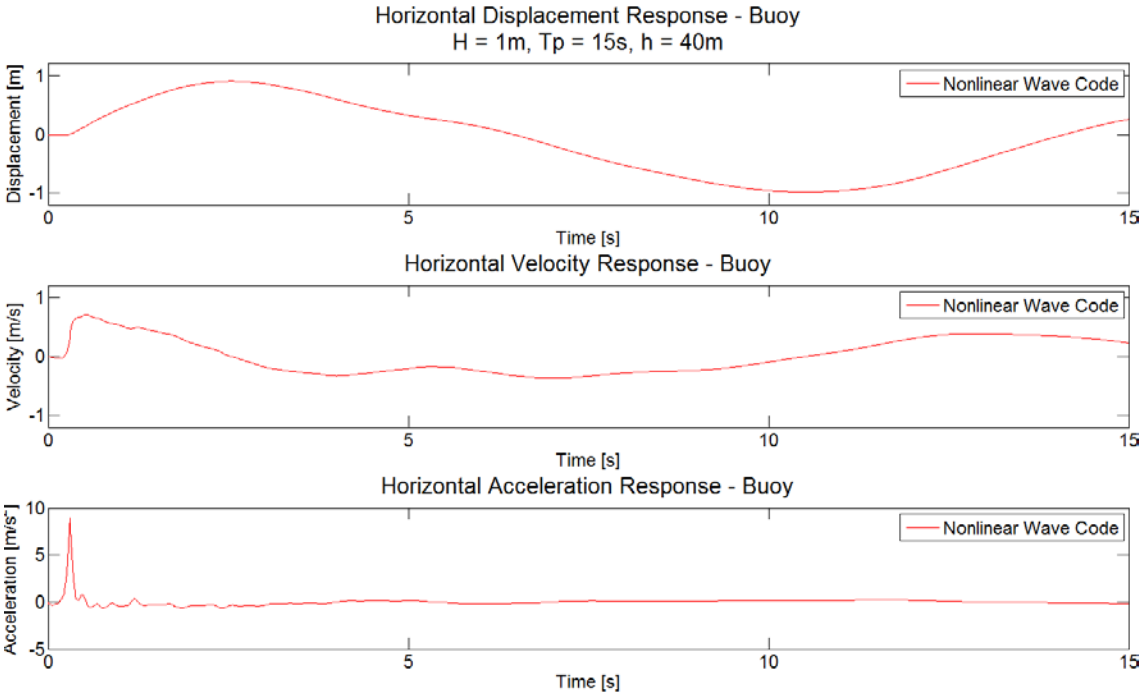

Figure 89: Horizontal dynamic response of the buoy.

As aforementioned the wave simulation is performed in a time duration of 15s which equals the duration of one wave period. In the initial configuration of the wave simulation, the floating structure is subjected to a wave crest in which the fluid velocity is maximum and the fluid acceleration is zero. This is remarked from the horizontal displacement response of the buoy as the displacement is positive in the duration of the wave crest while the displacement is negative during a wave trough. In Figure 90 the vertical response of the space frame structure is given.

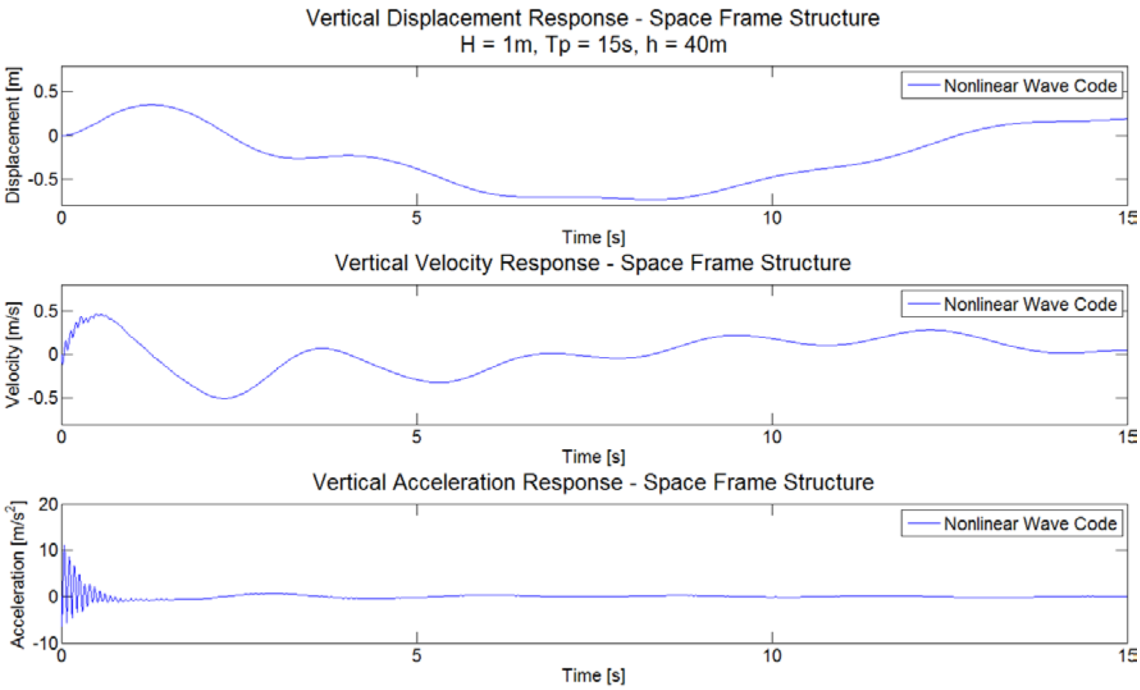

Figure 90: Vertical displacement response of space frame structure.

It is remarked from the vertical displacement response of the space frame structure that it yet again follows the motion of the wave. The structure is initially subjected to a wave crest which in interaction with the buoyancy moves the structure vertically. This is particularly observed by the first peak of the displacement response as a large part of the space frame structure initially is submerged. It is furthermore remarked that the magnitude of vertical displacement of the space frame structure equals the amplitude of the wave subjected to the structure. The motion of floating space frame structure is thus assessed to be physically realistic.

However, as aforementioned and remarked from Figure 89 and Figure 90 the Ansys Workbench has not been used as benchmark for the results obtained in the Nonlinear Wave Code. This is due to it has not been possible to model the anchoring ropes in Ansys Workbench. The limitation of the anchoring cable modelling in Ansys Workbench is explained in the following subsection.

Wave Modelling Limitation in Ansys Workbench

As aforementioned in subsection 8.1 the moment of inertia of the ropes is reduced in the Nonlinear Wave Code so that the ropes are without bending stiffness. To achieve the same structural properties in Ansys Workbench the ropes are tried modelled by two section types

- User Integrated cross-section
- LINK180-elements

Applying the User-supplied integrated section properties instead of basic geometry data, the area of section and moment of inertia are typed in manually as required by the user by means of APDL commands. However, the User Integrated cross-sections have no solid representation and are thus not able to represent the hydrodynamic forces. These User Integrated cross-sections do give a solution but not a valid representation of the hydrodynamic forces subjected to the structure.

Another approach of representing the ropes of the structure is to use the LINK180-elements, which is a uniaxial tension-compression element normally used to model trusses, cables and links. According to the Mechanical APDL reference in Ansys, the LINK180-element is able to represent hydrodynamic added mass and loading, while buoyant loading is available. However applying this bar-element the Ansys Workbench solver does not converge which according to the *Solution Information* in Ansys is due to the flooding option does not work with LINK180-element.

It has thus not been possible to represent the cable section properties in Ansys Workbench. A simulation is instead performed in both the Nonlinear Wave Code and Ansys Workbench to predict the response of the floating space frame structure without using cable specifications. The purpose is to validate that the Nonlinear Wave Code is able to represent the response of the coupled floating structure.

Dynamic Response of Coupled Floating Space Frame Structure

In the following subsection the predicted dynamic response obtained in the Nonlinear Wave Code and Ansys Workbench for the coupled floating space frame structure without structural cable properties is introduced.

A time-domain analysis with simulation duration of $15s$ and a time step of $0.01s$ is performed. The structure is subjected to a linear wave with the wave specifications set to $H = 1m$, $T_p = 15s$ and ocean depth $h = 40m$. The total number of beam elements is 212 while 10 extraction points are applied for each beam element. Both the horizontal and vertical displacement response is extracted from the model with the appertaining velocity and acceleration responses. The dynamic response of the buoy is illustrated in Figure 91.

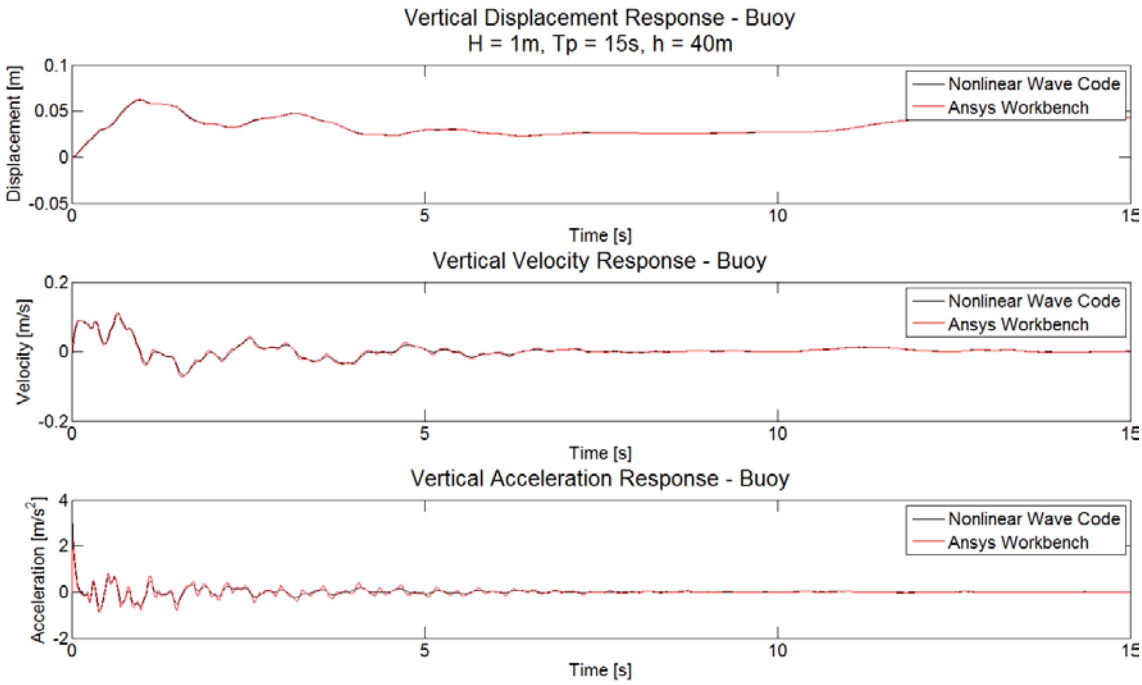

Figure 91: Comparison of vertical response for the buoy between the Nonlinear Wave Code and Ansys Workbench.

As no structural cable properties are applied, it is observed from Figure 91 that the vertical displacement of the buoy is small. The stiff cables damp the motion of the buoy. However, it is seen that the predicted response in the Nonlinear Wave Code is consistent with the wave modelling in Ansys Workbench. The deviation is determined to be 1.1%. In Figure 92 the horizontal response of the buoy is illustrated.

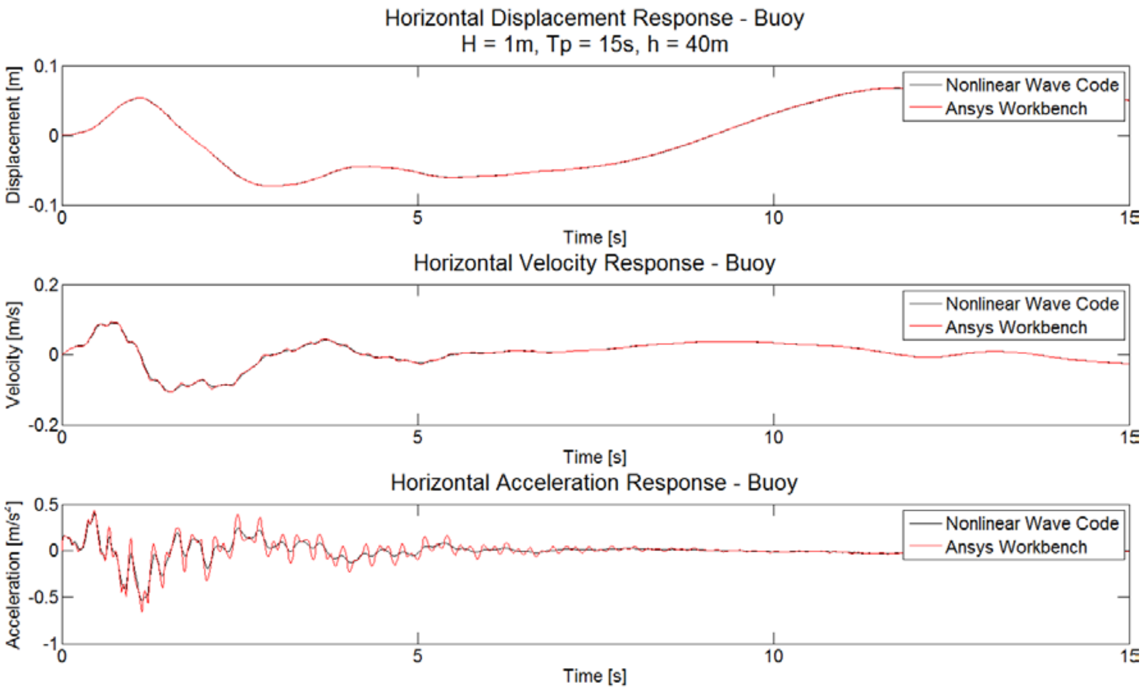

Figure 92: Horizontal displacement for the Nonlinear Wave Code compared to Ansys Workbench.

Yet again it is remarked that the predicted horizontal displacement of the buoy obtained by the Nonlinear Wave Code agrees with Ansys Workbench. The deviation of the displacement response between the Nonlinear Wave Code and Ansys Workbench is determined to be 1.7%. However, a clear deviation is observed for the acceleration response. A finer time step and finer mesh of the floating structure in the Nonlinear Wave Code implies a more accurate prediction of the dynamic response and hereby the acceleration response. The vertical response of the space frame structure is given in Figure 93.

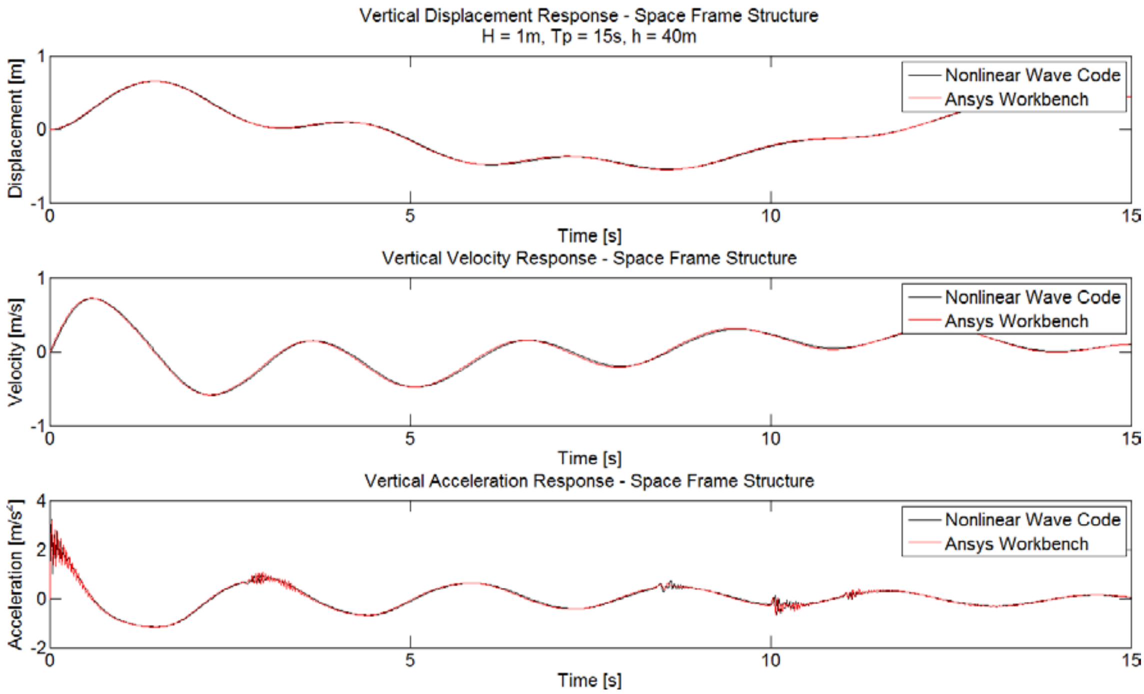

Figure 93: Comparison of vertical response of the space frame structure.

It is remarked from Figure 94, that the space frame structure follows the motion of the wave. The structure is initially subjected to a wave crest which in interaction with the buoyancy moves the structure vertically. The deviation of the vertical displacement response between the Nonlinear Wave Code and Ansys Workbench is for the space frame structure determined to be 6.4%. The deviation of the dynamic response for the space frame structure is in general larger than the deviation obtained for the buoy, which additionally is confirmed by a deviation of 14.3% for the horizontal displacement response between the Nonlinear Wave Code and Ansys Workbench. The horizontal displacement response of the space frame structure is illustrated in Figure 95.

The most interesting of the predicted response of the coupled floating structure is the response of the space frame structure. This is due to the space frame structure consist of vertical, horizontal and inclined elements while the buoy only consists of one vertical cylinder. Considering the limitation of the wave modelling in Ansys Workbench which is not able to deal with horizontal elements near the free ocean surface, a deviation is expected to occur when the horizontal elements of the space frame structure nears the free water surface. Trying to reduce this source of deviation the height of the space frame structure is set to $2m$ to avoid that the horizontal cylinders get in contiguity with the ocean water surface. However the inclined has also an influence on the deviation. The horizontal response is given in Figure 96.

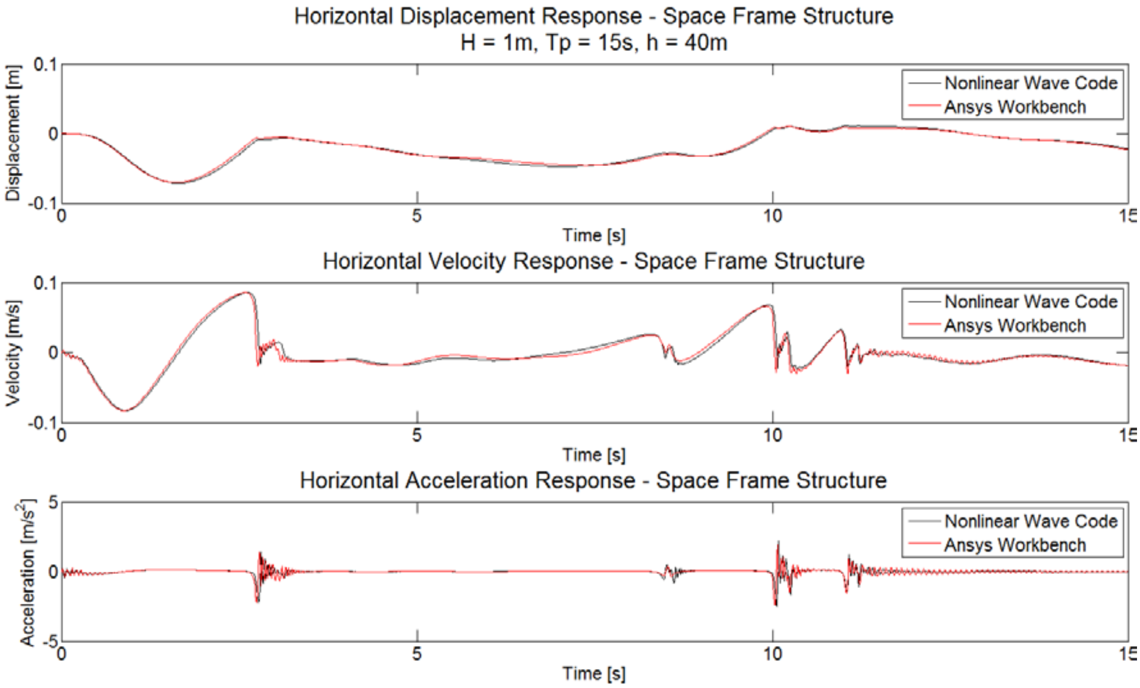

Figure 96: Horizontal response of the space frame structure.

Considering the horizontal displacement response of the space frame structure, it is remarked that the magnitude of the displacement is small. This is due to among other things the stiff cable connecting the buoy and the space frame structure which damps the motion of the space frame structure.

It is however remarked that the response obtained by the Nonlinear Wave Code generally agrees with Ansys Workbench. Considering the obtained results between the two programmes, it can be concluded that the Nonlinear Wave Code is able to predict the hydrostatics and hydrodynamic forces and the dynamic response of the coupled floating space frame structure.

9 Conclusion

The objective of this project is the prediction of the loads and the dynamic response of the floating slender space frame structure in the time-domain. The floating space frame structure is an integrated dynamic system consisting of a space frame floater, a buoy and moorings. All structural components are modelled by cylindrical beam elements based on the Bernoulli-Euler beam theory. All calculations in the project are performed numerically in the Nonlinear Wave Code, which is based on a corotational beam formulation. The implemented geometric nonlinear formulation allows the floating space frame structure to have arbitrarily large displacements and rotations at the global level. The Nonlinear Wave Code is capable of evaluating buoyancy forces and wave loading on arbitrarily designed restrained and floating slender offshore structures in different sea states.

The hydrodynamic forces are represented by two methods. In the first method the differential hydrodynamic forces are represented by a higher order polynomial regression. This method requires a high discretization of the beam elements near the free ocean surface to give an accurate prediction of the wave forces. This method gives an accurate hydrodynamic load prediction for fully submerged elements, while error estimation is introduced when the elements are partially submerged.

In the second method the hydrodynamic forces are represented by numerical integration, which is preferred compared to the polynomial regression, as this method gives sufficient accurate prediction of the wave forces for fully and partially submerged elements. The approach of representing the hydrodynamic forces is used in the prediction of the loads and dynamic response of the floating space frame structure.

Two buoyancy force formulations are implemented in the Nonlinear Wave Code, in which the first method evaluates the buoyancy forces as a function the submerged length of a cylinder. The buoyancy forces in the second method are determined as a function of the submerged cross-sectional area which is proven to be a more accurate and stable approach.

The floating space frame structure is modelled with a fine mesh to obtain a sufficient representation of the ocean loads and the dynamic response of the structure. A time-domain analysis with simulation duration of $15s$ is performed, in which the structure is subjected to a linear wave. The floating space frame structure is modelled in both the Nonlinear Wave Code and Ansys Workbench, in which the predicted loads and dynamic responses are consistent with each other. It is concluded that the Nonlinear Wave Code is able to predict the hydrostatics and hydrodynamic forces and the dynamic response of a floating slender space frame structure.

10 Reference List

[1] »»WEPTOS™ Innovating in Wave Energy,«,« [Online]. Available: http://www.weptos.com/wp-content/uploads/2011/12/Book-about-WEPTOS_144-dpi.pdf.

[2] »»Types of offshore wind turbine foundations,«,« [Online]. Available: http://www.aquaticbiosystems.org/content/10/1/8/figure/F4?highres=y.

[3] 2D Corotational Beam Formulation by Louie Yaw, Walla Walla University, Nov 30, 2009.

[4] Buoyancy forces and the 2D finite element analysis of flexible offshore pipes and risers by M. Yazdchi and M.A. Crisfield, Department of Aeronautics, London, 2002..

[5] Water Wave Mechanics by Thomas Lykke Andersen, Department of Civil Engineering, Aalborg University, August 2012.

[6] DNV, »Design of Offshore Wind Turbine Structures DNV-OS-J101,« 2013 January..

[7] »Phillystran,« [Online]. Available: http://www.phillystran.com/Markets2/Towing-Lines.

[8] Generation and Analysis of Random Waves by Zhou Liu, Laboratoriet for Hydraulik og Havnebygning, 3. udgave, Aalborg University, januar 2001.

[9] Analysis of Waves by Peter Frigaard, Department of Civil Engineering, Aalborg University, May 2012.

[10] DNV, »Enviromental Conditions and Enviromental Loads DNV-RP-C205« , October 2011..

[11] DNV, »Global performance of Deep Water Floating Structures DNV-RP-F205« , October 2004..

[12] DNV, »Design of Floating Wind Turbine Structures DNV-OS-J103,« 2013 June

[13] DNV, »Design of Offshore Steel Structures, General (LRFD Method) DNV-OS-J101,« 2011 April.

[14] Concepts and Application of Finite Element Analysis by Robert D. Cook, 4th Edition, University of Wisconcin - Madison..

[15] Engineering Vibration by DanielJ. Inman, 3rd Edition, 2007.

[16] Structural Analysis by Aslam Kassimali, 4th Edition, Cengage Learning,2011.

[17] Non-linear Modeling and Analysis of Solids and Structures by Steen Krenk, Cambridge University Press, 2009.

[18] T. Fischer, »WP4: Offshore Foundations and Support Structures,« UpWind, 2006.

[19] NAFEMS Introduction to Nonlinear Finite Element Analysis, Edited by E. Hinton, Published by NAFEMS Ltd, Scotland United Kingdom.

[20] Mechanics and Analysis of Beams, Columns and Cables, 2nd Edition by Professor Steen Krenk, Published by Polyteknisk Press, Denmark, 2000.

11 Appendix A

Method of Wave Modelling in Ansys Workbench

In the following Chapter the wave modelling in Ansys Workbench is described. The wave modelling is introduced by means of an extension pack available at the homepage of Ansys Workbench. The steps behind the wave modelling are described and graphical views of the options are introduced.

The wave modelling in Ansys Workbench is implemented by means of the Ocean Environment command, which is included in Ansys Workbench by installation of the Offshore Extensions Pack that is available on the Ansys homepage. By the Ocean Environment it is among other things possible to input the basic environment through OCTYPE, Basic along with the ability to adjust the mean water level and sea bed level from the global origin. Furthermore it is possible to control the flooding input of local variation of drag and inertia coefficients based on Z level as handled under OCZONE.

The first step of the wave modelling is to define the basic properties once the Ocean Basic load icon is clicked. The properties to be defined are the Ocean Mean Water Level and the Sea Bed Level which are measured from the global origin.

Offshore | Ocean Environment

General	
Ocean Mean Water Level	0 [m]
Ocean Sea Bed Level	-40 [m]
Ocean Depth	40 [m]
Ocean Density	1025 [kg m^-1 m^-1 m^-1]
Standard Earth Gravity	9,81 [m sec^-1 sec^-1]

Figure 97: Definition of the MWL and SBL.

The graphic of the position of the Mean Water Level and Sea Bed Level is automatically updated based in the user entry. Unless the density and standard earth gravity are user defined, they defaults to 1025 $\frac{kg}{m^3}$ and 9.81 $\frac{m}{s^2}$, respectively. The next step is to define the structural coefficients.

Structural Coefficients	
Default Member Flooding	True
Added mass ratio-Cay	1
Added mass ratio-Caz	1
Buoyancy Force Ratio	1
Tabular Input Options	Z Level
Coefficients By Depth	Tabular Data

Figure 98: Definition of the added mass ratio.

The added mass ratio defaults to the value 1, but can be set as required. The flooding behaviour of the structure is defined by either the true or false option as illustrated below here.

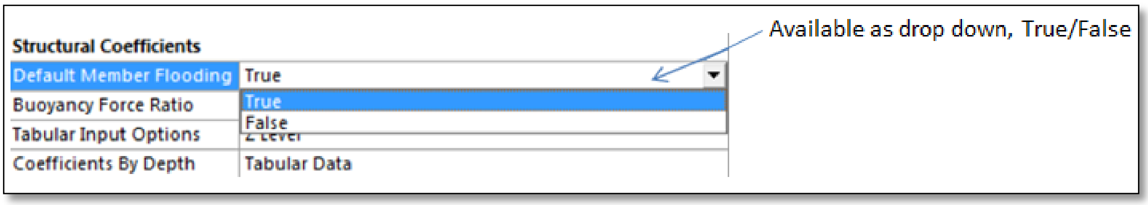

Figure 99: Selection of the flooding behaviour of the structure.

The Structural Coefficients consisting of the drag- and inertia coefficients are given as tabular data under the function "*Coefficients by Depth*".

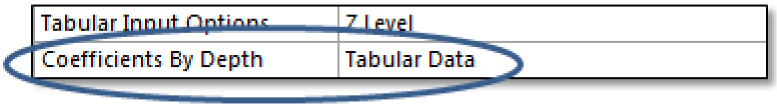

Z level	Drag Coefficient in Y, CDY	Drag Coefficient in Z, CDZ	Drag Coefficient in X, CTX	Mass Coefficient in Y, CMY	Mass Coefficient in Z, CMZ
0 [m]	1	1	1	2	2
-40 [m]	1	1	1	2	2

Figure 100: Definition of the structural coefficients as function of the ocean depth.

The Structural Coefficients are as shown in above-mentioned Figure 100 as function of the depth. It is possible to add more rows if the structural coefficients are varying with depth. The next step is to define the wave theory.

Wave Options	
Wave Theory	Airy
Wave Case Definition	Tabular Data
Force Application	Act on Elements at their actual location

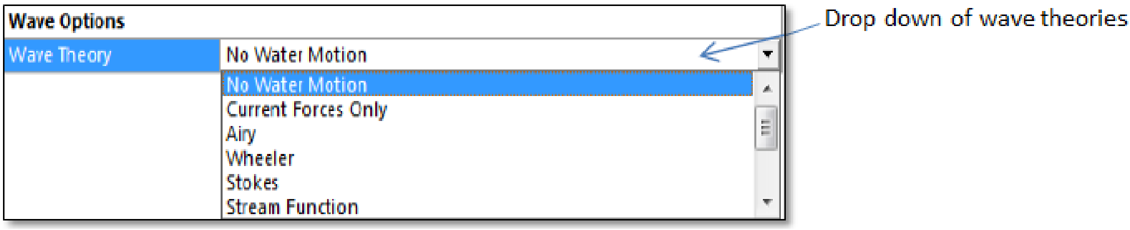

Figure 101: Selection of the wave theory.

After defining the General and Structural Coefficients properties, the wave options which are available under the drop down of Wave Theory has to be defined as illustrated in Figure 101. After selecting the wave theory, the parameters of the wave in the property table are to be defined as shown in Figure 102.

Load Step	Time duration	Wave Direction	Current Definition	Wave Period	Wave Height	Phase Shift	Case Name
1	10	0 [°]	Disable Current	10 [sec]	3 [m]	0 [°]	Wave Case No. 1:0 [°]:10 [sec]:3 [m]:0 [°]

Figure 102: Definition of the wave parameters in different load steps.

The rows are dynamically created based on the number of steps issued in the Analysis Settings. It is furthermore possible to define random waves by means of the JONSWAP spectrum.

12 Appendix B

In this appendix the Nonlinear Wave Code written in the programming language Matlab is introduced. Only the main scripts are included, while reference is made to the Appendix DVD for the complete version of the produced Nonlinear Wave Code.

```
#####################################################################
% M.sc. in Civil and Structural Engineering - Master Thesis
% Nonlinear Time-domain Analysis of Floating Space Frame Structures
% Nonlinaer Wave Code
% Authors: Alaa Taha & Arber Kadriu
% ------------------------------------------------------------------
% InputData
#####################################################################

function [nCoord,eTop,force,NodeFix,ch,NumberNewPoints,E,rhoS,eMat,...
A,I,eSec,waveTheory,MWL,h,H,T,Do,CDn,CDt,CM,CA,rhoW,ny,k,g,nf,...
phases,t] = InputData;

% Design of the Floating Space Frame Structure
%====================================================================
load('Coordinates.TXT');
mainCoord = Coordinates;

load('MainTopology.TXT')
mainTop = MainTopology;

% Discretization of Structure
for i=1:length(mainTop(:,1));
NumberNewPoint = 0;
xvals(i,:) = linspace(mainCoord(mainTop(i,1),1),
mainCoord(mainTop(i,2),...
             1), NumberNewPoint+2);
yvals(i,:) = linspace(mainCoord(mainTop(i,1),2),
mainCoord(mainTop(i,2),...
             2), NumberNewPoint+2);
end

xvals = xvals';
yvals = yvals';

x = xvals(:);
y = yvals(:);
xy = [x,y];

nCoord = unique(xy,'rows','stable');

load('Topology.TXT')
eTop = Topology;

% Static Boundary Conditions
%         Node    Force
force = [             ];
```

```
% Geometric Boundary Conditions: FixedDof(:,1)
%            node  dofs
NodeFix   = [  1   0 0 1
             103   0 0 1
             108   1 1 0
             113   1 1 0];

% Charnier at Node
%      Element  Node
ch = [  51       2
        52       1
       113       1
       132       2  ];

% Extra Points
%======================================================================
NumberNewPoints = 10 ;

% Material and cross section parameters of the structure
%======================================================================
E = [200e9    % Young Modulus
     200e9
     200e9
     200e9];

Do = [0.5     % Outer cylinder diameter [m]
      0.127
      0.032
      0.200];

Di = [Do(1,1)*0.96681   % Inner cylinder diameter [m]
      0.000
      0.000
      Do(4,1)*0.96681];

A = [((Do(1,1)/2)^2)*pi - ((Di(1,1)/2)^2)*pi % Cross-Sectional Area
     ((Do(2,1)/2)^2)*pi - ((Di(2,1)/2)^2)*pi
     ((Do(3,1)/2)^2)*pi - ((Di(3,1)/2)^2)*pi
     ((Do(4,1)/2)^2)*pi - ((Di(4,1)/2)^2)*pi];

I = [(pi*(Do(1,1)^4 - Di(1,1)^4)/64)         % Second Moment of Area
     (pi*(Do(2,1)^4 - Di(2,1)^4)/64)
     (pi*(Do(3,1)^4 - Di(3,1)^4)/64)
     (pi*(Do(4,1)^4 - Di(4,1)^4)/64)];

rhoS = [7850                              % Density of the Structure
        10.4/A(2,1)
        4.19/A(3,1)
        7850];

% Assign Materials to Elements
eMat = [ ones(1,102)*2 ones(1,10) ones(1,20)*3 ones(1,80)*4] ;
% Assign Cross-sections to Elements
eSec = [ ones(1,102)*2 ones(1,10) ones(1,20)*3 ones(1,80)*4] ;
```

```
% Wave Theory
%==================================================================
waveTheory = 'Airy';
% waveTheory = 'Wheeler';
% waveTheory = 'Stokes_5th_Order';
% waveTheory = 'Irregular_Wave';

% Input parameters
%==================================================================
MWL = 0;                       % Mean water level [m]
h = 40;                        % Water depth [m]
H = 1 ;                        % Wave height [m]
T = 15;                        % Apparent wave period [s]
CDn = 0.5;                     % Drag coefficient – tangential [-]
CDt = 0;                       % Drag coefficient - Perpendicular [-]
CM = 2;                        % Inertia coefficient [-]
CA = 1;                        % Added Mass coefficient [-]
rhoW = 1025;                   % Density [kg/m^3]
ny = 1.05e-6;                  % Fluid kinematic viscosity[m^2/s]
k = 5e-6;                      % Roughness height [m] - Painted steel
g = 9.81;                      % Gravity [m/s^2]
nf = 20;                       % Number of Airy waves
phases = 2*pi*rand(1,nf);      % Random phase in the interval [0,2*pi]
% Timestep
%==================================================================
tStep = 0.01;
t     = 0:tStep:15;
```

```
% ####################################################################
% MainNonlinearCode
% ####################################################################

Clear all; Close all; Clc;

% Input for Nonlinear Wave Code
======================================================================
[nCoord,eTop,force,NodeFix,ch,NumberNewPoints,E,rhoS,eMat,A,I,eSec,...
waveTheory,MWL,h,H,T,Do,CDn,CDt,CM,CA,rhoW,ny,k,g,nf,phases,t] =
Input_Data;

% Calculations
======================================================================
% Dof Per Node
dofPerNode = 3  ;

% Nodes Per Element
NodePerElem = 2 ;

% Numbers of Nodes and Elements in Global Model
Nn = length(nCoord(:,1)) ;
Ne = length(eTop(:,1)) ;

% Elements
for i=1:length(eTop(:,1));
    Elem(:,:,i) = [nCoord(eTop(i,1),:) ; nCoord(eTop(i,2),:)];
end

% Length of Each Element
for i=1:length(eTop(:,1));
    lElem(i) = pdist([nCoord(eTop(i,1),:);nCoord(eTop(i,2),:)]);
end
lElem = lElem;

% Number of Global Degrees of Freedom Without Charnier
Ndof = dofPerNode*Nn ;

%Ordering of Elements
if size(eTop,1) == 1
    ElemDof = 1:Ndof;
else
    Dofn = reshape(1:Ndof,dofPerNode,[])';
    Dofc = num2cell(Dofn,2);
    ElemDof = cell2mat(Dofc(eTop(:,1:2)));
End

% Implementation of Charnier
if numel(ch) > 0
for i=1:length(ch(:,1))
    ElemDof(ch(i,1),3*ch(i,2)) = max(ElemDof(:))+1;
end
% Number of Global Degrees of Freedom With Charnier
Ndof = dofPerNode*Nn + length(ch(:,1));
end

% Fixed Nodes
FixedDof=[];
for i=1:numel(NodeFix(:,1))
```

```
    for j=2:numel(NodeFix(i,:))
        if NodeFix(i,j) == 0
FixedDof = [FixedDof ((NodeFix(i,1)-1)*3)+(j-1)];
        end
    end
end
FreeDof = [1:Ndof];
FreeDof(FixedDof) = [];

% Static Boundary Conditions
f = zeros(Ndof,1);
if numel(force)>0
    for i=1:length(force(:,1))
f(force(i,1),1) = force(i,2);
    end
end

% Known Forces and Displacements
fKnown = zeros(Ndof,1);
fKnown(FreeDof,1)=1;                 % Forces are known
fKnown = logical(fKnown);

dKnown = ones(Ndof,1);
dKnown(FreeDof,1)=0;                 % Displacements are known
dKnown = logical(dKnown);

% Global Displacement Dofs
dxz = zeros(length(nCoord(:,1)),2);
dxz(1,:) = ElemDof(1,1:2);
for i=1:length(eTop(:,1))
dxz(1+i,:)=ElemDof(i,4:5);
end

% Definition of Variables
======================================================================
% Current Externally Applied Global Nodal Force Vector
fn = zeros(Ndof,1);
% Number of Load Increments
ninc = 100 ;
% Load Factor
lambda = 1/ninc ;
% Calculation of the Incremental Force Vector
dF = lambda*f ;
% Storage Vector of Local Forces
qL = zeros(3,Ne);
% Global Nodal Displacements
un = zeros(Ndof,1); Su = zeros(Ndof,1) ;
% Initial System Matrices
[beta0,L0,B,Ksys] = KbeamNon(Ndof,Ne,eTop,nCoord,un,ElemDof,E,eMat,...
A,eSec,I,qL);
% Initial Memberdata Values
[L,beta,qL,qi,Fint] = MemberData(Ndof,Ne,eTop,nCoord,un,ElemDof,...
                                 L0,E,eMat,A,eSec,beta0,I);
```

```
% Dynamic Analysis
======================================================================
% Global Mass Matrix
Msys = zeros(Ndof) ;

% Loop Over a Finite Number of Elements
for n = 1:Ne ;
  % Extract Global Node Numbers
  ne = eTop(n,:) ;
  % Coordinates of Element Nodes
  xe = nCoord(ne',:) ;
  % Extract Global Degrees of Freedom for Element
  eDof = [ElemDof(n,1:3);ElemDof(n,4:6)];
  % Calculate Element Mass Matrix
  Me = Mbeam(xe,rhoS,A,eMat(n),eSec(n));
  % Add Element Mass Matrix Into the Right Spot
  Msys(eDof',eDof') = Msys(eDof',eDof')+ Me ;
end

% Initial Conditions
M=Msys(fKnown,fKnown);
K=Ksys(fKnown,fKnown);
%[w0,f0,aC,C] = Cbeam(Ksys,fKnown,M);
C = 0*M;

u0 = zeros(length(K),1) ; % init. displacement
v0 = zeros(length(K),1) ; % init. velocity

% Nonlinear Newmark Scheme
======================================================================
% Time-domain Solutions
dt = t(2) - t(1) ; % time increment

% Gravity Acceleration Force Vector
[Fs] = SelfWeight(beta,Elem,lElem,ElemDof,rhoS,eMat,A,eSec,g);

% Maximum Particle Velocity
[uMax] =
Maximum_Particle_Vel(nCoord,eTop,NumberNewPoints,t,waveTheory,...
                              H,T,h,MWL,g,nf,phases);
% Integration parameters
% gammaC = 1/2;
% betaC  = 1/4;
Ndamp = 0.1;              % Numerical damping ratio
gammaC = 0.5+Ndamp;       % Newmark beta-method integration parameters
betaC = 0.25*(1+Ndamp)^2; % Newmark beta-method integration parameters
% Initialize the Vectors u, v and a
u = zeros(Ndof,length(t));
v = zeros(Ndof,length(t));
a = zeros(Ndof,length(t));
uu = zeros(Ndof,1);
vv = zeros(Ndof,1); aa = zeros(Ndof,1);
u(fKnown,1) = u0 ; % initial displacements
v(fKnown,1) = v0 ; % initial velocities
a(fKnown,1) = M\(Fs(fKnown,1)-C*v0-K*u0);

% Perform Loop over the Time Steps
  for j = 1 : numel(t)-1
```

```
  % Predicted Values of u and v
    aa(fKnown,1) = a(fKnown,1);
    vv(fKnown,1) = v(fKnown,1)+a(fKnown,1)*dt;
    uu(fKnown,1) = u(fKnown,1)+v(fKnown,1)*dt +  0.5*a(fKnown,1)*dt^2;

% Memberdata of Current Values
[L,beta,qL,qi,Fint] = MemberData(Ndof,Ne,eTop,nCoord,uu,ElemDof,L0,...
                                 E,eMat,A,eSec,beta0,I);

  % Updated Coordinate System
    for i=1:Nn
    ux(i) = nCoord(i,1)+u(dxz(i,1),1);
    uy(i) = nCoord(i,2)+u(dxz(i,2),1);
    end
    nCoordUp = [ux' uy'];
    [extP,dL] = Extrepoints(nCoordUp,eTop,NumberNewPoints);
  % Surface Elevation
    if strcmp(waveTheory,'Airy')==1 || strcmp(waveTheory,'Wheeler')==1
    [eta,hTot,Lwave] = Eta(H,T,h,MWL,j*dt-dt,extP);
    elseif strcmp(waveTheory,'Stokes_5th_Order') == 1
    [Lwave,D,E5th]=LDEStokes5thOrderWaves(H,T,h);
    [eta,hTot] = EtaStokes5(Lwave,E5th,T,MWL,j*dt-dt,extP);
    elseif strcmp(waveTheory,'Irregular_Wave') == 1
    [eta,hTot,Lwave] = EtaIrregular(h,H,T,MWL,j*dt-
dt,extP,nf,phases);
    end
    hdata(:,j) = [hTot(1,1); hTot(end,1)];
  % Buoyancy Force Vector
    [Fb] =
BuoyancyForce(Do,eSec,hTot,extP,nCoordUp,eTop,dL,L,beta,rhoW,...
              g,ElemDof);
  % Wave force vector
    [Fw] = WaveForce(Do,eSec,waveTheory,h,eta,H,T,nf,phases,extP,...
                  nCoordUp,eTop,dL,L,beta,rhoW,ny,k,uMax,g,ElemDof,...
                  CDn,CDt,CM,CA,j*dt-dt,v,a);
  % Gravity acceleration force vector
    [Fs] = SelfWeight(beta,Elem,lElem,ElemDof,rhoS,eMat,A,eSec,g);
  % Residual calculation
    r = Fs(fKnown,1) - M*aa(fKnown,1) - C*vv(fKnown,1) -
Fint(fKnown,1)...
        + Fb(fKnown,1) + Fw(fKnown,1);
  % Calculation of the Norm of the Residual
    rnorm = sqrt(r'*r);
  % Total Force Vector
    Ftot = (Fb+Fw+Fs);

    tol = norm(Ftot(fKnown,1))*1e-3; % Tolerance
    kiter = 0;      % Zero iteration counter
    maxiter = 100;  % Max iterations
    while rnorm>tol && kiter<maxiter;
  % System matrices
 [beta0,L0,B,Ksys]=KbeamNon(Ndof,Ne,eTop,nCoord,uu,ElemDof,E,...
                            eMat,A,eSec,I,qL);
Kmod = M*(1/(betaC*dt^2)) + C*((gammaC*dt)/(betaC*dt^2)) + ...
       Ksys(fKnown,fKnown);
  % Increment correction
    Su = Kmod\r;
  % Corrected values
    uu(fKnown,1) = uu(fKnown,1) + Su;
    vv(fKnown,1) = vv(fKnown,1) + (((gammaC*dt)/(betaC*dt^2)))*Su;
```

```
    aa(fKnown,1) = aa(fKnown,1) + ((1/(betaC*dt^2)))*Su ;
  % Updated Memberdata Regarding the Corrected Values
 [L,beta,qL,qi,Fint] = MemberData(Ndof,Ne,eTop,nCoord,uu,...
                                  ElemDof,L0,E,eMat,A,eSec,beta0,I);
  % Updated Coordinate System
    for i=1:Nn
    ux(i) = nCoord(i,1)+uu(dxz(i,1),1);
    uy(i) = nCoord(i,2)+uu(dxz(i,2),1);
    end
    nCoordUp = [ux' uy'];
    [extP,dL] = Extrepoints(nCoordUp,eTop,NumberNewPoints);
  % Surface elevation
    if strcmp(waveTheory,'Airy')==1 || strcmp(waveTheory,'Wheeler')==1
    [eta,hTot,Lwave] = Eta(H,T,h,MWL,j*dt-dt,extP);
    elseif strcmp(waveTheory,'Stokes_5th_Order') == 1
    [Lwave,D,E5th]=LDEStokes5thOrderWaves(H,T,h);
    [eta,hTot] = EtaStokes5(Lwave,E5th,T,MWL,j*dt-dt,extP);
    elseif strcmp(waveTheory,'Irregular_Wave') == 1
    [eta,hTot,Lwave] = EtaIrregular(h,H,T,MWL,j*dt-dt,extP,nf,phases);
    end
  % Buoyancy Force Vector
    [Fb] = BuoyancyForce(Do,eSec,hTot,extP,nCoordUp,eTop,dL,L,...
                         beta,rhoW,g,ElemDof);
  % Wave force vector
    [Fw] = WaveForce(Do,eSec,waveTheory,h,eta,H,T,nf,phases,extP,...
                nCoordUp,eTop,dL,L,beta,rhoW,ny,k,uMax,g,ElemDof,...
                CDn,CDt,CM,CA,j*dt-dt,vv,aa);
  % Gravity Acceleration Force Vector
    [Fs] = SelfWeight(beta,Elem,lElem,ElemDof,rhoS,eMat,A,eSec,g);
  % Residual Calculation
    r = Fs(fKnown,1)-M*aa(fKnown,1)-C*vv(fKnown,1)-Fint(fKnown,1)...
        + Fb(fKnown,1) + Fw(fKnown,1) ;
  % Calculation of the Norm of the Residual
    rnorm = sqrt(r'*r);
  % Update Iteration Counter
    kiter = kiter + 1;
    end

  % Error if No Convergence
    if rnorm>tol
    j
    error('Load Step Did not Converge: ')
    end
  % Final Values
    u = uu;
    v = vv;
    a = aa;
    udata(:,j+1) = u;
    vdata(:,j+1) = v;
    adata(:,j+1) = a;
    etadata(:,j+1) = eta(end,end);
  end
```

```
########################################################################
% MemberData
########################################################################
function [L,beta,qL,qi,Fint] = MemberData(Ndof,Ne,eTop,nCoord,uc,...
                               ElemDof,L0,E,eMat,A,eSec,beta0,I);
% === Description
=======================================================
% Input:    Ndof            Number of dof
%           Ne              Number of elements
%           eTop            Topology
%           nCoord          Coordinates
%           uc              Current nodal displacements
%           ElemDof         dof of each element
%           L0              Original length of each element
%           E               Young's modulus
%           eMat            Materialparameter of each element
%           A               Section area
%           eSec            Cross-sectionalparameter of each element
%           Beta0           Initial angle of each element
%           I               Area moment of inertia
%
% Output:   L               Length of members
%           beta            Angle of members
%           qL              Local forces
%           Fint            Internal force vector

% Update of Member Data
========================================================================
Fint = zeros(Ndof,1) ;

for n = 1:Ne
% Extract Global Node Numbers
ne = eTop(n,:) ;
% Coordinates of Element Nodes
xe = nCoord(ne',:) ;
% Calculation of the Distance between Nodes
dX(n) = xe(2,1)+uc(ElemDof(n,4))-(xe(1,1)+uc(ElemDof(n,1)));
dY(n) = xe(2,2)+uc(ElemDof(n,5))-(xe(1,2)+uc(ElemDof(n,2)));
% Update current length of members
L(n) = sqrt(dX(n)^2 + dY(n)^2);
% Update the Cosine and Sine of the Current Angle Beta for Members
c(n) = dX(n)/L(n); s(n) = dY(n)/L(n);
% Calculate the Axial Displacement of Members
uL(n) = (L(n)^2 - L0(n)^2)/(L(n) + L0(n));
% Calculate the Axial Force
N(n) = (E(eMat(n))*A(eSec(n))*uL(n))/L0(n);
% Calculate Beta
beta(n) = atan2(dY(n),dX(n)) ;

% Calculate Beta1 and Beta2
beta1(n) = (uc(ElemDof(n,3))+beta0(n));
beta2(n) = (uc(ElemDof(n,6))+beta0(n));

% Calculate Teta1L and Teta2L
theta1l(n) = atan((c(n)*sin(beta1(n)) - s(n)*cos(beta1(n)))/...
                 (c(n)*cos(beta1(n)) + s(n)*sin(beta1(n))));
theta2l(n) = atan((c(n)*sin(beta2(n)) - s(n)*cos(beta2(n)))/...
                 (c(n)*cos(beta2(n)) + s(n)*sin(beta2(n))));
```

```
if theta1l(n) == -(cos(pi/2)) &&  theta2l(n) == -(cos(pi/2))
   theta1l(n)=0;
   theta2l(n)=0;

elseif theta1l(n) == (cos(pi/2)) &&  theta2l(n) == (cos(pi/2))
theta1l(n)=0;
theta2l(n)=0;
end

% Calculate Nodal Rotations
M1(n) = 4*E(eMat(n))*I(eSec(n))*theta1l(n)/L0(n) + 2*E(eMat(n))*...
        I(eSec(n))*theta2l(n)/L0(n);
M2(n) = 2*E(eMat(n))*I(eSec(n))*theta1l(n)/L0(n) + 4*E(eMat(n))*...
        I(eSec(n))*theta2l(n)/L0(n);

% Update Local Forces
qL(:,n) = [N(n); M1(n); M2(n)];

% Calculation of Transformation Matrix
B(:,:,n) = [-c(n)        -s(n)      0   c(n)       s(n)        0
            -s(n)/L(n)   c(n)/L(n)  1   s(n)/L(n)  -c(n)/L(n)  0
            -s(n)/L(n)   c(n)/L(n)  0   s(n)/L(n)  -c(n)/L(n)  1];

% Calculating Internal Forces
======================================================================
% Internal Force Vector in Global Coordinates for Beam Element i
qi(:,n) = B(:,:,n)'*qL(:,n) ;

Fint(ElemDof(n,:),1) = Fint(ElemDof(n,:),1) + qi(:,n) ;
end
```

```
#####################################################################
% Tangent Stiffness Matrix
#####################################################################
function [beta0,L0,B,Ksys] =
KbeamNon(Ndof,Ne,eTop,nCoord,un,ElemDof,E,eMat,A,eSec,I,qL);

% === Description=======================================================
% Input:    Ndof            Number of dof
%           Ne              Number of elements
%           eTop            Topology
%           nCoord          Coordinates
%           un              Global nodal displacements
%           ElemDof         dof of each element
%           E               Young's modulus
%           eMat            Materialparameter of each element
%           A               Section area
%           eSec            Cross-sectionalparameter of each element
%           I               Area moment of inertia
%           qL              Local forces
%
% Output:   Ksys            6x6 Nonlinear Stiffness Matrix


Ksys = zeros(Ndof) ;

% Loop over a finite number of elements
for n = 1:Ne
% Extract global node numbers
ne = eTop(n,:) ;
% Coordinates of element nodes
xe = nCoord(ne',:) ;
% Vector of initial angles of beam members
beta0(n) = atan2((xe(2,2)-xe(1,2)),(xe(2,1)-xe(1,1)));
% Initial beam element length
L0(n) = sqrt((xe(2,1)-xe(1,1))^2 + (xe(2,2)-xe(1,2))^2);

% Vector of beam element length based on current u
L(n) = sqrt(((xe(2,1)+un(ElemDof(n,4)))-(xe(1,1)+...
       un(ElemDof(n,1))))^2 + ((xe(2,2)+un(ElemDof(n,5)))-...
       (xe(1,2)+un(ElemDof(n,2))))^2);

% Vectors of cosines and sines for each beam element angle
c(n) = ((xe(2,1)+un(ElemDof(n,4))) - (xe(1,1)+un(ElemDof(n,1))))/L(n);
s(n) = ((xe(2,2)+un(ElemDof(n,5))) - (xe(1,2)+un(ElemDof(n,2))))/L(n);

% Transformation Matrix B
    B(:,:,n) = [-c(n)        -s(n)      0   c(n)        s(n)        0
                -s(n)/L(n)   c(n)/L(n)  1   s(n)/L(n)  -c(n)/L(n)   0
                -s(n)/L(n)   c(n)/L(n)  0   s(n)/L(n)  -c(n)/L(n)   1];
CL(:,:,n) = ((E(eMat(n))*A(eSec(n)))/L0(n))*[1 0 0
0 4*(sqrt(I(eSec(n))/A(eSec(n))))^2 2*(sqrt(I(eSec(n))/A(eSec(n))))^2
0 2*(sqrt(I(eSec(n))/A(eSec(n))))^2 4*(sqrt(I(eSec(n))/A(eSec(n))))^2]
```

```
% Standard Transformed Global Tangent Stiffness
Kt1(:,:,n) = B(:,:,n)'*CL(:,:,n)*B(:,:,n);

% The Axial Force in the Beam
N(n) = qL(1,n);

% The Local Nodal Rotations
M1(n) = qL(2,n);
M2(n) = qL(3,n);

r(:,n) = [-c(n) -s(n) 0 c(n) s(n) 0]';
z(:,n) = [s(n) -c(n) 0 -s(n) c(n) 0]';

Kts(:,:,n) = (N(n)/L(n))*(z(:,n)*z(:,n)')+((M1(n)+M2(n))/...
              L(n)^2)*(r(:,n)*z(:,n)' + z(:,n)*r(:,n)');

% The Variationally Consistent Tangent Stiffness Matrix
KeNon(:,:,n) = Kt1(:,:,n) + Kts(:,:,n) ;

% Add Element Stiffness Matrix into the Right Spot
Ksys(ElemDof(n,:),ElemDof(n,:)) = Ksys(ElemDof(n,:),ElemDof(n,:))...
                                  + KeNon(:,:,n) ;
end
```

```
########################################################################
% Mbeam
########################################################################
%==== Description =====================================================
% Input:    xe              Coordinates of Element Nodes
%           rhoS            Structure Density
%           A               Cross-sectional Area
%           eMat            Material parameter of each element
%           eSec            Cross-sectional parameter of each element
%
% Output:   Me              Mass matrix

syms x
% Calculation of element length
Dxe = xe(2,:)-xe(1,:) ;
L   = norm(Dxe)       ;

mbar  = zeros(2) ;
mbeam = zeros(4) ;
Me    = zeros(6) ;

% Shape function bar
N1 =  -(1/L)*x+1;
N4 =  (1/L)*x;

% Shape function beam Bernoulli-Euler
N2 = 1 - (3*x^2)/L^2 + (2*x^3)/L^3  ;
N3 = x - (2*x^2)/L + (x^3)/L^2      ;
N5 = (3*x^2)/L^2 - (2*x^3)/L^3      ;
N6 = (-x^2)/L + (x^3)/L^2           ;

% Shape Functions
Nbar  = [N1 N4];
Nbeam = [N2 N3 N5 N6];

% Integration of Mass matrix
mbar=real(double(int(Nbar'*rhoS(eMat)*A(eSec)*Nbar,0,L)))    ;
mbeam=real(double(int(Nbeam'*rhoS(eMat)*A(eSec)*Nbeam,0,L))) ;

% Local Mass Matrix
bardof=[1 4]        ;
beamdof=[2 3 5 6]   ;

Me(bardof,bardof)   = mbar  ;
Me(beamdof,beamdof) = mbeam ;

% Transformation matrix
NodeDir1 = Dxe(1)/L ;
NodeDir2 = Dxe(2)/L ;

T = [ NodeDir1 NodeDir2   0    0            0        0
     -NodeDir2 NodeDir1   0    0            0        0
     0             0      1    0            0        0
     0             0      0  NodeDir1    NodeDir2    0
     0             0      0  -NodeDir2   NodeDir1    0
     0             0      0    0            0        1] ;

Me = T'*(Me)*T ;
```

```
######################################################################
% Wave Forces
######################################################################
function[Fw]=WaveForce(Do,eSec,waveTheory,h,eta,H,T,nf,phases,extP,...
nCoord,eTop,dL,L,beta,rhoW,ny,k,uMax,g,ElemDof,CDn,CDt,CM,CA,tc,v,a);

%==== Description
=========================================================
% Input:     Do               Cylinder Diameter
%            eSec             Cross-sectionalparameter of each element
%            waveTheory       Wave Theory
%            h                Waterdepth
%            eta              Surface Elevation
%            H                Wave Height
%            T                Wave Period
%            nf               Number of Airy Waves
%            phases           Random Phase in The Interval [0,2*pi]
%            extP             Element Extraction Points
%            nCoord           Coordinates
%            eTop             Topology
%            dL               Distance Between Extraction Points
%            L                Element Length
%            beta             Angle of Each Element
%            rhoW             Water density
%            ny               Fluid Kinematic Viscosity
%            k                Roughness Height - Painted steel
%            uMax             Maximum Particle Velocity
%            g                Gravity Acceleration
%            ElemDof          Dofs of Each Element
%            CDn              Drag coefficient - tangential
%            CDt              Drag coefficient - Perpendicular
%            CM               Inertia coefficient
%            CA               Added Mass coefficient
%            tc               Current Time Step
%            v                Current Structure Velocity
%            a                Current Structure Acceleration
%
% Output:    Fw               Buoyancy force vector


% Loop over Elements
%======================================================================
Fw = zeros(max(max(ElemDof,[],2)),1);
vS = zeros(max(max(ElemDof,[],2)),1);
aS = zeros(max(max(ElemDof,[],2)),1);

for i=1:length(eTop(:,1));

% Elements and Element Length
%======================================================================
Elem(:,:,i) = [nCoord(eTop(i,1),:) ; nCoord(eTop(i,2),:)];
lElem(i) = pdist([nCoord(eTop(i,1),:);nCoord(eTop(i,2),:)]);

% Unit Vectors
%======================================================================
j  = [0 1]';

e1(i,:) = [cosd(radtodeg(beta(i))) sind(radtodeg(beta(i)))];
e2(i,:) = [-sind(radtodeg(beta(i))) cosd(radtodeg(beta(i)))];
```

```
e12(:,:,i) = [e1(i,:); e2(i,:)]; % Transformation from global to local
e21(:,:,i) = e12(:,:,i)';        % Transformation from local to global

%======================================================================
% Outer radius
r(:,i) = Do(eSec(i))/2;

%======================================================================
for jj=1:length(extP(:,1,1))

% The Cross-sectional Top and Bottom elevations
Ht(jj,i) = (eta(jj,i))-((extP(jj,:,i)'+e2(i,:)'*r(:,i)))'*j ;
Hb(jj,i) = (eta(jj,i))-((extP(jj,:,i)'-e2(i,:)'*r(:,i)))'*j ;

% The submerged height
if Ht(jj,i) >= 0
Hs(jj,i) = 2*r(:,i) ;
elseif Hb(jj,i) > 0 && Ht(jj,i) < 0 ;
Hs(jj,i) = ((2*r(:,i))/(Hb(jj,i)-Ht(jj,i)))*Hb(jj,i) ;
else Hb(jj,i) <= 0 ;
Hs(jj,i) = 0 ;
end

% Cross-Sectional Area
As(jj,i) = (r(:,i)^2*acos((r(:,i)-Hs(jj,i))/r(:,i)))-(r(:,i)-
Hs(jj,i))*...
           sqrt(2*r(:,i)*Hs(jj,i)-Hs(jj,i)^2);

% Partical Velocities and Accelerations
%======================================================================
if strcmp(waveTheory,'Airy') == 1 || strcmp(waveTheory,'Wheeler') == 1
[u,w,ax,az] =
Particle_Vel_and_Acc_Airy(extP,waveTheory,eta,h,H,T,g,tc);

vel_n(jj,i) = e12(2,:,i)*[u(jj,i); w(jj,i)];
vel_t(jj,i) = e12(1,:,i)*[u(jj,i); w(jj,i)];
acc_n(jj,i) = e12(2,:,i)*[ax(jj,i); az(jj,i)];

elseif strcmp(waveTheory,'Stokes_5th_Order') == 1
[Lwave,D]=LDE_Stokes5thOrderWaves(H,T,h);
[u,w,aTot] =
Particle_Vel_and_Acc_Stokes_5th_Order(extP,h,T,Lwave,D,eta,tc);

vel_n(jj,i) = e12(2,:,i)*[u(jj,i); w(jj,i)];
vel_t(jj,i) = e12(1,:,i)*[u(jj,i); w(jj,i)];
acc_n(jj,i) = aTot(jj,i);

elseif strcmp(waveTheory,'Irregular_Wave') == 1
[u,w,ax,az] = JonswapFLS(H,T,h,tc,extP,g,nf,phases);

vel_n(jj,i) = e12(2,:,i)*[u(jj,i); w(jj,i)];
vel_t(jj,i) = e12(1,:,i)*[u(jj,i); w(jj,i)];
acc_n(jj,i) = e12(2,:,i)*[ax(jj,i); az(jj,i)];
end
```

```
% Shape Functions
%=====================================================================
dLcount(:,i) = [0 ; dL(:,i)];
x(jj,i) = sum(dLcount(1:jj,i));

% Shape Function Bar
N1(jj,i) =  -(1/L(i))*x(jj,i)+1;
N4(jj,i) =  (1/L(i))*x(jj,i);

% Shape Function Beam Bernoulli-Euler
N2(jj,i) = 1 - (3*x(jj,i)^2)/L(i)^2 + (2*x(jj,i)^3)/L(i)^3;
N3(jj,i) = x(jj,i) - (2*x(jj,i)^2)/L(i) + (x(jj,i)^3)/L(i)^2;
N5(jj,i) = (3*x(jj,i)^2)/L(i)^2 - (2*x(jj,i)^3)/L(i)^3;
N6(jj,i) = (-x(jj,i)^2)/L(i) + (x(jj,i)^3)/L(i)^2;

% Structural Velocity and Acceleration
%=====================================================================
vS(ElemDof(i,1:2),1) = e12(:,:,i)*v(ElemDof(i,1:2),1);
vS(ElemDof(i,3),1) = v(ElemDof(i,3),1);
vS(ElemDof(i,4:5),1) = e12(:,:,i)*v(ElemDof(i,4:5),1);
vS(ElemDof(i,6),1) = v(ElemDof(i,6),1);
aS(ElemDof(i,1:2),1) = e12(:,:,i)*a(ElemDof(i,1:2),1);
aS(ElemDof(i,3),1) = a(ElemDof(i,3),1);
aS(ElemDof(i,4:5),1) = e12(:,:,i)*a(ElemDof(i,4:5),1);
aS(ElemDof(i,6),1) = a(ElemDof(i,6),1);

velS_n(jj,i) = [0 N2(jj,i) N3(jj,i) 0 N5(jj,i)
N6(jj,i)]*vS(ElemDof(i,:),1);
velS_t(jj,i) = [N1(jj,i) 0 0 N4(jj,i) 0 0]*vS(ElemDof(i,:),1);

accS_n(jj,i) = [0 N2(jj,i) N3(jj,i) 0 N5(jj,i)
N6(jj,i)]*aS(ElemDof(i,:),1);

% Relative Fluid-Structure Kinematics
%=====================================================================
if extP(jj,2,i) <= eta(jj,i) && H > 0;
velR_n(jj,i) = vel_n(jj,i) - velS_n(jj,i);
velR_t(jj,i) = vel_t(jj,i) - velS_t(jj,i);
accR_n(jj,i) = acc_n(jj,i) - accS_n(jj,i);
else
velR_n(jj,i) = 0;
velR_t(jj,i) = 0;
accR_n(jj,i) = 0;
end

% Drag Coefficient
%=====================================================================
% Drag Coefficient for Steady State
if k/Do(eSec(i)) < 10e-4 % Smooth
CDS = 0.65;
elseif k/Do(eSec(i)) > 10e-4 && k/Do(eSec(i)) < 10e-2
CDS = 29 + 4 * log(k/Do(eSec(i)));
elseif k/Do(eSec(i)) > 10e-2 % Rough
CDS = 1.05;
end

% Keulegan-Carpenter number
KC(jj,i) = (uMax(jj,i)*T)/Do(eSec(i));
```

```
% Wake Amplification Factor
if (KC(jj,i)/CDS) < 1.1;
psi(jj,i) = ((0.3-1.8)/(1.1-0))*((KC(jj,i)/CDS)-0)+1.8;
elseif (KC(jj,i)/CDS) >= 1.1 && (KC(jj,i)/CDS) < 3;
psi(jj,i) = 0.3;
elseif (KC(jj,i)/CDS) >= 3 && (KC(jj,i)/CDS) < 18;
psi(jj,i) = ((1.3-0.3)/(18-3))*((KC(jj,i)/CDS)-3)+0.3;
elseif (KC(jj,i)/CDS) >= 18 && (KC(jj,i)/CDS) < 20;
psi(jj,i) = ((1.25-1.3)/(20-18))*((KC(jj,i)/CDS)-18)+1.3;
elseif (KC(jj,i)/CDS) >= 20 && (KC(jj,i)/CDS) < 60;
psi(jj,i) = ((1-1.25)/(60-20))*((KC(jj,i)/CDS)-20)+1.25;
elseif (KC(jj,i)/CDS) >= 60;
psi(jj,i) = 1;
end

% Drag Coefficient
CD(jj,i) = CDS * psi(jj,i);

% Distributed Wave Load
%===================================================================
% Relative Morison Formulation
fd_n(jj,i) = CM*rhoW*As(jj,i)*acc_n(jj,i) - rhoW*CA*As(jj,i)*...
accS_n(jj,i) + 0.5*rhoW*CDn*Hs(jj,i)*velR_n(jj,i)*abs(velR_n(jj,i));
fd_t(jj,i) = 0.5*rhoW*CDt*Hs(jj,i)*velR_t(jj,i)*abs(velR_t(jj,i));


% Function of the Distributed Force Regarding the Shape Functions
%===================================================================
fd1(jj,i) = N1(jj,i)'*fd_t(jj,i);
fd2(jj,i) = N2(jj,i)'*fd_n(jj,i);
fd3(jj,i) = N3(jj,i)'*fd_n(jj,i);
fd4(jj,i) = N4(jj,i)'*fd_t(jj,i);
fd5(jj,i) = N5(jj,i)'*fd_n(jj,i);
fd6(jj,i) = N6(jj,i)'*fd_n(jj,i);
end

% Numerical Integration - Trapezoidal Rule
%===================================================================
Fw1(i) = dL(1,i)*((fd1(1,i)/2)+sum(fd1(2:end-1,i))+(fd1(end,i)/2));
Fw2(i) = dL(1,i)*((fd2(1,i)/2)+sum(fd2(2:end-1,i))+(fd2(end,i)/2));
Fw3(i) = dL(1,i)*((fd3(1,i)/2)+sum(fd3(2:end-1,i))+(fd3(end,i)/2));
Fw4(i) = dL(1,i)*((fd4(1,i)/2)+sum(fd4(2:end-1,i))+(fd4(end,i)/2));
Fw5(i) = dL(1,i)*((fd5(1,i)/2)+sum(fd5(2:end-1,i))+(fd5(end,i)/2));
Fw6(i) = dL(1,i)*((fd6(1,i)/2)+sum(fd6(2:end-1,i))+(fd6(end,i)/2));

% Distributed Wave Load Fw
%===================================================================
Fwi(:,i) = [e21(:,:,i)*[Fw1(i); Fw2(i)]; Fw3(i);
e21(:,:,i)*[Fw4(i);...
            Fw5(i)]; Fw6(i)]';

Fw(ElemDof(i,:),1) = Fw(ElemDof(i,:),1) + Fwi(:,i);
end
```

```
########################################################################
% Buoyancy Forces
########################################################################

%==== Description=======================================================
% Calculation of buoyancy forces for each element
% Input:    Do              Cylinder Diameter
%           h               Waterdepth
%           extP            Element extraction points
%           nCoordUP        Current Coordinates
%           eTop            Topology
%           dL              Distance between extraction points
%           L               Element Length
%           beta            Angle of each element
%           rhoW            Water density
%           g               Gravity acceleration
%           ElemDof         Dofs of each element
%
% Output:   Fb              Buoyancy Force Vector

% Loop over elements
%=======================================================================
Fb = zeros(max(max(ElemDof,[],2)),1);

for i=1:length(eTop(:,1));

% Elements and element length
%=======================================================================
Elem(:,:,i) = [nCoordUp(eTop(i,1),:) ; nCoordUp(eTop(i,2),:)];

% Unit vectors
%=======================================================================
j  = [0 1]';

e1(i,:) = [cosd(radtodeg(beta(i))) sind(radtodeg(beta(i)))];
e2(i,:) = [-sind(radtodeg(beta(i))) cosd(radtodeg(beta(i)))];

e12(:,:,i) = [e1(i,:); e2(i,:)]; % Transformation from global to local
e21(:,:,i) = e12(:,:,i)';        % Transformation from local to global

% Distributed excess buoyancy Fbq and Fbp
%=======================================================================
% Outer radius
r(i) = Do(eSec(i))/2;

for jj=1:length(extP(:,1,1))
% The cross-sectional top and bottom elevations
Htj(jj,i) = h(jj,i)-((extP(jj,:,i)'+e2(i,:)'*r(i)))'*j ;
Hbj(jj,i) = h(jj,i)-((extP(jj,:,i)'-e2(i,:)'*r(i)))'*j ;

% The submerged height
if Htj(jj,i) >= 0
Hsj(jj,i) = 2*r(i) ;
elseif Hbj(jj,i) > 0 && Htj(jj,i) < 0 ;
Hsj(jj,i) = ((2*r(i))/(Hbj(jj,i)-Htj(jj,i)))*Hbj(jj,i) ;
else Hbj(jj,i) <= 0 ;
Hsj(jj,i) = 0 ;
end
```

```
% Sectional area at watersurface
Aj(jj,i) =(r(i)^2*acos((r(i)-Hsj(jj,i))/r(i)))-(r(i)-
Hsj(jj,i))*sqrt(2*r(i)*Hsj(jj,i)-Hsj(jj,i)^2);

% Distrubuted excess buoyancy Fbqi
Fbqi(jj,i) = Aj(jj,i)*rhoW*g*e2(i,:)*j;

% Distrubuted excess buoyancy Fbpi
Fbpi(jj,i) = Aj(jj,i)*rhoW*g*e1(i,:)*j;

% Shape functions
%===================================================================
dLcount(:,i) = [0 ; dL(:,i)];
x(jj,i) = sum(dLcount(1:jj,i));

% Shape function bar
N1(jj,i) =  -(1/L(i))*x(jj,i)+1;
N4(jj,i) =  (1/L(i))*x(jj,i);

% Shape function beam Bernoulli-Euler
N2(jj,i) = 1 - (3*x(jj,i)^2)/L(i)^2 + (2*x(jj,i)^3)/L(i)^3;
N3(jj,i) = x(jj,i) - (2*x(jj,i)^2)/L(i) + (x(jj,i)^3)/L(i)^2;
N5(jj,i) = (3*x(jj,i)^2)/L(i)^2 - (2*x(jj,i)^3)/L(i)^3;
N6(jj,i) = (-x(jj,i)^2)/L(i) + (x(jj,i)^3)/L(i)^2;

% Function of the distributed force regarding the shapefunctions
%===================================================================
f1(jj,i) = N1(jj,i)'*Fbpi(jj,i);
f2(jj,i) = N2(jj,i)'*Fbqi(jj,i);
f3(jj,i) = N3(jj,i)'*Fbqi(jj,i);
f4(jj,i) = N4(jj,i)'*Fbpi(jj,i);
f5(jj,i) = N5(jj,i)'*Fbqi(jj,i);
f6(jj,i) = N6(jj,i)'*Fbqi(jj,i);
end

% Numerical integration - trapezoidal rule
Fb1(i) = dL(1,i)*((f1(1,i)/2)+sum(f1(2:end-1,i))+(f1(end,i)/2));
Fb2(i) = dL(1,i)*((f2(1,i)/2)+sum(f2(2:end-1,i))+(f2(end,i)/2));
Fb3(i) = dL(1,i)*((f3(1,i)/2)+sum(f3(2:end-1,i))+(f3(end,i)/2));
Fb4(i) = dL(1,i)*((f4(1,i)/2)+sum(f4(2:end-1,i))+(f4(end,i)/2));
Fb5(i) = dL(1,i)*((f5(1,i)/2)+sum(f5(2:end-1,i))+(f5(end,i)/2));
Fb6(i) = dL(1,i)*((f6(1,i)/2)+sum(f6(2:end-1,i))+(f6(end,i)/2));

% Distributed excess buoyancy Fbq
Fbqp(:,i) = [e21(:,:,i)*[Fb1(i); Fb2(i)]; Fb3(i); e21(:,:,i)*[Fb4(i);
Fb5(i)]; Fb6(i)]';

% Buoyancy force
%===================================================================
=====
Fb(ElemDof(i,:),1) = Fb(ElemDof(i,:),1) + Fbqp(:,i);

end
```